Příloha č. 1

Clinical Biochemistry 48 (2015) 2–7

Contents lists available at ScienceDirect

Clinical Biochemistry

journal homepage: www.elsevier.com/locate/clinbiochem

Screening for adenylosuccinate lyase deficiency using tandem mass spectrometry analysis of succinylpurines in neonatal dried blood spots

Marie Zikanova *, Jakub Krijt, Vaclava Skopova, Matyas Krijt, Veronika Baresova, Stanislav Kmoch

Institute of Inherited Metabolic Disorders, First Faculty of Medicine, Charles University in Prague and General University Hospital in Prague, Ke Karlovu 2, 128 08 Praha 2, Czech Republic

ARTICLE INFO

Article history:
Received 3 September 2014
Received in revised form 14 October 2014
Accepted 15 October 2014
Available online 23 October 2014

Keywords:
Dried blood spots
DBS
Screening
Adenylosuccinate lyase deficiency
Purine metabolism
Tandem mass spectrometry
LC–MS/MS

ABSTRACT

Objectives: Stable isotope dilution coupled with liquid chromatography–tandem mass spectrometry (LC–MS/MS) is the sensitive method for screening for various inherited metabolic disorders using dried blood spots (DBSs). We present a method for LC–MS/MS determination of succinyladenosine (SAdo) and succinylaminoimidazole carboxamide riboside (SAICAr), biomarkers for adenylosuccinate lyase deficiency (dADSL), in DBS.

Design and methods: SAICAr and SAdo were separated on a Symmetry-C18 column and detected using positive electrospray ionisation in selected reaction monitoring mode. The quantification was performed using the isotopically labelled internal standards SAdo-$^{13}C_4$ and SAICAr-$^{13}C_4$, which were prepared via ADSL-catalysed reactions of fumarate-$^{13}C_4$ with adenosine monophosphate and aminoimidazole carboxamide ribotide, respectively, and subsequent alkaline phosphatase-catalysed dephosphorylation of the resulting products.

Results: The detection of SAICAr and SAdo in DBS was linear over the range of 0–25 μmol/L. The respective intra-assay and inter-assay imprecision values were less than 10.7% and 15.2% for SAICAr and 4.7% and 5.7% for SAdo. The recoveries from DBS spiked with different concentrations of SAICAr and SAdo were between 94% and 117%. The concentrations of SAICAr and SAdo were higher in the archived DBS from dADSL patients (SAICAr, 0.03–4.7 μmol/L; SAdo, 1.5–21.3 μmol/L; n = 5) compared to those of the control subjects (SAICAr, 0–0.026 μmol/L; SAdo, 0.06–0.14 μmol/L; n = 31), even after DBSs from dADSL patients were stored for 2–23 years.

Conclusions: We developed and validated a method of succinylpurine analysis in DBS that improves selective screening for dADSL in the paediatric population and may be used for retrospective diagnosis to aid the genetic counselling of affected families.

Introduction

Liquid chromatography coupled with tandem mass spectrometry (LC–MS/MS) is a powerful tool for the measurement of metabolic profiles in biological samples. It allows simultaneous profiling of diverse groups of metabolites in limited clinical materials such as dried blood spots (DBSs). For high-quality quantitative analysis, the use of isotope-labelled internal standards is highly recommended to reduce the variability caused by matrix effects, sample preparation errors or detection sensitivity changes. High reliability, sensitivity and throughput make stable isotope dilution tandem mass spectrometry an optimal technique for selective or neonatal screening of various groups of inherited metabolic disorders [1,2].

Screening procedures for disorders of purine and pyrimidine metabolism are mostly based on the detection of abnormal metabolites in urine [3–11]. However, collection of this material may be difficult, especially in newborns. Furthermore, the instability of some metabolites requires deep freezing of the collected material before transportation to metabolic laboratories. In contrast, DBS can be stored at room temperature and requires no special shipping policy; additionally, their use precludes false negative results due to bacterial infections [12]. Moreover, DBS samples are routinely collected on a Guthrie card from all neonates in many countries for the screening of inborn errors of metabolism and may be available for the screening of purine disorders without the need for additional sample (urine, blood) collection.

In this work, we describe methods for the preparation of the isotopically labelled purine metabolites succinylaminoimidazole carboxamide riboside-$^{13}C_4$ (SAICAr-$^{13}C_4$) and succinyladenosine-$^{13}C_4$ (SAdo-$^{13}C_4$) and demonstrate their use in quantitative LC–MS/MS analysis of SAdo and SAICAr in neonatal DBS. This method allows inexpensive selective

Abbreviations: ADSL, adenylosuccinate lyase; SAdo, succinyladenosine; SAICAr, succinylaminoimidazole carboxamide riboside; PEI-TLC, polyethylenimine cellulose thin-layer chromatography; HPLC–DAD, high-performance liquid chromatography with diode array detection; LC–MS/MS, liquid chromatography–tandem mass spectrometry.

* Corresponding author. Fax: +420 224 967 081.
E-mail addresses: marie.zikanova@lf1.cuni.cz (M. Zikanova), jkrijt@lf1.cuni.cz (J. Krijt), vaclava.skopova@lf1.cuni.cz (V. Skopova), Matyas.Krijt@staff.cuni.cz (M. Krijt), veronika.baresova@lf1.cuni.cz (V. Baresova), skmoch@lf1.cuni.cz (S. Kmoch).

http://dx.doi.org/10.1016/j.clinbiochem.2014.10.004
0009-9120/

screening of adenylosuccinate lyase (ADSL) deficiency (MIM# 103050), which is an inherited metabolic disorder of purine metabolism [13,14], in patients with an unspecific neurological manifestation.

Material and methods

Chemicals

Calf intestinal alkaline phosphatase (CIP) and NEB3 buffer were purchased from New England Biolabs (Ipswich, MA). All other chemicals were purchased from SIGMA Chemical Company (St. Louis, MO).

Preparation and purification of $^{13}C_4$-labelled compounds

SAdo-$^{13}C_4$

A reaction mixture consisting of 10 mM Tris–Cl (pH 8), 10 mM KCl, 2 mM EDTA, 70 mM AMP, 6 mM fumaric acid-$^{13}C_4$ and 50 μg/mL human recombinant ADSL [15,16] was incubated for 4 h at 37 °C, concentrated under a stream of nitrogen, applied to PEI-TLC plates (CEL 300 PEI/UV254, 10 cm × 20 cm; Macherey-Nagel) and developed in 1 M ammonium acetate. Adenylosuccinic acid-$^{13}C_4$ (SAMP-$^{13}C_4$) was detected under UV254 (RF 0.02), scraped off and extracted with 2 M ammonium hydroxide. The PEI cellulose was removed by centrifugation at 5000 *g* for 10 min. The supernatant was concentrated under a stream of nitrogen and analysed by high-performance liquid chromatography with diode array detection (HPLC–DAD) as described below. To each reaction, 20 U of CIP and NEB3 buffer was added, and the samples were incubated for 1 h at 37 °C. The concentration of SAdo-$^{13}C_4$ after HPLC–DAD analysis was determined spectrophotometrically at 269 nm (NanoDrop, Thermo Scientific) and calculated using the extinction coefficient 19,200 L mol^{-1} cm^{-1} [17].

SAICAr-$^{13}C_4$

A reaction mixture of 10 mM Tris–Cl (pH 8), 10 mM KCl, 2 mM EDTA, 6 mM aminoimidazole carboxamide ribotide (AICAR), 70 mM fumaric acid-$^{13}C_4$ and 50 μg/mL human recombinant ADSL [15,16] was incubated for 3 h at 37 °C. Then, 20 U of CIP and NEB3 buffer was added, incubated for 1 h at 37 °C and analysed by HPLC–DAD (as described below). The reaction mixture was applied onto a Dowex 50W column, washed with water and eluted with 2 M ammonium hydroxide [16]. The alkaline fractions containing SAICAr-$^{13}C_4$ were pooled and concentrated under a stream of nitrogen. After HPLC–DAD analysis, the SAICAr-$^{13}C_4$ concentration was determined spectrophotometrically at 269 nm (NanoDrop, Thermo Scientific) and calculated using the extinction coefficient 13,100 L mol^{-1} cm^{-1} [17].

HPLC–DAD analysis

The HPLC–DAD analysis of the prepared $^{13}C_4$-labelled compounds was performed using a 10A Shimadzu Liquid Chromatography System with a diode array detector.

Twenty microlitre aliquots of the reaction mixture were injected onto the Prontosil 120-3 C18-AQ column (200 * 4 mm, 3 μm) (Bischoff, Leonberg, Germany) and subjected to gradient elution beginning with 100% phase A containing 0.1 M KH_2PO_4 and 5 mM tetrabutylammonium hydrogen sulphate (pH 3) and 0% phase B containing phase A and 30% acetonitrile at a flow rate of 0.7 mL/min. The analysis progressed linearly to 100% B over 0–12 min, followed by 100% B from 12 to 14 min, and 100–0% B (0–100% A) from 14 to 15 min. Then, the column was regenerated with 100% A for 10 min.

Samples

For this study, we used DBS collected on a Whatman 903® filter paper (Whatman, Dassel, Germany) from 31 anonymous control samples and 6 ADSL-deficient patients identified in a newborn screening. The samples were protected from light and humidity and stored for several months or years at room temperature.

The project was approved by the Ethics Committee of the General University Hospital in Prague and informed consents were obtained from the patients. Authors have complied with the World Medical Association Declaration of Helsinki regarding the ethical conduct of research involving human subjects.

Sample preparation for DBS screening

Using a manual punch, three 3-mm diameter disks from the centre of each DBS sample area were removed, placed in 100 μL of extraction buffer containing acetonitrile:methanol:water (1:1:1 ratio) with 100 nM SAdo-$^{13}C_4$ and SAICAr-$^{13}C_4$ and incubated for 15 min in an ultrasonic bath.

An 80-μL aliquot of the extract was transferred to a clean tube and centrifuged for 5 min at 8000 *g*. Then, the supernatant was evaporated to dryness under a stream of nitrogen and dissolved in 30 μL of water for LC–MS/MS analysis.

Preparation of calibrators

Aliquots of whole blood were spiked with 0.01, 0.05, 0.25, 1 and 10 μmol/L of the succinylpurines SAICAr and SAdo. The DBSs were processed as described above, and calibration curves were constructed by plotting the ratio of the peak areas of the succinylpurines and the corresponding internal standard against the concentration of succinylpurine added to the calibration blood sample.

LC–MS/MS instrumentation and experimental conditions

The LC–MS/MS system consisted of the Agilent 1290 Infinity LC System (Agilent Technologies, Palo Alto, CA, USA) coupled with an API 4000 triple quadrupole mass spectrometer with an electron ion source. The system was operated using Analyst software, version 1.4 (Applied Biosystems, Foster City, CA, USA).

The separation was performed on a Symmetry C18 column (100 * 2.1 mm, 3.5 micron particle size, Waters Corporation, Milford, USA). The gradient elution was performed with 0.1% formic acid solution in water (phase A) and 0.1% formic acid solution in acetonitrile (phase B). The gradient profile began with 100% A, followed by a linear increase to 30% B over 7 min and an increase to 60% B at 8 min. The column was then regenerated with 100% A for another 7 min. The flow rate was 0.25 mL/min.

The detection of the analytes was carried out using the positive electrospray ionisation technique and the selected reaction monitoring mode. The precursor ions m/z 375 and m/z 384 correspond to protonated molecular ions of SAICAr and SAdo. The product ions m/z 252.2 and m/z 243 correspond to protonated fragments after the cleavage of the glycosidic C–N bond. The parameters of the mass spectrometer are listed in Table 1.

Table 1
LC–MS/MS parameters for analytes and internal standards.

Compound	Retention time (min)	MRM transitions (m/z)	Dwell time (ms)	DP[a] (V)	CE[b] (V)
SAdo	4.0	384.2/252.2	100	34	22
SAICAr	3.1	375.2/243	100	35	26
SAdo-$^{13}C_4$	4.0	388.2/256.2	100	34	22
SAICAr-$^{13}C_4$	3.1	379.2/247.2	100	35	26

[a] Declustering potential.
[b] Collision energy.

Results

Preparation of the $^{13}C_4$-labelled standards

The ADSL metabolites SAdo-$^{13}C_4$ and SAICAr-$^{13}C_4$ were prepared for LC–MS/MS analysis by two enzymatic reactions. In the first reaction, fumaric acid-$^{13}C_4$ and AMP (or AICAR) were converted to SAMP-$^{13}C_4$ (or SAICAR-$^{13}C_4$) by human recombinant ADSL [15]. In the second reaction, the resulting SAMP-$^{13}C_4$ (or SAICAR-$^{13}C_4$) was dephosphorylated to SAdo-$^{13}C_4$ (or SAICAr-$^{13}C_4$) by CIP (Fig. 1). The excess AMP, which is considerably less expensive than fumaric acid-$^{13}C_4$, was used in the SAdo-$^{13}C_4$ preparation reaction. The disadvantage of this procedure is the necessity of separating SAMP-$^{13}C_4$ from AMP by TLC after the first enzymatic reaction. This step reduces the yield and is time consuming. Thus, excess fumarate-$^{13}C_4$ was used rather than AICAR in the SAICAr-$^{13}C_4$ preparation reaction, due to the simpler purification and similar price of both input substrates. The purity of the prepared metabolites as determined by HPLC–DAD analysis was 96%.

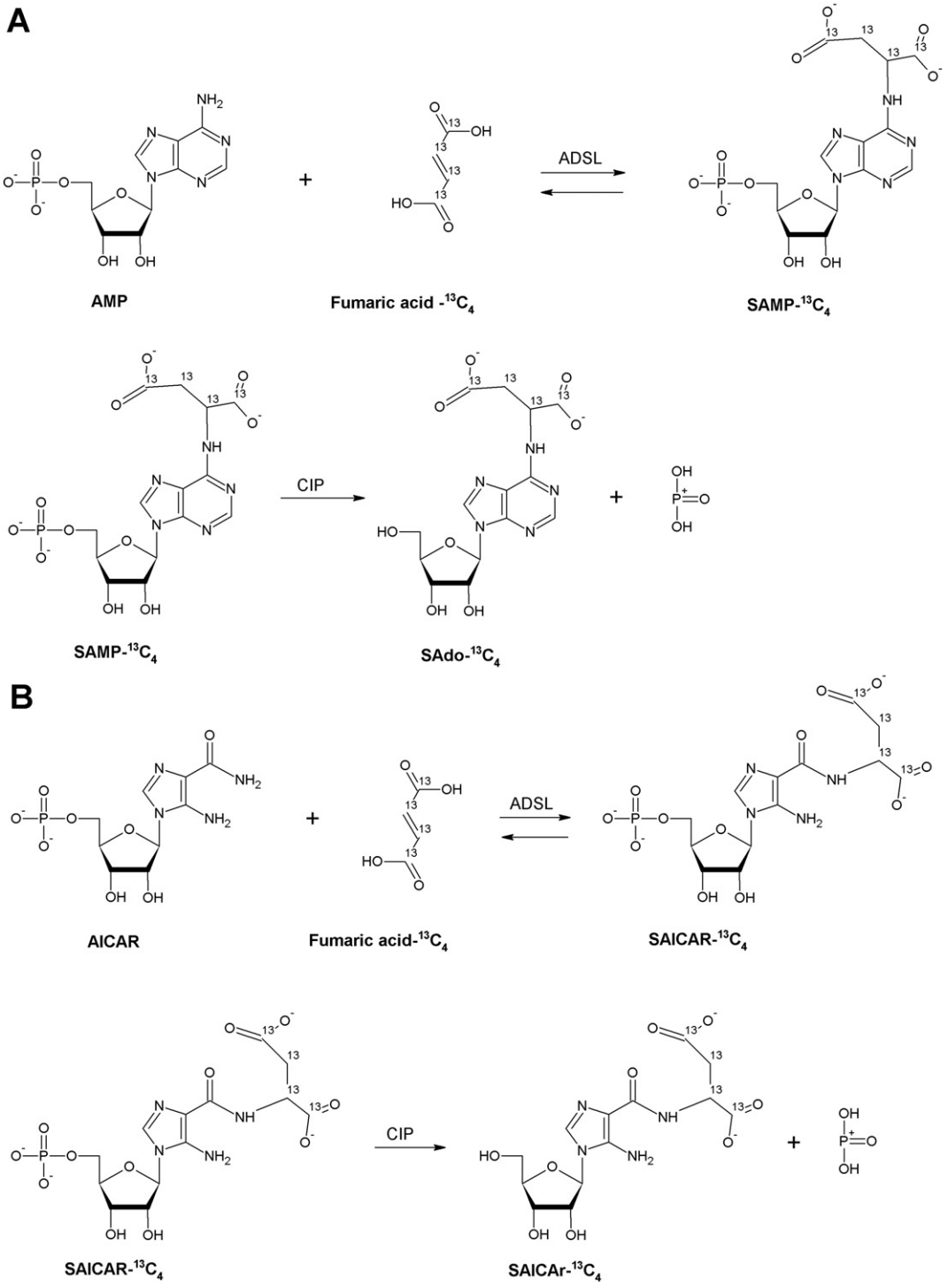

Fig. 1. Preparation of the isotopically labelled standards. In the first reaction, human recombinant ADSL binds fumaric acid-$^{13}C_4$ to AMP (A/) or AICAR (B/). Subsequently, the SAMP-$^{13}C_4$ product is dephosphorylated to SAdo-$^{13}C_4$ (A/) and SAICAR-$^{13}C_4$ is dephosphorylated to SAICAr-$^{13}C_4$ by calf intestinal alkaline phosphatase (CIP).

Table 2
Intra- and inter-assay method imprecision and the lower limits of quantification and the limits of detection for the LC–MS/MS method.

Sample	Compounds	Concentration μmol/L	Imprecision (CV %)		LLOQ μmol/L	LOD μmol/L
			Intra-day	Inter-day		
Control	SAICAr	0.01	10.7	15.2	0.01	0.004
Patient		2.1	2.4	2.8		
Control	SAdo	0.12	4.7	5.7	0.01	0.002
Patient		2.2	4.2	5.7		

Determination of SAdo and SAICAr in DBS

Linearity

The linearity of the method was demonstrated by high correlation coefficients ($r > 0.996$) for the calibration curves, which covered clinically relevant concentrations ranging from 0.01 μmol/L up to 25 μmol/L for both metabolites (see Data Supplement 1 for calibration curves). The linearity within the monitored concentration range was confirmed by Mandel's fitting test.

Imprecision and limits of detection and quantification

The method imprecision was determined using normal and high concentrations of SAdo and SAICAr by analysing DBS samples from one control and one ADSL-deficient patient. Intra-assay imprecision was determined by analysing six replicates from a single DBS sample in one day and ranged between 2.4% and 10.7% for SAICAr and between 4.2% and 4.7% for SAdo. Inter-assay imprecision was examined by analysing two DBSs six times over a period of 14 days; the observed range of inter-assay imprecision was between 2.8% and 15.2% for SAICAr and 5.7% for SAdo (Table 2).

The limits of detection (LOD) were assessed using a signal-to-noise ratio of 3:1 and were determined to be 0.004 μmol/L for SAICAr and 0.002 μmol/L for SAdo.

The lower limits of quantification (LLOQ) were determined as the lowest spiked concentration of each analyte which, upon addition to the blood sample, was experimentally determined in the DBS with imprecision better than 20% and recovery of 100 ± 20%. The determined LLOQ were 10 nmol/L for both succinylpurines.

Recovery

Recovery was determined by analysis of DBS prepared from control blood sample spiked with 5 concentration levels of SAdo and SAICAr. Six replicate analyses of each DBS were performed. The percentage recovery was determined by comparing the mean concentration of the analytes determined in the spiked DBS to the expected value (mean concentration in unspiked DBS + concentration of the spike).

The results of the studies are summarised in Table 3. The recoveries ranged from 94% to 117% depending on the concentration of the succinylpurines added to the DBS.

Matrix effects

The ion suppression effects were evaluated in post-column infusion experiments by directly infusing SAdo and SAICAr dissolved in 0.1% formic acid while the DBS extract was simultaneously injected via the autosampler. Signal suppression was observed between 0.7 and 1.2 min and 1.4 and 2 min with no signal enhancement present during the analysis. Neither SAICAr nor SAdo (retention times 3.1 and 4.1 min, respectively) did elute in the region of signal suppression (Data Supplement 2).

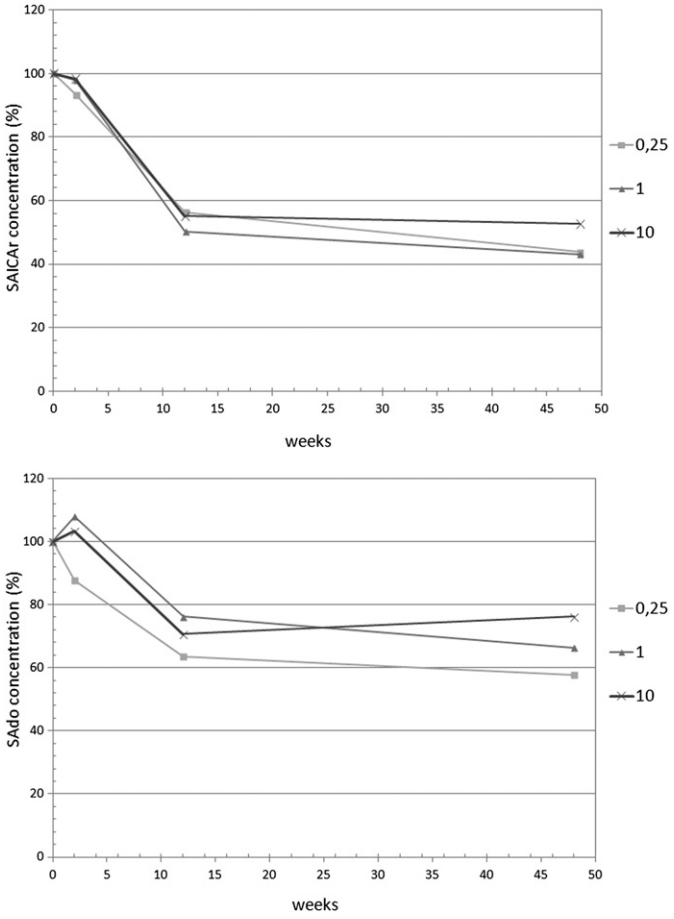

Fig. 2. The long-term stability of SAICAr and SAdo in DBS. Squares, set-squares and crosses represent the addition of 0.25, 1 and 10 μmol/L succinylpurines to the blood, respectively.

Stability study

To evaluate the usefulness of the method in routine clinical practice, we tested the stability of SAICAr and SAdo in DBS over a 2-week period. We also tested the long-term stability of both metabolites in DBS over a period of 3 to 12 months to evaluate metabolite changes in the archived DBS from ADSL patients.

The sample stability was tested by analysing spiked DBS samples prepared as described in the section "Preparation of calibrators" and stored at room temperature. After 2 weeks, 3 months and 12 months, these DBS samples were analysed, and the results were compared to the succinylpurine determinations in the spiked DBS calibration samples, which were stored at −80 °C.

The results showed that both metabolites are stable in DBS stored for 2 weeks and that the metabolite concentrations decreased from 24% to 42% for SAdo and from 44% to 57% for SAICAr in the spiked DBS stored for 3 or 12 months (Fig. 2).

Table 3
The recovery of SAICAr and SAdo from DBS spiked with defined amounts of SAdo and SAICAr.

	SAdo					SAICAr				
Concentration added (μmol/L)	0.01	0.05	0.25	1	10	0.01	0.05	0.25	1	10
Mean recovery (%)	111	94	102	105	102	117	104	100	106	97

SAICAr and SAdo in DBS samples

The concentrations of SAICAr and SAdo were higher in DBS from ADSL-deficient patients (SAICAr, 0.03–4.7 μmol/L; SAdo, 1.5–21.3 μmol/L; n = 5) compared to control subjects (SAICAr, 0–0.026 μmol/L; SAdo, 0.06–0.14 μmol/L; n = 31) (see Data Supplement 3 for LC–MS/MS analyses). The decrease in SAICAr concentrations determined in DBS stored for 2 to 23 years confirms the instability of SAICAr over time (Fig. 3).

Discussion

The current trends for population and selective screening of metabolic disorders are to use methods based on the profiling of a wide spectrum of metabolites in DBS using LC–MS/MS. LC–MS/MS is more sensitive and specific than traditional assays such as HPLC–DAD. These methods replace classical screening techniques and offer an alternative diagnostic test for many metabolic disorders. One such disorder is ADSL deficiency, an inherited disorder of purine metabolism.

Affected individuals present a variety of non-specific neurological symptoms [15,18]. The correct diagnosis of ADSL deficiency prevents further costly clinical examination and is essential for predicting the risks associated with a subsequent pregnancy and for the possibility of prenatal diagnosis [19].

There is strong evidence that ADSL deficiency is under-diagnosed [20]. To date, approximately 80 patients have been reported worldwide [20–25] (http://udmp.lf1.cuni.cz/adsl). Underestimation of the prevalence of ADSL deficiency may be partially due to assessment based on the detection of the less stable biomarker SAICAr by TLC with Pauly's reagent or the Bratton–Marshall test, which may produce false negative results [12]. The benefits of using LC–MS/MS in the diagnosis of ADSL deficiency are well illustrated in the case of the state of Victoria, Australia, where no cases of ADSL deficiency were diagnosed, despite the availability of the Bratton–Marshall test and HPLC-based purine and pyrimidine screening. Immediately after introduction of the new tandem mass spectrometry screening method in urine, which included detection of SAdo in the negative ion mode (transitions _382.1 to _206.1 m/z) and quantification using hexanoyl-$^{13}C_2$-glycine as an internal standard, three new cases of ADSL deficiency were diagnosed [20].

In a previous study, the possibility of using DBS for the diagnosis of ADSL deficiency was tested [26]. In this study, the authors focused on testing for ADSL activity. However, this enzyme was shown to be unstable in DBS. In our laboratory, we developed a reliable and sensitive analytical method for screening ADSL deficiency in neonatal DBS based on LC–MS/MS analysis of the ADSL metabolites SAdo and SAICAr. Precise quantification of SAICAr and SAdo in DBS was accomplished using the isotopically labelled standards SAdo-$^{13}C_4$ and SAICAr-$^{13}C_4$.

This is the first report of SAICAr and SAdo concentrations in newborn DBS samples from ADSL-deficient patients. Due to the rarity of the disease, the number of DBS from ADSL-deficient patients was limited. Moreover, these archived DBSs were stored at room temperature for a long period of time (2–23 years). The stability of biomarkers for ADSL deficiency in DBS stored for such a long time is questionable. A long-term stability study showed a decrease in both metabolites in spiked

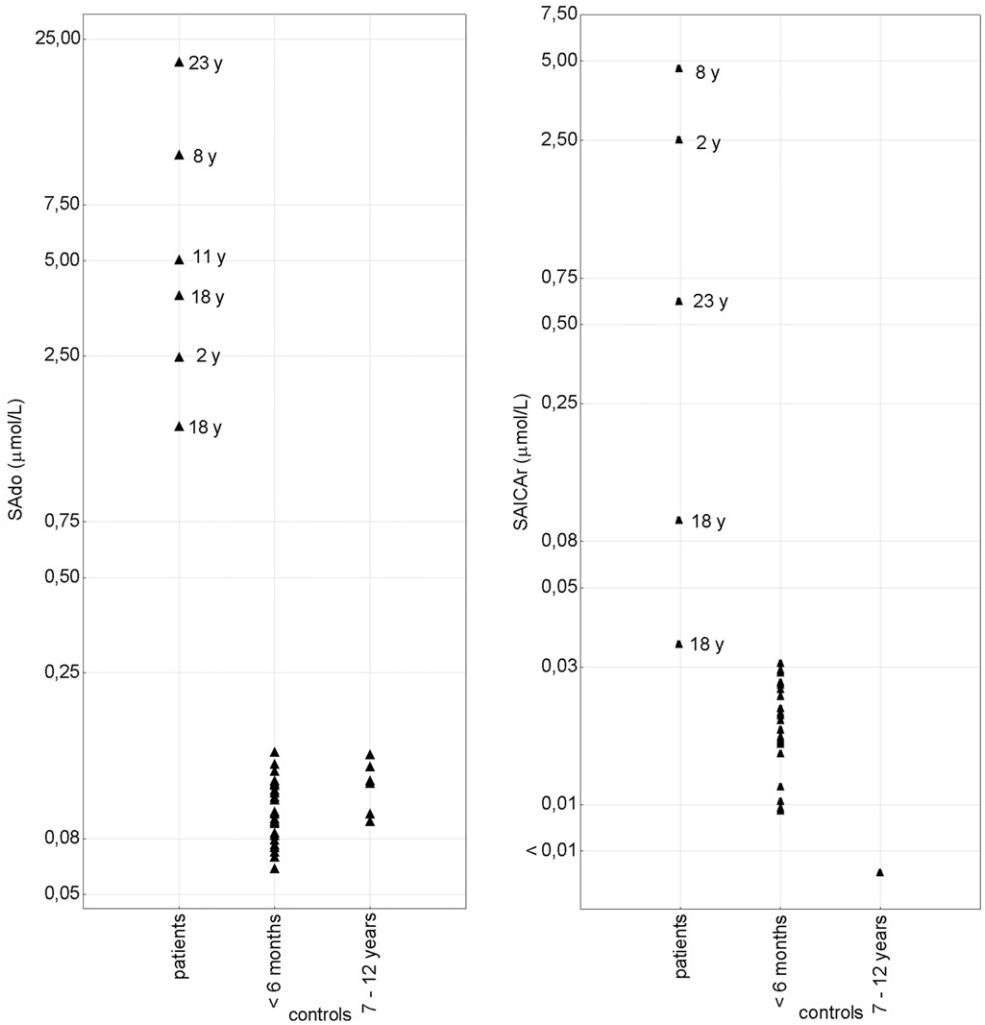

Fig. 3. Concentrations of SAdo and SAICAr in the DBS of ADSL-deficient patients archived for 2 to 23 years (n = 6), controls < 6 months old (n = 25) and controls 7–12 years old (n = 6).

DBS stored for 3 or 12 months. SAICAr was less stable than SAdo, showing an approximate 50% decrease in concentration after storage for more than 3 months. These results explain the lower SAICAr levels determined in the archived DBS samples from patients with ADSL deficiency. The SAICAr concentration in one DBS stored for 18 years before analysis was similar to the upper range in the control samples, which were stored for less than 6 months. In other examined DBS samples from ADSL-deficient patients, SAICAr concentrations were above the levels present in control DBS samples. The SAdo levels in archived DBS from ADSL-deficient patients were greater than one order of magnitude above the levels determined in control DBS, which demonstrates the usefulness of the presented method in screening ADSL deficiency in newborn DBS from patients with non-specific neurological manifestations.

Conclusions

The presented method allows extensive screening of ADSL deficiency in a population of patients with neurological involvement and opens up opportunities for the further development of screening methods for other, not-yet-identified defects in de novo purine synthesis. Due to the long-term stability of the metabolite SAdo in DBS, the presented method may be used for retrospective diagnosis to aid genetic counselling of affected families.

Supplementary data to this article can be found online at http://dx.doi.org/10.1016/j.clinbiochem.2014.10.004.

Competing interests

The authors declare that they have no competing interests.

Acknowledgements

This work was supported by grant P305/12/P419 from the Czech Science Foundation. Institutional support was provided by the UNCE 204011, PRVOUK-P24/LF1/3 and SVV 260 022 programmes of Charles University in Prague and by the Ministry of Health of the Czech Republic — conceptual development of research organization VFN64165 and BIOCEV — Biotechnology and Biomedicine Centre of the Academy of Sciences and Charles University (CZ.1.05/1.1.00/02.0109), from the European Regional Development Fund.

References

[1] Chrastina P, Bartl J, Stastna S, Paulova M, Koubikova H, Elleder M, et al. Screening of inherited metabolic disorders by tandem mass spectrometry. J Inherit Metab Dis 2007;30:2.
[2] Wilcken B, Wiley V, Hammond J, Carpenter K. Screening newborns for inborn errors of metabolism by tandem mass spectrometry. N Engl J Med 2003;348:2304–12.
[3] Adam T, Friedecky D, Fairbanks LD, Sevcik J, Bartak P. Capillary electrophoresis for detection of inherited disorders of purine and pyrimidine metabolism. Clin Chem 1999;45:2086–93.
[4] Bartl J, Martincova O, Krijt J, Zeman J, Sebesta I. Diagnostic approach to adenosine deaminase deficiency. J Inherit Metab Dis 2007;30:135.
[5] de Bree PK, Wadman SK, Duran M, Fabery de Jonge H. Diagnosis of inherited adenylosuccinase deficiency by thin-layer chromatography of urinary imidazoles and by automated cation exchange column chromatography of purines. Clin Chim Acta 1986;156:279–87.
[6] Hartmann S, Okun JG, Schmidt C, Langhans CD, Garbade SF, Burgard P, et al. Comprehensive detection of disorders of purine and pyrimidine metabolism by HPLC with electrospray ionization tandem mass spectrometry. Clin Chem 2006;52:1127–37.
[7] la Marca G, Casetta B, Malvagia S, Pasquini E, Innocenti M, Donati MA, et al. Implementing tandem mass spectrometry as a routine tool for characterizing the complete purine and pyrimidine metabolic profile in urine samples. J Mass Spectrom 2006;41:1442–52.
[8] Maddocks J, Reed T. Urine test for adenylosuccinase deficiency in autistic children [letter]. Lancet 1989;1:158–9.
[9] Sebesta SM, Krijt J, Simmonds HA. Screening tests for adenylosuccinase deficiency. Screening 1995;4:117–24.
[10] van Kuilenburg AB, van Lenthe H, Loffler M, van Gennip AH. Analysis of pyrimidine synthesis "de novo" intermediates in urine and dried urine filter-paper strips with HPLC–electrospray tandem mass spectrometry. Clin Chem 2004;50:2117–24.
[11] Castro M, Carrillo R, Garcia F, Sanz P, Ferrer I, Ruiz-Sala P, et al. Thirteen years experience with selective screening for disorders in purine and pyrimidine metabolism. Nucleosides Nucleotides Nucleic Acids 2014;33:233–40.
[12] Krijt J, Skopova V, Adamkova V, Cermakova R, Jurecka A, Kmoch S, et al. The need for vigilance: false-negative screening for adenylosuccinate lyase deficiency caused by deribosylation of urinary biomarkers. Clin Biochem 2013;46:1899–901.
[13] Jaeken J, Wadman SK, Duran M, van Sprang FJ, Beemer FA, Holl RA, et al. Adenylosuccinase deficiency: an inborn error of purine nucleotide synthesis. Eur J Pediatr 1988;148:126–31.
[14] Jurecka A, Zikanova M, Kmoch S, Tylki-Szymanska A. Adenylosuccinate lyase deficiency. J Inherit Metab Dis 2014. http://dx.doi.org/10.1007/s10545-014-9755-y.
[15] Kmoch S, Hartmannova H, Stiburkova B, Krijt J, Zikanova M, Sebesta I. Human adenylosuccinate lyase (ADSL), cloning and characterization of full-length cDNA and its isoform, gene structure and molecular basis for ADSL deficiency in six patients. Hum Mol Genet 2000;9:1501–13.
[16] Zikanova M, Krijt J, Hartmannova H, Kmoch S. Preparation of 5-amino-4-imidazole-n-succinocarboxamide ribotide, 5-amino-4-imidazole-n-succinocarboxamide riboside and succinyladenosine, compounds usable in diagnosis and research of adenylosuccinate lyase deficiency. J Inherit Metab Dis 2005;28:493–9.
[17] Van den Bergh F, Vincent MF, Jaeken J, Van den Berghe G. Radiochemical assay of adenylosuccinase: demonstration of parallel loss of activity toward both adenylosuccinate and succinylaminoimidazole carboxamide ribotide in liver of patients with the enzyme defect. Anal Biochem 1991;193:287–91.
[18] Mouchegh K, Zikanova M, Hoffmann GF, Kretzschmar B, Kuhn T, Mildenberger E, et al. Lethal fetal and early neonatal presentation of adenylosuccinate lyase deficiency: observation of 6 patients in 4 families. J Pediatr 2007;150:57–61 [e2].
[19] Marie S, Flipsen JW, Duran M, Poll-The BT, Beemer FA, Bosschaart AN, et al. Prenatal diagnosis in adenylosuccinate lyase deficiency. Prenat Diagn 2000;20:33–6.
[20] van Werkhoven MA, Duley JA, McGown I, Munce T, Freeman JL, Pitt JJ. Early diagnosis of adenylosuccinate lyase deficiency using a high-throughput screening method and a trial of oral *S*-adenosyl-l-methionine as a treatment method. Dev Med Child Neurol 2013;55:1060–4.
[21] Gitiaux C, Ceballos-Picot I, Marie S, Valayannopoulos V, Rio M, Verrieres S, et al. Misleading behavioural phenotype with adenylosuccinate lyase deficiency. Eur J Hum Genet 2009;17:133–6.
[22] Jurecka A, Zikanova M, Jurkiewicz E, Tylki-Szymanska A. Attenuated adenylosuccinate lyase deficiency: a report of one case and a review of the literature. Neuropediatrics 2014;45:50–5.
[23] Lundy CT, Jungbluth H, Pohl KR, Siddiqui A, Marinaki AM, Mundy H, et al. Adenylosuccinate lyase deficiency in the United Kingdom pediatric population: first three cases. Pediatr Neurol 2010;43:351–4.
[24] Perez-Duenas B, Sempere A, Campistol J, Alonso-Colmenero I, Diez M, Gonzalez V, et al. Novel features in the evolution of adenylosuccinate lyase deficiency. Eur J Paediatr Neurol 2012;16:343–8.
[25] Spiegel EK, Colman RF, Patterson D. Adenylosuccinate lyase deficiency. Mol Genet Metab 2006;89:19–31.
[26] Bierau J, Pooters IN, Visser D, Bakker JA. An HPLC-based assay of adenylosuccinate lyase in erythrocytes. Nucleosides Nucleotides Nucleic Acids 2011;30:908–17.

Příloha č. 2

Molecular Genetics and Metabolism 119 (2016) 270–277

Contents lists available at ScienceDirect

Molecular Genetics and Metabolism

journal homepage: www.elsevier.com/locate/ymgme

CRISPR-Cas9 induced mutations along de novo purine synthesis in HeLa cells result in accumulation of individual enzyme substrates and affect purinosome formation

Veronika Baresova [1], Matyas Krijt [1], Vaclava Skopova, Olga Souckova, Stanislav Kmoch, Marie Zikanova *

Institute of Inherited Metabolic Disorders, First Faculty of Medicine, Charles University in Prague, General University Hospital in Prague, Ke Karlovu 2, 128 08 Praha 2, Czech Republic

ARTICLE INFO

Article history:
Received 15 June 2016
Received in revised form 19 August 2016
Accepted 19 August 2016
Available online 24 August 2016

Keywords:
De novo purine synthesis
Adenylosuccinate lyase deficiency
AICA-ribosiduria
CRISPR
Human cellular model
Purinosome

ABSTRACT

Purines are essential molecules for nucleic acid synthesis and are the most common carriers of chemical energy in all living organisms. The cellular pool of purines is maintained by the balance between their de novo synthesis (DNPS), recycling and degradation. DNPS includes ten reactions catalysed by six enzymes. To date, two genetically determined disorders of DNPS enzymes have been described, and the existence of other defects manifested by neurological symptoms and the accumulation of DNPS intermediates in bodily fluids is highly presumable.

In the current study, we prepared specific recombinant DNPS enzymes and used them for the biochemical preparation of their commercially unavailable substrates. These compounds were used as standards for the development and validation of quantitative liquid chromatography-tandem mass spectrometry (LC-MS/MS). To simulate manifestations of known and putative defects of DNPS we prepared CRISPR-Cas9 genome-edited HeLa cells deficient for the individual steps of DNPS (CR-cells), assessed the substrates accumulation in cell lysates and growth media and tested how the mutations affect assembly of the purinosome, the multi-enzyme complex of DNPS enzymes. In all model cell lines with the exception of one, an accumulation of the substrate(s) for the knocked out enzyme was identified. The ability to form the purinosome was reduced.

We conclude that LC-MS/MS analysis of the dephosphorylated substrates of DNPS enzymes in bodily fluids is applicable in the selective screening of the known and putative DNPS disorders. This approach should be considered in affected individuals with neurological and neuromuscular manifestations of unknown aetiology. Prepared in vitro human model systems can serve in various studies that aim to provide a better characterization and understanding of physiology and pathology of DNPS, to study the role of each DNPS protein in the purinosome formation and represent an interesting way for the screening of potential therapeutic agents.

1. Introduction

Purines comprise essential molecules for nucleic acid synthesis and are the most common carriers of chemical energy in all living organisms. The cellular pool of purines is maintained by the balance between their de novo synthesis (DNPS), recycling and degradation. DNPS includes ten reactions catalysed by six enzymes (Fig. 1). To date, two genetically determined defects of DNPS have been identified, including the adenylosuccinate lyase (ADSL, EC 4.3.2.2) deficiency (OMIM 103050) [1] and AICA-ribosiduria (OMIM 608688) [2]; both defects

Abbreviations: ADSL, adenylosuccinate lyase; AICAR, aminoimidazolecarboxamide ribotide; AICAr, aminoimidazolecarboxamide riboside; AIR, aminoimidazole ribotide; AIr, aminoimidazole riboside; AMP, adenosine monophosphate; ATIC, bifunctional enzyme 5-aminoimidazole-4-carboxamide ribonucleotide transformylase/inosine monophosphate cyclohydrolase; CAIR, carboxyaminoimidazole ribotide; CAIr, carboxyaminoimidazole riboside; CHO, Chinese hamster ovarian cells; CIP, calf intestinal alkaline phosphatase; CRISPR, clustered regularly interspaced short palindromic repeats; DMEM, Dulbecco's minimum essential medium; DNPS, de novo purine synthesis; FAICAR, formylaminoimidazolecarboxamide ribotide; FGAM, formylglycineamidine ribotide; FGAR, formylglycineamide ribotide; FGAr, formylglycineamide riboside; GAR, glycineamide ribotide; GART, trifunctional enzyme glycinamide ribonucleotide synthetase/aminoimidazole ribonucleotide synthetase/glycinamide ribonucleotide transformylase; HPLC-DAD, high performance liquid chromatography with diode-array detection; LC-MS/MS, liquid chromatography-tandem mass spectrometry; MBP, maltose binding protein; N^{10}-formyl-THF, N^{10}-formyl-tetrahydrofolate; PAICS, bifunctional enzyme phosphoribosylaminoimidazole carboxylase/phosphoribosylaminoimidazole succinocarboxamide synthetase; PFAS, phosphoribosylformylglycinamidine synthetase; PPAT, phosphoribosyl pyrophosphate amidotransferase; PRA, phosphoribosyl amine; PRPP, phosphoribosyl pyrophosphate; SAICAR, succinylaminoimidazolecarboxamide ribotide; SAICAr, succinylaminoimidazolecarboxamide riboside; S-Ado, succinyladenosine; SAMP, succinyladenosine monophosphate.

* Corresponding author at: Institute of Inherited Metabolic Disorders, Ke Karlovu 2, 128 08 Prague 2, Czech Republic.
E-mail address: mzika@lf1.cuni.cz (M. Zikanova).

[1] These two authors contributed to the work equally.

http://dx.doi.org/10.1016/j.ymgme.2016.08.004
1096-7192/

are accompanied by serious neurological involvement and are caused by missense mutations in the *ADSL* and *ATIC* genes, respectively. Defects in the other four genes have not been identified.

The range of the genetic variabilities and allele frequencies available in the Exome Aggregation Consortium (ExAc) database indicate that similar to the *ADSL* and *ATIC* genes, there is (with the exception of the *PPAT* gene) no evolutionary constraints against loss of function or missense mutations in other DNPS genes *GART*, *PFAS* and *PAICS* (Supplementary data 1). Thus, it may be expected that individuals with biallelic mutations in these genes should exist and, similar to the other DNPS defects, may manifest nonspecific neurological and neuromuscular symptoms and the accumulation of specific DNPS intermediates in bodily fluids.

The main limitation regarding the diagnosis of these defects is the absence of a method for their detection. In the current work, we utilize the technique of liquid chromatography-tandem mass spectrometry (LC-MS/MS) for the determination of accumulated DNPS intermediates. The major constraint was the lack of standards. We previously developed procedures for the preparation of ADSL substrates and used them as standards in the diagnosis of ADSL deficiency via the LC-MS/MS method [3,4]. We subsequently prepared substrates of the DNPS enzymes phosphoribosylformylglycinamidine synthetase (PFAS, EC 6.3.5.3), bifunctional PAICS - phosphoribosylaminoimidazole carboxylase (EC 4.1.1.21)/phosphoribosylaminoimidazole succinocarboxamide synthetase (EC 6.3.2.6), and together with the commercially available substrate of 5-aminoimidazole-4-carboxamide ribonucleotide transformylase (EC 2.1.2.3)/inosine monophosphate cyclohydrolase (ATIC, EC 3.5.4.10), we used these substrates as the standards in the LC-MS/MS detection of DNPS defects and as substrates for the development of individual enzyme activity assays. To model the situation in the bodily fluids of patients with DNPS disorders, we prepared clustered regularly interspaced short palindromic repeats (CRISPR)-Cas9 genome-edited HeLa cells (CR-cells) deficient for specific steps of DNPS and analysed DNPS metabolites in cell lysates and growth media. We also tested the ability of the CR-cells to form purinosome, a multi-enzyme complex of DNPS enzymes, which cells transiently assemble in their cytoplasm upon depletion or an increased demand for purines [5,6].

2. Materials and methods

2.1. Chemicals and standard solutions

Succinylaminoimidazolecarboxamide ribotide (SAICAR), SAICA-riboside (SAICAr), succinyladenosine (S-Ado) and N^{10}-formyl-tetrahydrofolate (N^{10}-formyl-THF) were prepared as previously described [3,7]. Calf intestinal alkaline phosphatase (CIP) and NEB3 buffer were purchased from New England Biolabs (NEB), and Dulbecco's minimum essential medium (DMEM), F12 nutrition mix and foetal bovine serum (FBS) were obtained from Life Technologies, Thermofisher Scientific, Czech Republic. All other chemicals were purchased from Sigma-Aldrich, Czech Republic.

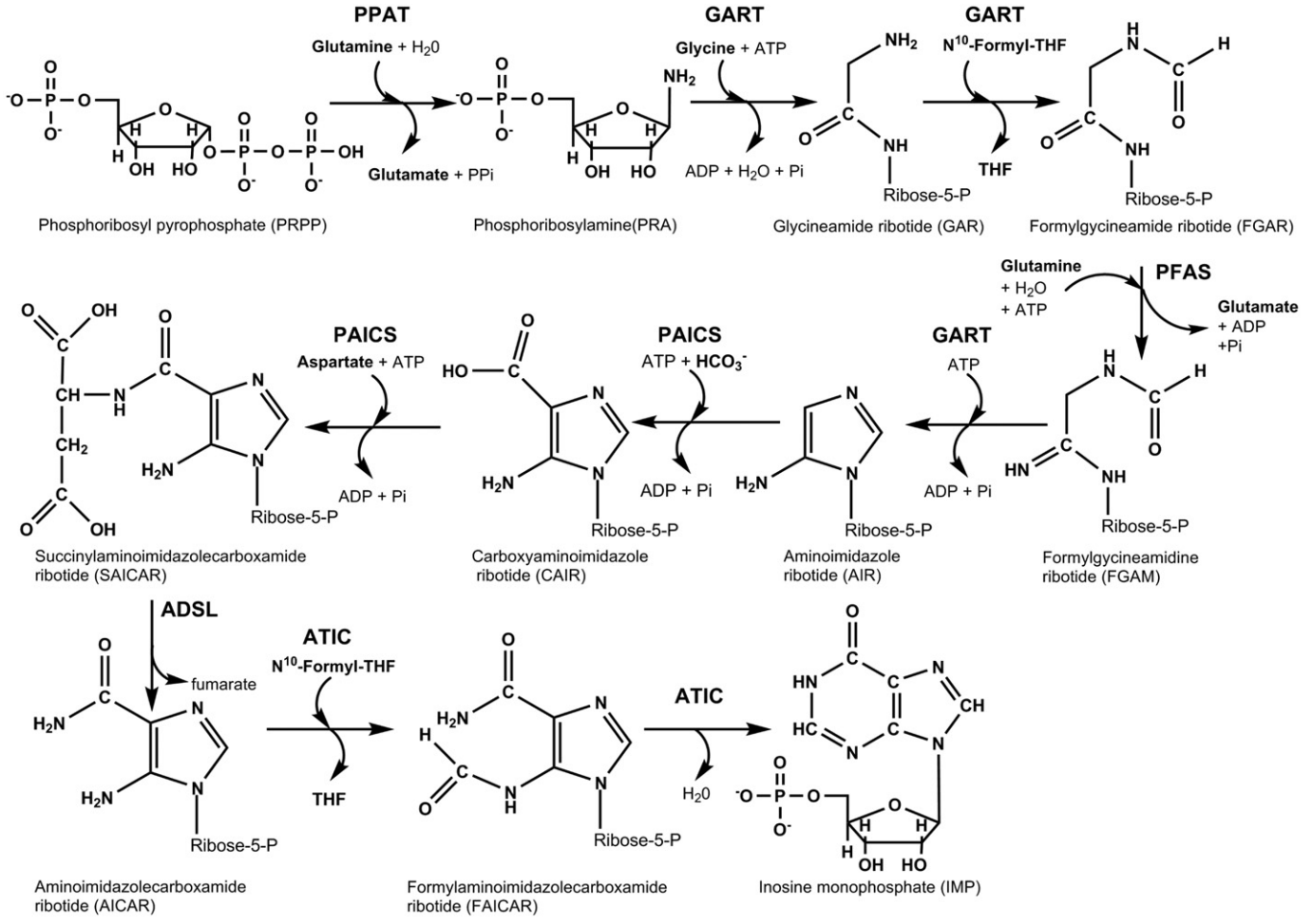

Fig. 1. De novo purine synthesis (DNPS): The basic molecule of purine inosine monophosphate (IMP) is generated within 10 reactions from organic and inorganic acids, amino acids and phosphoribosyl pyrophosphate (PRPP) using six enzymes. In the first reaction, glutamine transfers an NH_2 group to PRPP, creating a phosphoribosylamine and the side products glutamate and pyrophosphate. In subsequent reactions, other functional groups are added (from glycine, N^{10}-formyl tetrahydrofolate, glutamine, hydrogen carbon acid, aspartate and again from N^{10}-formyl tetrahydrofolate) to initiate the imidazole cycle followed by the pyrimidine cycle, the completion of which results in IMP formation.

2.2. Recombinant protein preparation

We prepared the cDNA trifunctional glycinamide ribonucleotide synthetase (EC 6.3.4.13)/aminoimidazole ribonucleotide synthetase (EC 6.3.3.1)/glycinamide ribonucleotide transformylase (EC 2.1.2.2.) (*GART*), *PFAS*, *PAICS*, *ADSL* and *ATIC* genes using previously described methods [8]. We introduced constructs with the correct sequences into the *E. coli* strain DH5αF'IQ (Invitrogen) and expressed the recombinant protein via IPTG. The pellets were resuspended in buffer A (10 mM Tris [pH 8.2], 2 mM EDTA, 10 mM KCl, 1 mM DTT, and 4% glycerol), sonicated four times for 15 s at 40 W, and centrifuged (9000*g*, 30 min); the lysates were applied to amylose affinity columns (NEB). We subsequently eluted the recombinant protein fused with maltose binding protein (MBP) from the column and performed SDS–PAGE analysis according to standard procedures.

2.3. Preparation and purification of substrates

2.3.1. Aminoimidazole ribotide (AIR) and AI-riboside (AIr)

We incubated 400 μl of a reaction mixture that contained 100 mM sodium phosphate (pH 6), 35 mM $MgCl_2$, 6 mM ADP, 6 mM SAICAR and 0.5 mg/ml human recombinant MBP-PAICS at 37 °C for 5 h and analysed the mixture via high performance liquid chromatography with diode-array detection (HPLC-DAD). We applied the reaction mixture to an activated Strata X-AW (33 μm; 200 mg/3 ml) column (Phenomenex) and immediately eluted the column using 100 mM sodium acetate pH 5.1. AIR was not captured by the column in contrast to SAICAR, ADP and ATP. We concentrated the single fractions under a stream of nitrogen and analysed them via HPLC-DAD. AIR was determined at 250 nm using a NanoDrop spectrophotometer (Thermo Scientific), and the concentration was calculated using an extinction coefficient of 3830 M^{-1} cm^{-1} [9]. We subsequently prepared AIr from the 3 mM AIR solution in the standard reaction mixture of 1xNEB3 buffer and 1 U CIP via incubation for 2 h at 37 °C.

2.3.2. Carboxyaminoimidazole ribotide (CAIR) and CAI-riboside (CAIr)

Four hundred microliters of a reaction mixture that contained 50 mM Tris-Cl (pH 8), 1.3 mM $MgCl_2$, 500 mM $NaHCO_3$, 3 mM AIR and 0.5 mg/ml human recombinant MBP-PAICS were incubated at 37 °C for 4 h and analysed via HPLC-DAD. We applied the reaction to an activated Strata XL-A (100 μm; 200 mg/3 ml) column, washed the column with 3 ml of 100 mM ammonium acetate (pH 8.2) and 3 ml of methanol and dried it under a vacuum. CAIR was eluted with 5% formic acid in methanol and analysed via HPLC-DAD. The amount of CAIR was determined at 250 nm using a NanoDrop spectrophotometer, and the concentration was calculated using an extinction coefficient of 10,580 M^{-1} cm^{-1} [9]. We subsequently prepared CAIr from the 3 mM CAIR solution in the standard reaction previously described.

2.3.3. Formylglycineamide ribotide (FGAR) and FGA-riboside (FGAr)

Four hundred microliters of a reaction mixture that contained 85 mM Tris-Cl (pH 9), 5.7 mM $MgCl_2$, 10 mM NH_4OH, 11 mM glycine, 0.7 mM ATP, 30 mM ribose-5-phosphate, 0.1 mM N^{10}-formyl-THF and 0.5 mg/ml human recombinant MBP-GART were incubated at 37 °C for 4 h and analysed via LC-MS/MS. We dephosphorylated the obtained FGAR to formylglycineamide riboside (FGAr) in the standard reaction previously described. We applied the reaction mixture to the activated column Strata X-C (33 μm; 200 mg/3 ml) and washed it with 3 ml of 0.1 N HCl. FGAr was not captured by the column in contrast to the other compounds. The FGAr fractions were concentrated under a stream of nitrogen and analysed via LC-MS/MS.

2.4. HPLC-DAD detection

The HPLC analyses were performed using a 10A Shimadzu Liquid Chromatography System with a PDA detector.

2.4.1. AIR/AIr

We applied 20 μl of the reaction mixture to a Prontosil 120–3 C18-AQ column (200 * 4 mm, 3 μm) (Bischoff Chromatography), which was subsequently eluted using a gradient initiated with 100% of phase A (0.1 M potassium phosphate buffer [pH 1.5] and 5 mM tetrabutylammonium hydrogensulfate) and 0% of phase B (phase A plus 30% of acetonitrile) at a flow rate of 0.7 ml/min. The mobile phase was adjusted linearly to 100% phase B over 0–13 min, followed by 100% B at 13–15 min and 100–0% B and 0–100% A at 15–16 min. The column was regenerated with 100% A for 19 min.

2.4.2. CAIR/CAIr

CAIR/CAIr detection was performed using the same column as the AIR detection. The gradient started with 100% of phase C (5 mM potassium dihydrogen phosphate, 75 mM dipotassium hydrogen phosphate buffer [pH 8.1] and 10 mM tetrabutylammonium bromide) and 0% of phase D (phase C plus 30% of acetonitrile) at a flow rate of 1 ml/min for 10 min. The mobile phase was adjusted linearly to 100% D and 0% C over 10–15 min, followed by 100% D at 15–17 min and 100–0% D and 0–100% C at 17–18 min. The column was regenerated with 100% C for 17 min.

2.5. CR-cell preparation

We used the GeneArt® CRISPR Nuclease Vector with an OFP Reporter Kit (Life Technologies) to knockout the genes that encoded DNPS enzymes in HeLa cells. We prepared the vectors according to the manufacturer's protocol. We transfected 5×10^6 HeLa cells using the Neon® Transfection System (Life Technologies, pulse voltage 1005 V, pulse width 35 ms, 2 pulses and 10 μl tip). The cells were seeded on 40 mm diameter Petri dishes. At 24 h post-transfection, we selected single cells positive for OFP and seeded them onto 96-well plates. We maintained the cells in DMEM with 10% FBS, 1% penicillin/streptomycin and 0.03 mM adenine. We tested the cells for protein deletion, the presence of mutations and DNPS substrate accumulation.

2.6. Mutation analysis

We isolated genomic DNA (gDNA), transcribed cDNA from the total RNA of the HeLa cells and performed PCR analysis according to standard procedures. The PCRs were conducted in 25 μl reaction mixtures that contained Red PCR Master Mix (Rovalab), 1.5 mM $MgCl_2$, 8% DMSO and 0.4 μM specific primers. We gel-purified the amplification products and sequenced the amplicons using the ABI BigDye method (Applied Biosystems).

2.7. Preparation of cell lysates

A pellet of 1×10^6 HeLa cells was dissolved in 50 μl of buffer A with Protease Inhibitor Cocktail Tablets (Roche), sonicated four times for 15 s and centrifuged at 17,000*g* for 20 min at 4 °C.

2.8. Activity assays

2.8.1. GART

The reaction was performed for 6 h at 37 °C in a 30 μl reaction mixture that contained 85 mM Tris (pH 9.0), 5.7 mM $MgCl_2$, 10 mM NH_4OH, 11.4 mM glycine, 0.7 mM ATP, 5.7 mM ribose-5-phosphate, 0.1 mM N^{10} formyl-THF and cell lysate (12.6 μg of protein). We analysed the formed FGAR/FGAr using the LC/LC-MS method.

2.8.2. PAICS

The reaction was performed for 30 min at 37 °C in a 50 μl reaction mixture that contained 50 mM Tris (pH 7.4), 13 mM $MgCl_2$, 0.45 mM ATP, 180 mM $KHCO_3$, 0.2 mM AIR and cell lysate (20 μg of protein). We measured the concentration of the formed SAICAR using the

Table 1
LC-MS/MS parameters for analytes.

Compound	Retention time (min)	MRM transitions (*m/z*)	Dwell time (ms)	DP[a] (V)	CE[b] (V)
GAr	4.51	207.1–133/73	100	35	25
FGAr	5.48	235.1–217.1/103.1/86.1	100	41	25
AIr	5.01	216.3–94/84	100	35	25
CAIr	6.89	260.2–110.0/128.2	100	35	25
SAICAr	11.31	375.2–243.0	100	35	22
AICAr	8.52	259.2–127.2/110.0	100	20	18
S-Ado	13.53	384.2–252.2	100	34	26

[a] Declustering potential.
[b] Collision energy.

HPLC-DAD method according to the previously described AIR/AIr detection procedure.

2.8.3. ADSL

The reaction was performed for 20 min at 37 °C in 50 μl of buffer A with 0.12 mM adenosine5′-(α,β-methylene) diphosphate and cell lysate (16 μg of the protein). The substrate concentrations were 0.14 and 0.09 mM for succinyladenosine monophosphate (SAMP) and SAICAR, respectively. We measured the concentrations of the formed adenosine monophosphate (AMP) and aminoimidazolecarboxamide ribotide (AICAR) using the previously described HPLC-DAD method.

2.8.4. ATIC

The reaction was performed for 1 h at 37 °C in 100 μl of solution that contained 33 mM Tris (pH 7.4), 25 mM KCl, 2.3 mM beta-mercaptoethanol, 0.1 mM N^{10}-formyl-THF, 0.5 mM AICAR and cell lysate (20 μg of protein). We analysed the concentration of the formed IMP using the previously described HPLC-DAD method.

2.9. Western blots of cell lysates

We separated the denatured protein samples via 10% SDS-PAGE and blotted them onto a PVDF membrane. The membrane was blocked with 5% BSA in PBS and probed with the following primary antibodies: mouse monoclonal anti-GART (Abnova), rabbit polyclonal anti-PFAS, mouse monoclonal anti-ATIC (Abcam), mouse monoclonal anti-PAICS (Origene) or rabbit polyclonal anti-ADSL (Atlas) diluted in 5% BSA in PBS. The target proteins were detected using species appropriate HRP labelled secondary antibodies. Chemiluminescent detection was performed using the Clarity Western ECL Substrate (Bio-Rad) and X-ray visualized.

2.10. LC-MS/MS analysis

We added 12.5 μl of 5% perchloric acid to 30 μl of the prepared lysate/medium sample, incubated for 5 min on ice, centrifuged and adjusted to pH 5–8 by the addition of 2.5 M $KHCO_3$.

The LC-MS/MS system consisted of an Agilent 1290 Infinity LC System (Agilent Technologies) coupled with an API 4000 triple quadrupole mass spectrometer with an electron ion source, which was operated using the Analyst software (Applied Biosystems).

We applied 5 μl of the sample to a Symmetry C18 column (100 * 2.1 mm, 3.5 μm, Waters Corporation). The gradient elution was initiated with 100% of A (0.1% formic acid), followed by a linear increase to 30% of B (0.1% formic acid solution in acetonitrile) over 7 min, an increase to 60% of B at 8 min and regeneration with 100% of A for 7 min. The flow rate was 0.25 ml/min. The detection of the analytes was conducted using the positive electrospray ionization technique in the reaction monitoring mode. The mass spectrometry parameters are listed in Table 1, and chromatographs are presented in Supplementary data 2.

2.11. Purinosome formation

2.11.1. Cell culture

Knockout and control HeLa cells were maintained in Dulbecco's minimum essential medium (DMEM, Gibco, Invitrogen), supplemented with 10% foetal bovine serum (FBS) (Gibco, Invitrogen) and penicillin/streptomycin (Sigma Aldrich); knockout cells were enriched with 3×10^{-5} M of adenine (purine rich (PR) medium). The purine depleted (PD) media were supplemented with dialysed 10% FBS [5] and 1% penicillin/streptomycin (Sigma Aldrich). The cells were seeded in the PR or PD medium for the immunofluorescence experiments. After 24 h, the immunofluorescence labelling was performed.

2.11.2. Immunofluorescence

The cells were fixed with 4% paraformaldehyde in PBS, permeabilized in 0.1% TRITON, blocked with 5% BSA in PBS and incubated at 4 °C overnight with the following primary antibodies: anti-rabbit polyclonal IgG anti- phosphoribosyl pyrophosphate amidotransferase (PPAT, Sigma Aldrich), mouse polyclonal IgG anti-GART (Novus Biologicals), and mouse monoclonal IgG anti-ATIC (Abcam). Species appropriate secondary antibodies, Alexa Fluor® 488 and 555 (Molecular Probes, Invitrogen), were used. Slides were mounted in ProLong® Gold Antifade

Table 2
Mutations and predicted protein changes in the CR-cells.

Cells	Edited gene	cDNA change	Predicted protein change
CR_GART1	*GART*	c.368delA	p.(Gln123Hisfs*16)
		c.367_368insA	p.(Trp124Metfs*8)
CR_GART2	*GART*	c.368delA	p.(Gln123Hisfs*16)
		c.367_368insTTGATAGAGTTCTCATGAGATCTGGTTGTCTAAAAGTGT	p.(Gln123Leufs*14)
CR_PFAS	*PFAS*	c. 2683_2684insA	p.(Thr895Asnfs*17)
		c.2683_2700insAGGCCCTCCTGGCCCCAGACTCTGTTGGACCCCCAACTCCCCCTCCAGCAGGCATCTGG + c.2684_2699delTCACTCAGGGGCTGCTGAA	p.(Thr895Lysfs*31)
CR_PAICS	*PAICS*	c.284_5insT	p.(Glu97*)
		c.285delT	p.(Ile96Metfs*8)
CR_ADSL1	*ADSL*	c.113_114insA	p.(Trp39Metfs*22)
		c.115delT	p.(Trp39Glyfs*27)
CR_ADSL2	*ADSL*	c.114_115insT	p.(Trp39Leufs*22)
		c.115_125delTGGCGGCAGCT	p.(Trp39Valfs*18)
CR_ATIC1	*ATIC*	c.81_92delTGGTTTGAATCT	p.(Gly28_Leu31del)
		Second allele is not expressed	
CR_ATIC2	*ATIC*	c. 81_91delTGGTTTGAATC	p.(Leu29Argfs*21)
		c. 81_91delTGGTTTGAATC	

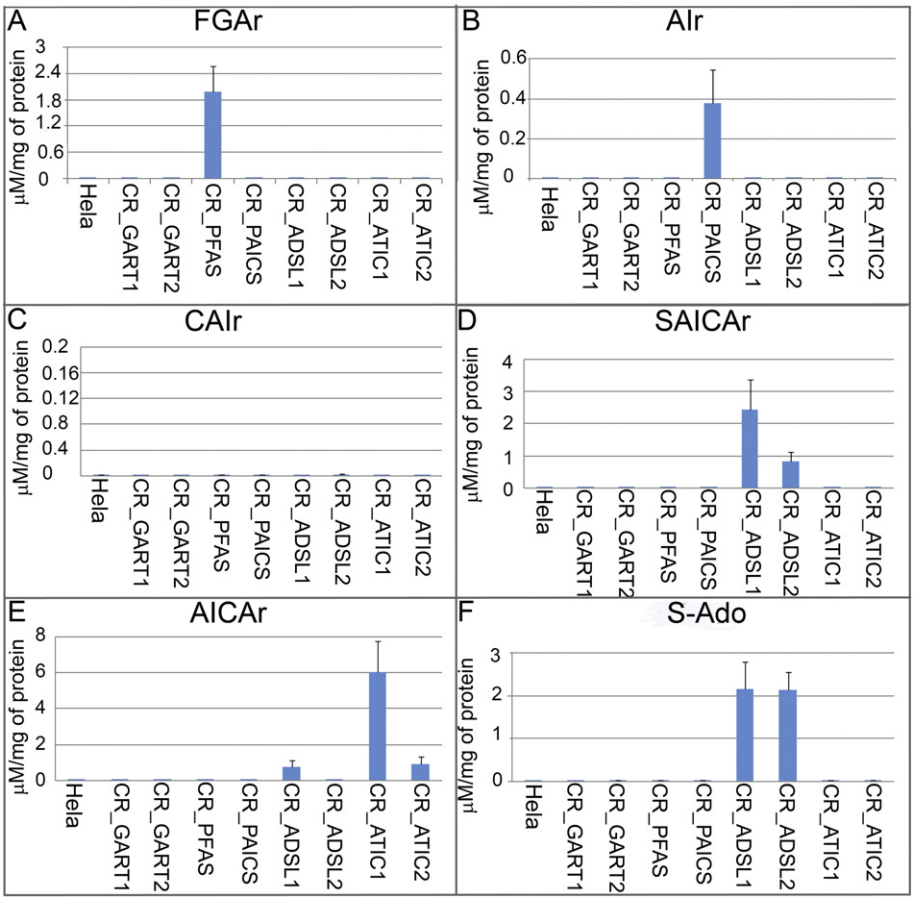

Fig. 2. Accumulation of the DNPS intermediates in HeLa cell lines deficient in specific steps of DNPS: The intermediates of the DNPS were measured by LC-MS/MS method in the cell growth media. A) FGAr was accumulated in the growth media of CR_PFAS cells. B) AIr was accumulated in the growth media of CR_PAICS cells. C) No accumulation of CAIr in growth media of any cells was observed. D) SAICAr was accumulated in the growth media of CR_ADSL cells. E) AICAr was accumulated in the growth media of CR_ATIC and in one line of CR_ADSL cells. F) S-Ado was accumulated in the growth media of CR_ADSL cells.

Mountant with DAPI (ThermoFisher Scientific). All immunofluorescence experiments were repeated at least twice.

2.11.3. Image acquisition and analysis

Prepared slides were analysed via confocal microscopy. XYZ images were sampled according to the Nyquist criterion using a LeicaSP8X confocal microscope, HC PL APO OIL CS2 objective (60×, N.A.1.40), and 470–670 nm 80 MHz pulse continuum WLL2 (488 and 543 laser lines). Images were restored using a classic maximum likelihood restoration algorithm in Huygens Professional Software (SVI). The colocalization maps, which employed single pixel overlap coefficient values that ranged from 0 to 1, were created in Huygens Professional Software. The resulting overlap coefficient values are presented as pseudocolors, and the scale is shown in the corresponding lookup tables (LUT).

3. Results

3.1. Preparation and purification of DNPS intermediates

The strategies used for substrate production were based on the preparation of the human recombinant enzymes MBP-GART and MBP-PAICS.

The PAICS metabolite AIR was converted from SAICAR in an enzymatic reaction with MBP-PAICS and purified on a weak anion-exchange functionalized polymeric sorbent with a production yield of 22%. The purity of the prepared metabolite determined by HPLC-DAD analysis was 84%. In the second reaction, we dephosphorylated the resulting AIR to AIr via CIP.

CAIR was produced from AIR in a forward reaction catalysed by MBP-PAICS and purified on a strong anion-exchange polymeric sorbent. CAIR was contaminated by AIR, and the purity determined by HPLC-DAD was 60%. The resulting CAIR was dephosphorylated to CAIr by CIP.

The PFAS substrate, FGAR, is the resulting product of three reactions that occurred in one step. The first reaction is the formation of 5-phosphoribosylamine (PRA) from ribose-5-phosphate and ammonium hydroxide as a function of the pH [10]. In the second and third enzymatic reactions, PRA is converted by MBP-GART to form FGAR via the intermediate glycineamide ribotide. Due to FGAR instability, we immediately dephosphorylated FGAR to FGAr via CIP and purified the product on a strong cation-exchange polymeric sorbent.

3.2. Preparation of HeLa cells deficient for specific steps of DNPS

We knocked out genes that coded DNPS enzymes in HeLa cells using the CRISPR-Cas9 genome editing system. We detected positive clones via cDNA and gDNA sequencing, western blot analysis, LC-MS/MS and activity assays, if available. We prepared cell lines with knocked-out *GART*, *PFAS*, *PAICS*, *ADSL* and *ATIC*. All mutations in the targeted genes comprised insertions or deletions of at least one nucleotide, which resulted in a disrupted reading frame (Table 2) and no detectable protein expression.

3.3. Determination of DNPS metabolites in HeLa cells deficient for specific steps of DNPS

3.3.1. Linearity, limits of detection (LOD) and quantification (LOQ)

We confirmed the linearity of the method via the generation of linear calibration curves with high correlation coefficients ($r > 0.9911$) in the range of the indicated concentrations.

The LOD and LOQ were defined using signal-to-noise ratios of 3:1 and 10:1, respectively. The LOD and LOQ values were determined to be 0.0094 and 0.031 μmol/l, respectively, for FGAr, 0.048 and 0.16 μmol/l, respectively, for AIr, 0.077 and 0.25 μmol/l, respectively, for CAIr, 0.0023 and 0.0076 μmol/l, respectively, for AICAriboside (AICAr), 0.019 and 0.063 μmol/l, respectively, for SAICAr and 0.014 and 0.0046 μmol/l, respectively, for S-Ado.

3.3.2. DNPS metabolites in CR-cell lysates and growth media

We analysed the metabolites in the CR-cell lysates and growth media using the LC-MS/MS method with DNPS intermediate inner standards. We detected increased levels of FGAr in the growth medium of the PFAS-deficient cells (CR_PFAS, Fig. 2A), increased levels of AIr in the growth medium of the PAICS-deficient cells (CR_PAICS, Fig. 2B), increased levels of SAICAr (Fig. 2D) and S-Ado (Fig. 2F) in the growth medium of the ADSL-deficient cells (CR_ADSL), in the growth medium of CR_ADSL1 cells was further observed slightly increased level of AICAr (Fig. 2E) and increased levels of AICAr (Fig. 2E) and SAICAr (Fig. 2D) in the growth medium of the ATIC-deficient cells (CR_ATIC). We did not detect CAIr (Fig. 2C) or the GAr metabolite (data not shown) in the cell media or lysates. No metabolite of DNPS was identified in the cell lysates.

3.4. Activity assays

The enzyme activity was measured by HPLC in the CR_PFAS, CR_PAICS, CR_ADSL, CR_ATIC and control cell lysates. The protein activity measured in the control cells was set to 100%, and the activity of specific proteins in the CR-cells was set to relative numbers to the controls. We did not identify activity of the knockout protein in the CR_PFAS, CR_PAICS or CR_ATIC cells, and in the CR_ADSL cells, the activity decreased to 2.6 ± 3% of the control cells (Fig. 3A).

3.5. Western blots

To determine the ability of the CR-cells to process the proteins, we performed Western blot analyses of the cell lysates. The CR-cells did not produce a specific knockout protein (Fig. 3B).

3.6. Purinosome formation

To determine whether the mutations of the *GART*, *PFAS*, *PAICS*, *ADSL* and *ATIC* genes affect the intracellular compartmentalization of DNPS proteins in vivo, we investigated purinosome formation in CR-cells. To detect purinosome formation, we cultured Hela cells in PD and PR media, and we immuno-labelled the combination of PPAT and ATIC in the CR_GART cells and PPAT and GART in the remaining cells.

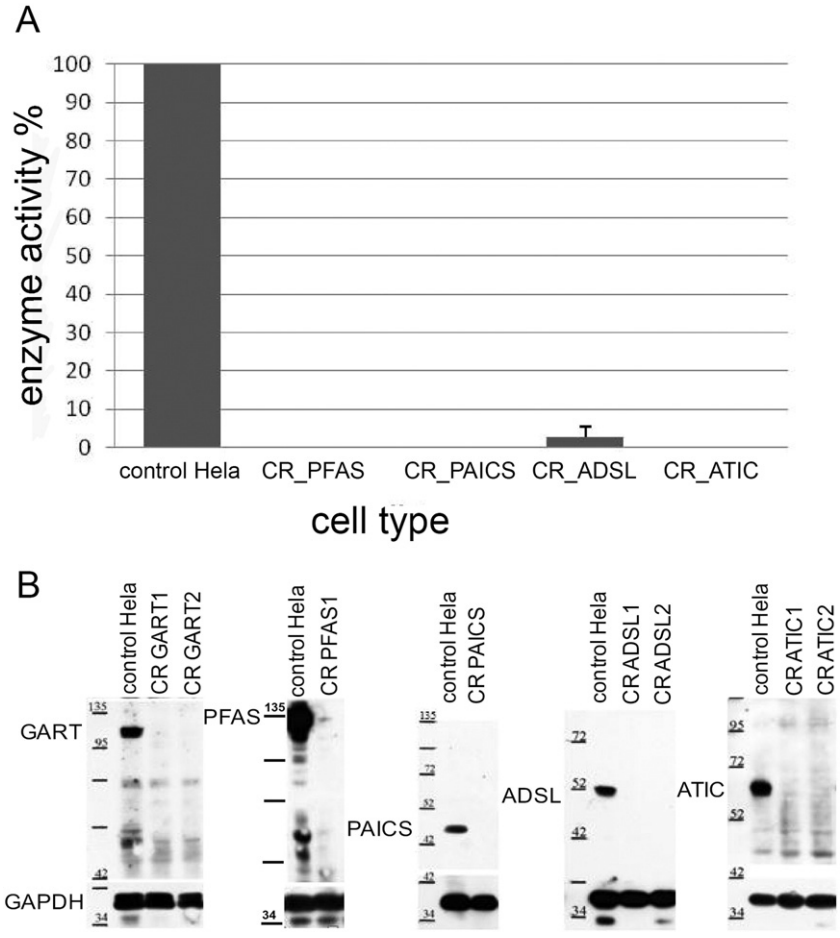

Fig. 3. Characterization of the CR-cells: A) Activity assays: The activity of GART, PFAS, ADSL and ATIC in control Hela cells was set as 100%. Compared to controls CR_GART cells have 0% activity of GART, CR_PFAS have 0% activity of PFAS, CR_ADSL have 1,7% activity of ADSL and CR_ATIC have 0% activity of ATIC. B) Western blot analysis of DNPS proteins in cell lysates demonstrating absence of GART, PFAS, PAICS, ADSL or ATIC in the knockout cells.

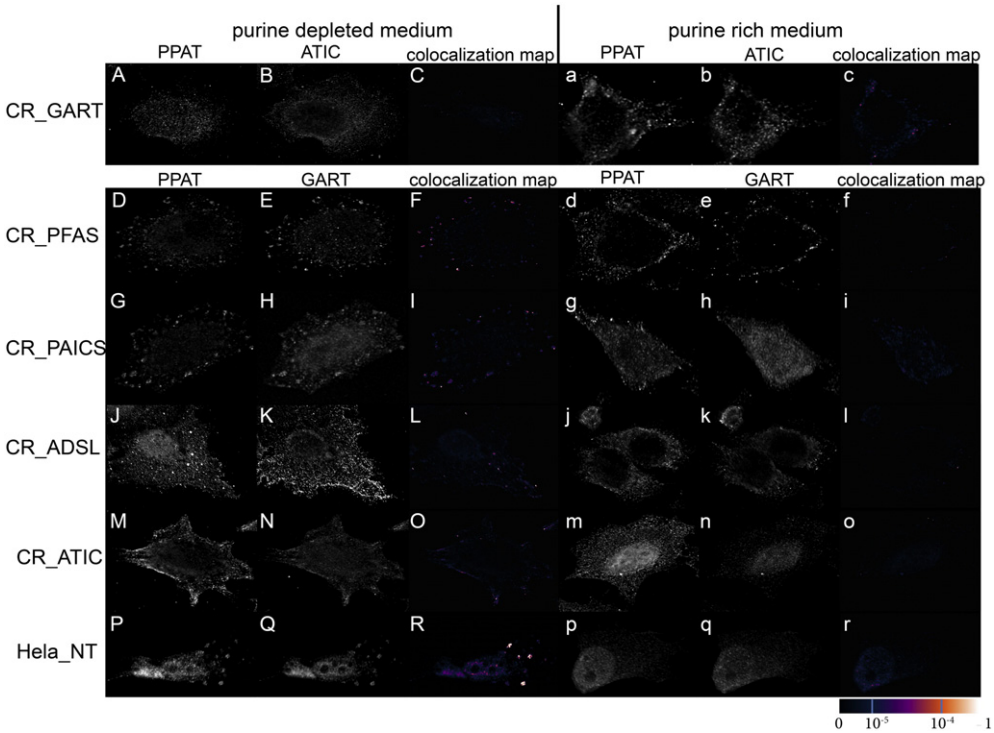

Fig. 4. Purinosome formation: The purinosome formation in the purine depleted medium was disrupted in cell lines where GART (A, B, C), ADSL (J, K, L) and bifunctional enzyme ATIC (M, N, O) were knocked-out. In cell lines with the knockout of PFAS (D, E, F) and PAICS (G, H, I) was the purinosome formation reduced when compared to control Hela cells (P, Q, R). In the purine rich medium the proteins remained diffuse and did not colocalize (a–r). Colocalization maps (C, F, I, L, O, R; c, f, i, l, o, r) display the values of the coefficients of the fluorescent signals overlaps. The values are transformed into pseudocolor which scale is shown at right bottom in corresponding LUT.

In the CR_GART (Fig. 4A, B, C), CR_ADSL (Fig. 4J, K, L) and CR_ATIC (Fig. 4M, N, O) cells grown in the PD medium, there was no granular staining of the immunolabelled proteins with no signal overlaps (Fig. 4C, L, O), which suggests the disruption of purinosome formation. In the CR_ PFAS (Fig. 4D, E, F) and CR_PAICS (Fig. 4G, H, I) cell lines grown in the PD medium, there was fine granular staining, and the image analysis indicated very low signal overlaps (Fig. 4F, I), which suggests highly reduced purinosome formation compared with the control Hela cells (Fig. 4P, Q, R). Regarding the cells grown in the PR medium, the proteins remained diffuse and did not exhibit colocalization (Fig. 4a–r). The colocalization maps (Fig. 4C, F, I, L, O, R; c, f, i, l, o, r) indicate the values of the coefficients of the fluorescent signal overlaps.

4. Discussion

As a result of the low incidence of known DNPS disorders, including 80 published cases of ADSL deficiency [11] and one case of AICA-ribosiduria worldwide [2], these diseases are most likely under-diagnosed. Patients with DNPS disorders are disadvantaged because of the broad, unspecific neurological symptoms; therefore, screening for known DNPS metabolic disorders is delayed. In cases with a severe phenotype, which typically end with early death, the diseases remain undiagnosed. Prenatal diagnosis in a subsequent pregnancy is therefore excluded.

Furthermore, specialized laboratory screening for metabolic disorders may not produce satisfactory results because of the limits of the diagnostic methods. Thus, laboratories primarily focus on ADSL deficiency and rarely on AICA-ribosiduria. To date, no other genetically determined defects of the DNPS have been described; however, the existence of defects is highly likely.

In the current study, we prepared individual recombinant enzymes of the DNPS pathway and used them in the biochemical preparation of the commercially unavailable enzyme substrates. These compounds were used in parallel as standards for the development and validation of their quantitative LC-MS/MS detection, as well as substrates for the development of enzyme activity assays.

We subsequently prepared CRISPR-Cas9 genome-edited HeLa cells deficient for specific steps of DNPS to demonstrate the potential situation in the bodily fluids of patients with genetically determined defects of the DNPS enzymes. It is a first human cellular model of all possible genetically determined defects of DNPS. Previously there were described and characterized models of Chinese hamster ovary (CHO) cells defected in PAICS and ADSL enzymes. The authors detected the accumulation of AIR in lysates of PAICS defected CHO cells. The accumulation of SAICAR, SAMP and in presence of SAICAR in growth media AIR was detected in lysates of ADSL deficient CHO cells [12,13]. In contrast to our findings, the DNPS intermediates were undetectable by LC-MS/MS in cell lysates of all prepared human model CR-cells. However, we identified an accumulation of the dephosphorylated substrate(s) for the defective enzyme in the growth media of model cells, with the exception of the cells with defective GART enzyme. This finding is a result of the instability of the GART substrate phosphoribosylamine, which has a half-life of 5 s under physiological conditions and is hydrolysed to ribose 5-phosphate, an intermediate of the pentose phosphate pathway [14]. Furthermore, we have unexpectedly detected, together with dephosphorylated ADSL substrates, dephosphorylated enzyme product AICAr in the CR_ADSL1 cells. AICAR crossroads between two metabolic pathways - DNPS and histidine metabolism. After the blockage of the ADSL reaction, a significant amount of AICAR can be provided through the alternative pathway [15]. Thus the accumulation of the AICAr in the growth media of CR_ADSL1 cells may be a result of the regulatory crosstalk between these two pathways.

We did not analyze substrates of affected enzymes such as amino acids, N^{10}-formyl-THF and bicarbonate considering their role in multiple pathways in organism. Therefore, we did not expect a measurable increase in their concentration.

Finally, using fluorescence microscopy, we determined that each of the DNPS enzyme deficiencies disrupted the formation of the purinosome in CR_cells. It is in accordance with previously published results that the

purinosome formation in ADSL deficient and AICAribusiduria fibroblasts is fully dependent on the presence of structurally intact ATIC and ADSL protein complexes and presumably also on the presence of all the other DNPS proteins [6]. CR_cells with mutated DNPS genes resulting in no detectable DNPS protein expression can serve as useful human model systems for the analysis of purinosome assembly and function. The study of purinosome formation by the endogenous proteins immunodetection in previously prepared CHO cells [12,13] has failed due to the unavailability of functional primary antibodies against hamster proteins (unpublished results).

5. Conclusion

We conclude that LC-MS/MS analysis of the dephosphorylated substrates of PFAS, PAICS, ADSL and ATIC enzymes in bodily fluids, such as urine, plasma and cerebrospinal fluid, is applicable in the selective screening of known and putative DNPS disorders. Similar to known disorders ADSL deficiency and AICA-ribosiduria, which are manifested by accumulation of metabolites SAICAr and S-Ado, or AICAr, respectively, in the bodily fluids of patients, the putative genetically determined defects of the enzymes PFAS and PAICS will manifest by the accumulation of their dephosphorylated substrates FGAr or AIr, respectively. Moreover, this approach should be considered in patients with neurological and neuromuscular diseases of unknown aetiology. In the case of positive results, a molecular biological examination of individual genes may follow, and genetic counselling may be established.

Human cellular models of HeLa cells deficient in particular steps of DNPS provide important insights about the pathogenesis of DNPS disorders and represent an interesting way for the screening of potential therapeutic agents. Furthermore, these cellular models offer advantages in various studies that investigate the mechanisms of purinosome formation and regulation.

Acknowledgements

The authors acknowledge Prof. Tomas Adam for providing us with control FGAr.

This work was supported by from the Ministry of Health of the Czech Republic [grant AZV 15-28979A] and by the Charles University in Prague [grant GAUK 818416]. Institutional support was provided by the Charles University in Prague [programs UNCE 204011, PRVOUK-P24/LF1/3 and SVV UK 260256/2016], by the Ministry of Education, Youth and Sports of CR [LQ1604 National Sustainability Program II], by the project "BIOCEV" [CZ.1.05/1.1.00/02.0109], by OP Prague Competitiveness [project CZ.2.16/3.1.00/24012].

Appendix A. Supplementary data

Supplementary data to this article can be found online at http://dx.doi.org/10.1016/j.ymgme.2016.08.004.

References

[1] G. Van den Berghe, J. Jaeken, Adenylosuccinase deficiency, Adv. Exp. Med. Biol. 195 (1986) 27–33.
[2] S. Marie, B. Heron, P. Bitoun, T. Timmerman, G. Van Den Berghe, M.F. Vincent, AICA-ribosiduria: a novel, neurologically devastating inborn error of purine biosynthesis caused by mutation of ATIC, Am. J. Hum. Genet. 74 (2004) 1276–1281.
[3] M. Zikanova, J. Krijt, H. Hartmannova, S. Kmoch, Preparation of 5-amino-4-imidazole-N-succinocarboxamide ribotide, 5-amino-4-imidazole-N-succinocarboxamide riboside and succinyladenosine, compounds usable in diagnosis and research of adenylosuccinate lyase deficiency, J. Inherit. Metab. Dis. 28 (2005) 493–499.
[4] M. Zikanova, J. Krijt, V. Skopova, M. Krijt, V. Baresova, S. Kmoch, Screening for adenylosuccinate lyase deficiency using tandem mass spectrometry analysis of succinylpurines in neonatal dried blood spots, Clin. Biochem. 48 (2015) 2–7.
[5] S. An, R. Kumar, E.D. Sheets, S.J. Benkovic, Reversible compartmentalization of de novo purine biosynthetic complexes in living cells, Science 320 (2008) 103–106.
[6] V. Baresova, V. Skopova, J. Sikora, D. Patterson, J. Sovova, M. Zikanova, S. Kmoch, Mutations of ATIC and ADSL affect purinosome assembly in cultured skin fibroblasts from patients with AICA-ribosiduria and ADSL deficiency, Hum. Mol. Genet. 21 (2012) 1534–1543.
[7] P.B. Rowe, A simple method for the synthesis of N5,N10-methenyltetrahydrofolic acid, Anal. Biochem. 22 (1968) 166–168.
[8] S. Kmoch, H. Hartmannova, B. Stiburkova, J. Krijt, M. Zikanova, I. Sebesta, Human adenylosuccinate lyase (ADSL), cloning and characterization of full-length cDNA and its isoform, gene structure and molecular basis for ADSL deficiency in six patients, Hum. Mol. Genet. 9 (2000) 1501–1513.
[9] E. Meyer, N.J. Leonard, B. Bhat, J. Stubbe, J.M. Smith, Purification and characterization of the purE, purK, and purC gene products: identification of a previously unrecognized energy requirement in the purine biosynthetic pathway, Biochemistry 31 (1992) 5022–5032.
[10] D.P. Nierlich, B. Magasanik, Phosphoribosylglycinamide synthetase of aerobacter aerogenes. purification and properties, and nonenzymatic formation of its substrate 5′-phosphoribosylamine, J. Biol. Chem. 240 (1965) 366–374.
[11] A. Jurecka, M. Zikanova, S. Kmoch, A. Tylki-Szymanska, Adenylosuccinate lyase deficiency, J. Inherit. Metab. Dis. 38 (2015) 231–242.
[12] N. Duval, K. Luhrs, T.G. Wilkinson 2nd, V. Baresova, V. Skopova, S. Kmoch, G.N. Vacano, M. Zikanova, D. Patterson, Genetic and metabolomic analysis of AdeD and AdeI mutants of de novo purine biosynthesis: cellular models of de novo purine biosynthesis deficiency disorders, Mol. Genet. Metab. 108 (2013) 178–189.
[13] L.K. Vliet, T.G. Wilkinson 2nd, N. Duval, G. Vacano, C. Graham, M. Zikanova, V. Skopova, V. Baresova, A. Hnizda, S. Kmoch, D. Patterson, Molecular characterization of the AdeI mutant of Chinese hamster ovary cells: a cellular model of adenylosuccinate lyase deficiency, Mol. Genet. Metab. 102 (2011) 61–68.
[14] J. Rudolph, J. Stubbe, Investigation of the mechanism of phosphoribosylamine transfer from glutamine phosphoribosylpyrophosphate amidotransferase to glycinamide ribonucleotide synthetase, Biochemistry 34 (1995) 2241–2250.
[15] K. Rebora, B. Laloo, B. Daignan-Fornier, Revisiting purine-histidine cross-pathway regulation in *Saccharomyces cerevisiae*: a central role for a small molecule, Genetics 170 (2005) 61–70.

PLOS ONE

RESEARCH ARTICLE

Mass spectrometric analysis of purine *de novo* biosynthesis intermediates

Lucie Mádrová[1,2], Matyáš Krijt[3], Veronika Barešová[3], Jan Václavík[1,2], David Friedecký[1,2,4], Dana Dobešová[1], Olga Součková[3], Václava Škopová[3], Tomáš Adam[1,2,4], Marie Zikánová[3]*

1 Institute of Molecular and Translational Medicine, Faculty of Medicine and Dentistry, Palacký University and University Hospital in Olomouc, Olomouc, Czech Republic, **2** Department of Clinical Biochemistry, University Hospital in Olomouc, Olomouc, Czech Republic, **3** Research Unit for Rare Diseases, Department of Pediatrics and Adolescent Medicine, First Faculty of Medicine, Charles University and General University Hospital in Prague, Prague, Czech Republic, **4** Laboratory of Inherited Metabolic Disorders, Department of Clinical Chemistry, University Hospital in Olomouc, Olomouc, Czech Republic

* marie.zikanova@lf1.cuni.cz

OPEN ACCESS

Citation: Mádrová L, Krijt M, Barešová V, Václavík J, Friedecký D, Dobešová D, et al. (2018) Mass spectrometric analysis of purine *de novo* biosynthesis intermediates. PLoS ONE 13(12): e0208947. https://doi.org/10.1371/journal.pone.0208947

Editor: Timothy James Garrett, University of Florida, UNITED STATES

Received: September 20, 2018

Accepted: November 26, 2018

Published: December 10, 2018

Data Availability Statement: All relevant data are within the manuscript and its Supporting Information files.

Funding: This work was supported by the Ministry of Health of the Czech Republic [grant AZV 15-28979A, http://www.azvcr.cz, recipient MZ], by The Charles University Grant Agency [grant GAUK 818416, recipient MK and GAUK 1102217, recipient OS, https://www.cuni.cz/UK-33.html] and by The Czech Science Foundation [grant GACR 18-12204S, recipient TA, https://gacr.cz/en/].

Abstract

Purines are essential molecules for all forms of life. In addition to constituting a backbone of DNA and RNA, purines play roles in many metabolic pathways, such as energy utilization, regulation of enzyme activity, and cell signaling. The supply of purines is provided by two pathways: the salvage pathway and *de novo* synthesis. Although purine *de novo* synthesis (PDNS) activity varies during the cell cycle, this pathway represents an important source of purines, especially for rapidly dividing cells. A method for the detailed study of PDNS is lacking for analytical reasons (sensitivity) and because of the commercial unavailability of the compounds. The aim was to fully describe the mass spectrometric fragmentation behavior of newly synthesized PDNS-related metabolites and develop an analytical method. Except for four initial ribotide PDNS intermediates that preferentially lost water or phosphate or cleaved the forming base of the purine ring, all the other metabolites studied cleaved the glycosidic bond in the first fragmentation stage. Fragmentation was possible in the third to sixth stages. A liquid chromatography-high-resolution mass spectrometric method was developed and applied in the analysis of CRISPR-Cas9 genome-edited HeLa cells deficient in the individual enzymatic steps of PDNS and the salvage pathway. The identities of the newly synthesized intermediates of PDNS were confirmed by comparing the fragmentation patterns of the synthesized metabolites with those produced by cells (formed under pathological conditions of known and theoretically possible defects of PDNS). The use of stable isotope incorporation allowed the confirmation of fragmentation mechanisms and provided data for future fluxomic experiments. This method may find uses in the diagnosis of PDNS disorders, the investigation of purinosome formation, cancer research, enzyme inhibition studies, and other applications.

Institutional support was provided by Charles University [programmes PRIMUS/17/MED/6, recipient MZ, PROGRES Q26/LF1, UNCE 204064 and SVV 260367/2017 http://www.cuni.cz] and by the Ministry of Education, Youth and Sports of CR [LO1304 National Sustainability Programme I and LQ1604 National Sustainability Programme II, http://www.msmt.cz/]. The funders had no role in study design, data collection and analysis, decision to publish, or preparation of the manuscript.

Competing interests: The authors have declared that no competing interests exist.

Introduction

Purine nucleotides have vital functions in numerous pathways in both prokaryotes and eukaryotes. As a part of many essential biomolecules, purine nucleotides participate in nucleic acid synthesis, transcription, translation, cell signaling processes, and maintaining energetic homeostasis and act as cofactors, neuromodulators, and cotransmitters. The supply of purine nucleotides is provided by two pathways: the salvage pathway and *de novo* synthesis. Purine *de novo* synthesis (PDNS) is a sequence of ten reactions catalyzed by six enzymes. Three of these enzymes are multifunctional in PDNS (Fig 1), and bifunctional adenylosuccinate lyase (ADSL) also participates in the purine nucleotide cycle, catalyzing the conversion of adenylosuccinic acid (SAMP) to adenosine monophosphate (AMP).

Initially, ribose-5-phosphate (R5P), which is synthesized in the pentose phosphate pathway, is converted by ribose-phosphate pyrophosphokinase (PRPS, EC 2.7.6.1) to PRPP, the first metabolite of PDNS. The formation of PRA is catalyzed by amidophosphoribosyltransferase (PPAT, EC 2.4.2.14). The trifunctional enzyme GART (phosphoribosylglycinamide synthetase, EC 6.3.4.13; phosphoribosylglycinamide formyltransferase, EC 2.1.2.2; and phosphoribosylaminoimidazole synthetase, EC 6.3.3.1) catalyzes steps 2, 3, and 5, respectively. Formation of FGAMR from FGAR is catalyzed by phosphoribosylformylglycinamidine synthase (PFAS, EC 6.3.5.3). The bifunctional enzyme PAICS consists of phosphoribosylaminoimidazole carboxylase (EC 4.1.1.21, step 6) and phosphoribosylaminoimidazolesuccinocarboxamide synthase (EC 6.3.2.6, step 7). The enzyme ADSL (EC 4.3.2.2) catalyzes the formation of AICAR from SAICAR. The last two steps are catalyzed by the bifunctional ATIC enzyme phosphoribosylaminoimidazolecarboxamide formyltransferase (EC 2.1.2.3, step 9) and IMP cyclohydrolase (EC 3.5.4.10, step 10). PDNS contributes to the cellular pool of purines at times when there is an increased demand for purines, particularly during the G1 and S phases of the cell cycle, and supplies enough purines for the synthesis of RNA and DNA [1]. The highest activity of PDNS has been found in the skeletal muscles, even exceeding the activity in the liver. In contrast, minimal activity has been found in the heart and brain (except developing brains). Erythrocytes, as an example of nondividing cells, lack an intact purine *de novo* synthetic pathway [2].

Recent studies focusing on protein-protein interactions have revealed that the individual enzymes of PDNS group together sequentially to form multienzyme complexes called purinosomes, which facilitate the synthesis of purines. It has been proposed that the formation of purinosomes inside cells occurs in the G1 and S phases of the cell cycle [1]. This is well described by immunofluorescence imaging of mammalian cells under purine-rich or purine-depleted conditions [1, 3, 4] and by monitoring the overall flux through the pathway [4]. Direct tracing of the intermediates of the pathway has thus far only been possible with the use of radioactive labeling [5].

To date, two genetically determined defects of this metabolic pathway (out of ten that are theoretically possible) have been identified: ADSL deficiency (OMIM 103050) and AICA-ribosiduria (ATIC deficiency, OMIM 608688). Almost eighty cases of ADSL deficiency [6] and only one case of AICA-ribosiduria [7] have been reported worldwide to date. There are three possible explanations for this limited number of cases: the first two are that the clinical conditions associated with these particular enzyme deficiencies are either benign or incompatible with fetal development. The third reason is that the available screening/diagnostic tools are relatively laborious and expensive, which limits their widespread use. The methods used for studying purine metabolism and diagnosing related metabolic diseases include proton nuclear magnetic resonance, electrophoresis, and chromatography. Chromatography dominates the field and has historically used UV absorbance, radiometric and tandem mass spectrometric detection [4, 8–10]. PDNS ribosides excreted into growth media in four genetically modified

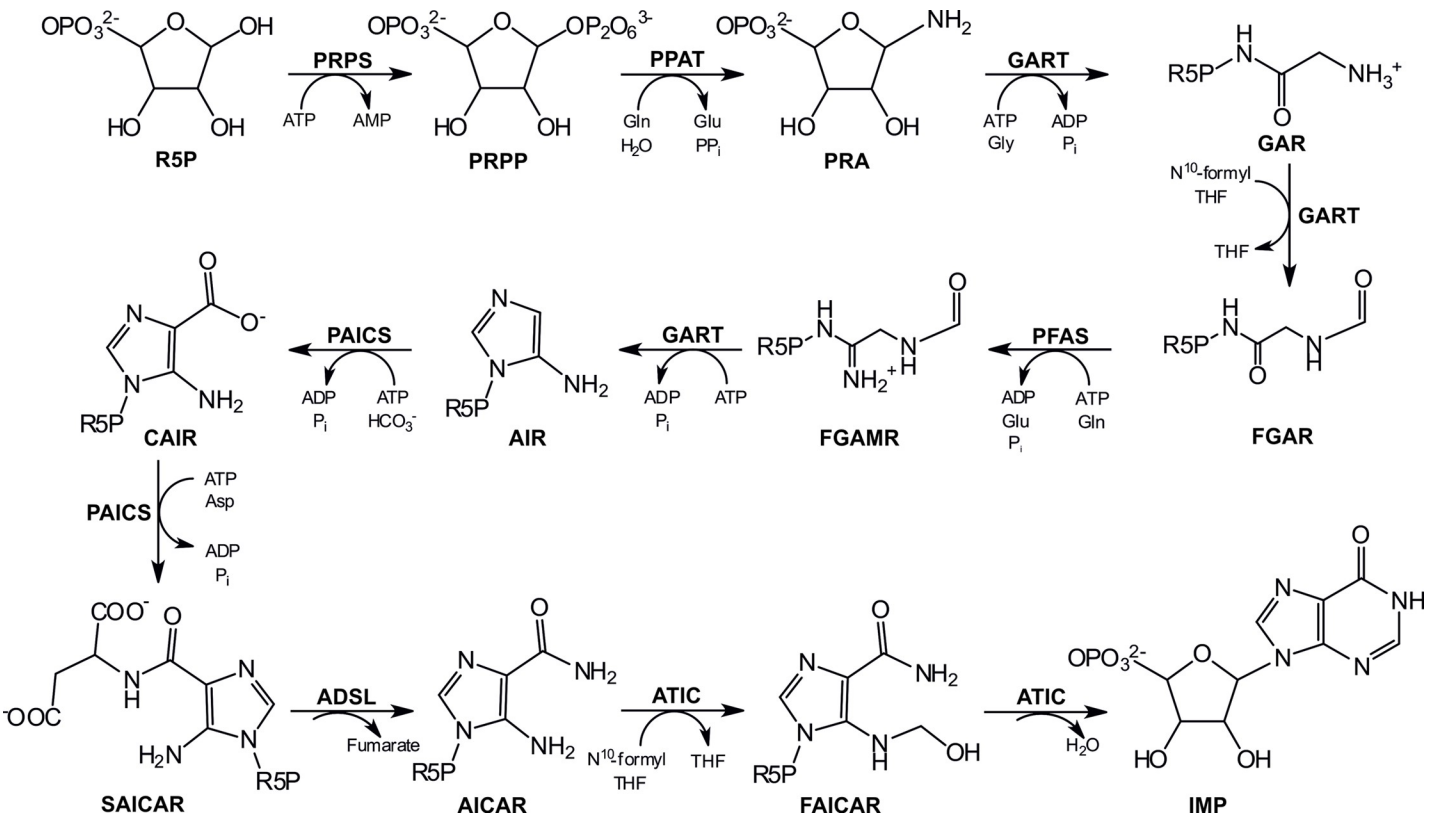

Fig 1. Purine *de novo* synthesis in humans. Abbreviations: phosphoribosylamine (PRA), glycinamideribonucleotide (GAR), N-formylglycinamide ribonucleotide (FGAR), N-formylglycinamidine ribonucleotide (FGAMR), aminoimidazole ribonucleotide (AIR), carboxyaminoimidazole ribonucleotide (CAIR), N-succinocarboxamide-5-aminoimidazole ribonucleotide (SAICAR), 5-aminoimidazole-4-carboxamide ribonucleotide (AICAR), 5-formamido-4-imidazolecarboxamide ribonucleotide (FAICAR), inosine-5-monophosphate (IMP), glutamine (Gln), glutamate (Glu), pyrophosphate (PPi), adenosine-5'-triphosphate (ATP), adenosine 5'-diphosphate (ADP), glycine (Gly), phosphate (Pi), N^{10}-formyl tetrahydrofolate (N^{10}-formyl THF), tetrahydrofolate (THF), hydrogen carbonic acid (HCO^{3-}), aspartate (Asp). For enzyme abbreviations, see the second paragraph of the Introduction.

https://doi.org/10.1371/journal.pone.0208947.g001

cell lines were detected in a recent study [11]. Currently, there is no published method for the detection of all natural PDNS intermediates. The only published report utilizes radioactive tracing [5]. Mass spectrometric fragmentation analysis of the compounds is of value because of the biological importance of such compounds and the lack of experimental fragmentation spectra. Mass spectral databases contain either no PDNS metabolites or *in silico* fragmentation spectra of the metabolites, as these compounds are not commercially available (except AICAR, AICAr and SAMP).

The aim of this work is to fully describe the mass spectrometric fragmentation behavior of PDNS metabolites. Based on this knowledge, we analyzed individual PDNS-defective cell lines to describe metabolic changes in the pathway with the objective of predicting metabolic changes in analogous human conditions. The method that was developed for the detection of PDNS intermediates could serve in pathway kinetic studies (enzyme activity measurements or inhibition experiments, since a number of compounds are claimed to be PDNS inhibitors) and in the diagnostics of inherited metabolic disorders. The method can also be applied in cancer research, as some genes encoding PDNS enzymes have been reported to be up- or downregulated in some tumors [12, 13]. In the first part, we synthesized 16 metabolites of PDNS and their dephosphorylated analogues and performed in-depth multistage mass spectrometric fragmentation analysis.

In the second part, we analyzed edited HeLa cells that were enzymatically deficient in the individual steps of PDNS and treated with isotopically labeled glycine. The aim was to confirm the identity of the newly synthesized intermediates of PDNS by comparing the fragmentation patterns of the synthesized intermediates with those produced by cells (formed under pathological conditions of known and theoretical possible defects of PDNS). Data obtained from the comparison of high-resolution mass spectrometry (HRMS) fragmentation and mass shifts in labeled and natural intermediates provided additional structural certainty in the form of knowledge of the labeling position.

Finally, experiments with PDNS-deficient HeLa cell lines provided data for stable isotope fluxomic analysis and allowed a deeper understanding to be gained of the biochemical changes under those circumstances.

Materials and methods

Chemicals

Isotopically labeled glycine (U-$^{13}C_2$, ^{15}N) was purchased from Cambridge Isotope Laboratories (Andover, MA, USA). AICAR, 5-aminoimidazole-4-carboxamide riboside (AICAr) and adenylosuccinic acid (SAMP) were purchased from Toronto Research Chemicals Inc. (North York, Canada). SAICAR, succinylaminoimidazolecarboxamide riboside (SAICAr), succinyladenosine (SAdo), AIR, 5-aminoimidazole riboside (AIr), CAIR, carboxyaminoimidazole riboside (CAIr), and N^{10}-formyl-tetrahydrofolate (N^{10}-formyl-THF) were prepared as previously described [11, 14]. Calf intestinal alkaline phosphatase (CIP) and NEB3 buffer were purchased from New England Biolabs (NEB, Ipswich, MA, USA), and Dulbecco's minimum essential medium (DMEM), F12 nutrient mix, and fetal bovine serum (FBS) were obtained from Life Technologies, ThermoFisher Scientific (MA, USA). Minimum Essential Medium (MEM) was obtained from BioSera (Nuaille, France). All other chemicals were purchased from Sigma-Aldrich (St. Louis, USA).

Preparation and purification of substrates

GAR, FGAR, and FGAMR intermediates were synthesized biochemically using bacterial recombinant enzymes. FAICAR was prepared by inorganic synthesis. We did not attempt to synthesize PRA, as it is known to be unstable *in vivo* [15, 16].

The initial concentration of all compounds ranged from 57 μM in samples of FGAMR/r to 124 μM in samples of GAR/r (see S1 Table).

The bacterial recombinant enzymes phosphoribosylglycinamide synthetase (GARS) and phosphoribosylglycinamide formyltransferase (GARTF) were expressed and purified as fused protein maltose binding protein MBP-GARS and MBP-GARTF using the pMAL^{TM} Protein Fusion and Purification System (New England Biolabs Inc., USA), as described previously [17].

To produce recombinant bacterial phosphoribosylformylglycinamide synthetase fused with a C-terminal polyhistidine tag (6H-PurL), the gene was introduced into the p6H vector, expressed in *Escherichia coli*, and purified on a Co^{2+}-immobilized metal affinity chromatography column (GE Healthcare) according to standard procedure.

GAR/r preparation. The reaction mixture containing 5.7 mM ribose-5-phosphate, 0.7 mM ATP, 10 mM glycine, 10 mM ammonium hydroxide, 12.7 mM magnesium chloride, 20 mM phosphate buffer pH 7.4, and 0.4 μg/μL purified MBP-GARS was incubated at 37˚C for four hours. The reaction was analyzed by high-performance liquid chromatography coupled with mass spectrometry (HPLC-MS). The riboside form was prepared by dephosphorylation with 1 U of CIP from NEB at 37˚C for four hours.

FGAR/r preparation. The reaction mixture containing 5.7 mM ribose-5-phosphate, 0.7 mM ATP, 10 mM glycine, 10 mM ammonium hydroxide, 12.7 mM magnesium chloride, 0.1

mM N^{10}-formyl-THF, 20 mM phosphate buffer pH 7.4, 0.4 μg/μL MBP-GARS, and 0.4 μg/μL MBP-GARTF was incubated at 37˚C for four hours. The subsequent procedure was the same as in GAR/r preparation.

FGAMR/r preparation. A total of 200 μL of the reaction mixture from the synthesis of FGAR was incubated with 2 mM glutamine, 2 mM ATP, and 0.25 μg/μL of purified 6H-PurL at 37˚C for four hours. The subsequent procedure was the same as in GAR/r preparation.

FAICAR/r preparation. FAICAr was prepared according to Lukens et al. [18]. FAICAR was prepared by adjusting the procedure used for the synthesis of FAICAr. In brief, we incubated 10 mg of AICAR with 11 mg of NaOH, 136 μL of formic acid and 250 μL of acetic anhydride for 1 hour at 37˚C. The product of the reaction was analyzed by HPLC-MS.

Cell cultivation and harvesting

We used the CRISPR-Cas9 genome-edited HeLa cells CR-GART, CR-PFAS, CR-PAICS, CR-ADSL, and CR-ATIC prepared by Baresova et al. in 2016 [11]. CR-HGPRT cells (hypoxanthine-guanine phosphoribosyltransferase deficient) were prepared analogously [19]. HeLa cells were cultured in a humidified atmosphere and incubated with 5% CO_2 at 37˚C. All cells (knockout and control) were maintained in DMEM/F12 nutrient mix medium supplemented with 10% FBS (Gibco, Invitrogen) and 1% penicillin/streptomycin. The medium of the knockout cells was enriched with $3x10^{-5}$ M of adenine. Twenty-four hours prior to the experiment, all the cell types were cultivated in purine-depleted DMEM supplemented with dialyzed 10% FBS [11] and 1% penicillin/streptomycin. Two hours prior to cell harvesting, the cells were washed with PBS and placed into 5 mL of glycine-free MEM with 500 μM of isotopically labeled glycine (U-$^{13}C_2$, ^{15}N) added. Each deficient cell line was cultivated in hexaplicate in 75-cm^2 flasks (approx. 5 million cells).

Cells were harvested by means of the modified quenching method described by Wojtowicz et al. [20]. Initially, the medium was transferred into a 15-mL plastic tube for subsequent analytical preparation. Cellular metabolism was quenched by spraying 40 mL of 60% aqueous cold methanol (v/v, -50˚C) by means of a plastic syringe with a needle. The culture flasks were kept on ice and extracted with 1 mL of 80% methanol (v/v, -50˚C), and the cells were mechanically detached using a cell scraper. The cell debris was drained out with a pipette. For an additional extraction, another 2 mL of cold methanol was added. The methanol extracts were combined, sonicated (30 s), and centrifuged (1800 *g*, 5 min, 4˚C), and the supernatants were freeze-dried.

Preparation of cell lysates

A total of 500 μL of cold 80% methanol was added to each lyophilizate and thoroughly mixed. The samples were centrifuged at 15,000 *g* for 15 min at 4˚C, and the supernatants were taken for analysis.

Preparation of cell media

The media were mixed using a vortex; then, 100 μL of each sample was taken and 300 μL of 80% methanol was added. The samples were left at -80˚C overnight. The extracts were centrifuged at 15,000 *g* for 15 min at 4˚C, and the supernatants were analyzed.

Fragmentation analysis of PDNS intermediates and their dephosphorylated analogues (HPLC-$HRMS^n$)

Chromatographic separation was achieved with hydrophilic interaction liquid chromatography using an Ultimate 3000 RS (ThermoFisher Scientific, MA, USA). The aminopropyl column (Luna NH_2 3 μm 100 Å, 100 x 2 mm, Phenomenex, Torrance, USA) was maintained at

35˚C. The mobile phase consisted of 20 mM ammonium acetate in water at pH 9.75 (mobile phase A) and acetonitrile (mobile phase B). The gradient elution was performed as follows: t = 0.0, 95% B; t = 7.0–13.0, 10% B; t = 14.0–17.0, 95% B. The flow rate was set to 0.3 mL/min, and the injection volume was 2 μL.

Multistage fragmentation analysis was performed on an Orbitrap Elite (ThermoFisher Scientific, MA, USA) operating in positive mode using electrospray ionization (capillary temperature 350˚C, source heater temperature 300˚C, sheath gas 10 arb. units, auxiliary gas 35 arb. units, sweep gas 0 arb. units). The electrospray voltage was set at +3.0 kV. Fragmentation for the most abundant fragments with intensities higher than 1E4 was performed using data-dependent analysis (DDA) or TreeRobot (HighChem, SK); otherwise, the selection of fragments was performed manually. Up to five of the most intense signals in MS^2 were isolated and further fragmented. Then, one to six of the most intense signals from each MS^3 spectrum were subjected to fragmentation to MS^4. The subsequent MS^n stages were also dependent on the intensities of the emerging fragments, usually producing spectra of the one or two most intense fragments from MS^4/MS^5. The fragmentation spectra were produced via collision-induced dissociation (CID) using 30 units of normalized collision energy; the isolation width was 2 Da, and the injection time was 200 ms. All the fragmentation spectra were measured with a resolution of 120,000 full-width at half-maximum (FWHM) and with a mass error below 3 ppm. The multistage fragmentation spectra of each compound were organized into mass spectral trees. In every spectrum, the structures of the fragments belonging to the precursor (target) compound/fragment were identified with the predictive fragmentation software MassFrontier 7.0.5.09 SP3 (HighChem, SK).

Analysis of cell lysates and media

The chromatographic conditions were the same as in the HPLC-$HRMS^n$ analysis mentioned above. Detection was performed on an Orbitrap Elite operating in positive ionization mode with the same setting as above. The detection method was divided into four time segments. Full scan analysis within the mass range *m/z* 70–1000 was performed in the first (0.0–3.0 min) and fourth (12.0–17.0 min) segments. The selected ion monitoring (SIM) method was applied in the second segment (3.0–7.0 min) for the analysis of ribosides (*m/z* 177–417) and in the third segment (7.0–12.0 min) for the analysis of ribotides (*m/z* 257–497) to enhance the sensitivity towards these metabolites (except for the measurement of SAdo and SAMP, which had different *m/z* ranges: 379–389 and 459–469, respectively). The resolution was set to 60,000 FWHM. The mass error was below 3 ppm. All cell lines were measured in hexaplicate, and the intensity values are presented as averages. The identities of the accumulated compounds in both cell lysates and media were confirmed by MS^2 fragmentation analysis. Fragmentation spectra were produced via CID with the fragmentation energy set to 30 units of normalized collision energy.

Results and discussion

Preparation and purification of PDNS intermediates and their dephosphorylated analogues

The ribosides AIr, CAIr, SAICAr, AICAr, FAICAr, and SAdo and ribotides AIR, CAIR, and SAICAR were synthesized according to previously published procedures [11, 14]. AICAR and SAMP were commercially available.

New methods have been developed for the preparation of GAR, FGAR, and FGAMR. The strategies were based on the preparation of the bacterial recombinant enzymes MBP-GARS,

MBP-GARTF, and 6H-PurL. The GAR metabolite was produced in two reactions that occurred in one step from ribose-5-phosphate. The first reaction was the formation of PRA from ribose-5-phosphate and ammonium hydroxide as a function of pH as described earlier [11]. In the second reaction, PRA was converted by MBP-GARS to GAR with a production yield of 10%. Then, GAR was dephosphorylated to GAr via CIP. FGAR was produced in the same reaction as GAR with added N^{10}-formyl THF and MBP-GARTF. The resulting FGAR was dephosphorylated to FGAr by CIP. FGAMR was prepared from FGAR in the reaction catalyzed by the 6H-PurL enzyme and dephosphorylated by CIP to FGAMr.

FAICAR/FAICAr was prepared inorganically from AICAR/AICAr. We applied a formylating environment consisting of formic acid, acetic anhydride, and NaOH to convert AICAR to FAICAR within one hour at 37˚C.

MS^n fragmentation analysis of PDNS intermediates and their dephosphorylated analogues

In total, eight biologically stable PDNS intermediates (GAR, FGAR, FGAMR, AIR, CAIR, AICAR, SAICAR, and FAICAR) and their dephosphorylated forms (GAr, FGAr, FGAMr, AIr, CAIr, AICAr, SAICAr, and FAICAr) were subjected to $HRMS^n$ fragmentation analysis. Moreover, other PDNS-related purine metabolites, SAMP, SAdo, and IMP, were measured.

The compounds were sequentially fragmented up to MS^6. The structure of the fragmented compound or fragment is shown in every spectrum, and up to six of the most intense fragments are depicted in the structure (see one example in Fig 2; the rest are provided in S1 Fig). More than half of the compounds were fragmented up to MS^4. The number of fragmentation steps was determined by the concentration of the synthesized compound in the reaction mixture (57–124 μM), molecular mass, ionization efficiency in positive mode and ion suppression (relatively minor effect due to experimental set-up). In our view, the richest information about the fragmentation behavior of PDNS metabolites lies within the MS^3 and MS^4 spectra. Higher MS stages (MS^5 and MS^6) usually offered just one or two additional fragments to the whole spectral tree (e.g., FAICAR, SAdo, SAICAr). The loss of intensity observed in increasing MS stages caused higher noise levels, making the spectra less reliable for interpretation. Nevertheless, even these spectra could help with the identification of unknown molecules in mass spectral databases. One of the greatest advantages of spectral trees is based on the comparison of substructural information of similar compounds—precursor ion fingerprinting (PIF)—assuming that similar compounds share identical substructures and the uniqueness of a compound is given by the way in which substructures combine [21–23].

Generally, the instability of the majority of ribotides and ribosides was observed as a result of ion-source fragmentation. MS^2 fragments were visible in full MS scans of nearly all compounds, most often not exceeding 5% of the intensity of a molecular ion. The intensity of some MS^2 fragments in full MS scans reached 17, 20, and 540% of the intensity of the molecular ions for GAr, SAdo, and FGAr, respectively. GAr was the first compound to be identified with such profound in-source fragmentation and was chosen for the optimization of the measurement conditions. The initial parameters of the electrospray ionization (ESI) source were a 3 kV spray voltage, 300˚C source heater temperature, 350˚C capillary temperature, and 60% S-Lens RF level. ESI measurements under various conditions were performed (spray voltage 2.5 and 2 kV; heater and capillary temperatures lowered to 250 and 300˚C, respectively; and S-lens parameters of 10, 20, and 40%) to reduce the ion-source fragmentation of fragile ions. No change in these parameters resulted in significantly better stability (see S2–S4 Figs). For compounds suffering from ion-source fragmentation and with low molecular ion intensity, the

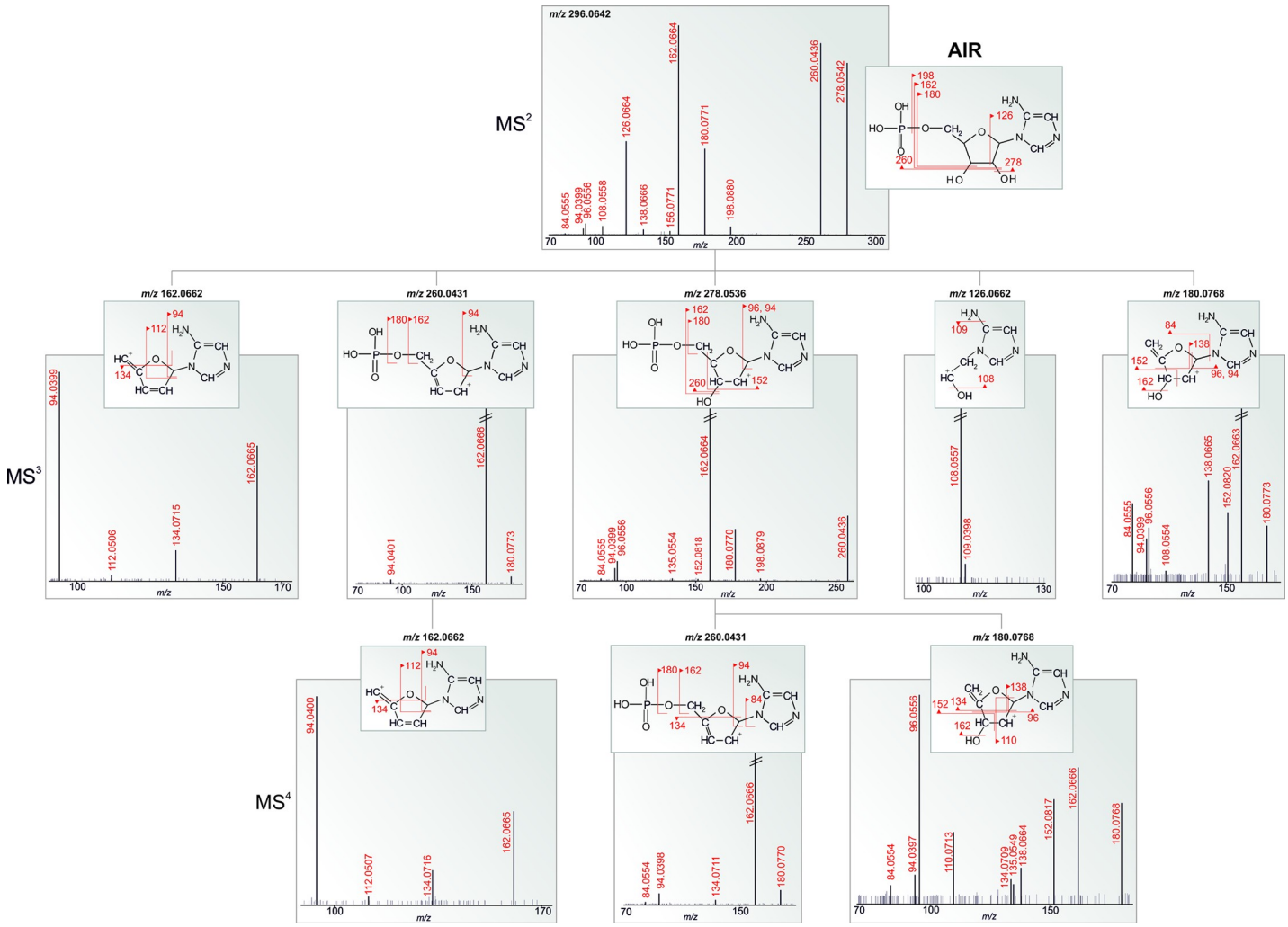

Fig 2. Fragmentation spectral tree of AIR. Every *m/z* assigned with accurate mass in the spectra (in red) belongs to the fragmented structure. The other *m/z* represent coeluting compounds or masses belonging to the fragmented structure that could not be identified using the given procedure.

https://doi.org/10.1371/journal.pone.0208947.g002

strategy for obtaining MS^n spectra was modified. MS^2 analysis of the ion-source fragments (corresponding to MS^3) belonging to the compound in the full MS spectrum was performed.

Ribotides showed considerable variability in their fragmentation patterns compared to ribosides (Fig 3). Losses of water or the phosphate group from ribose were the dominant events for the most intense fragments of the first part of the PDNS pathway (up to AIR). Other fragments appeared with the build-up of the purine ring, starting with CAIR and proceeding to consecutive PDNS intermediates. The most intense fragments of the ribotides of the second part of the pathway originated from the breaking of the N-glycosidic bond and the loss of an amino group from the base, similar to their dephosphorylated analogues.

All the ribosides shared common fragmentation behavior when the MS^2 spectra were compared (see S5 Fig). The most intense fragment ion always belonged to the part of the base forming the purine ring, suggesting that the N-glycosidic bond had the highest susceptibility to breaking. In some cases (FAICAr and SAdo), the formation of this fragment greatly predominated, and all the other fragments were found at below 1% of the intensity of the dominant fragment ion but still above the lowest detectable signal. The majority of the second-

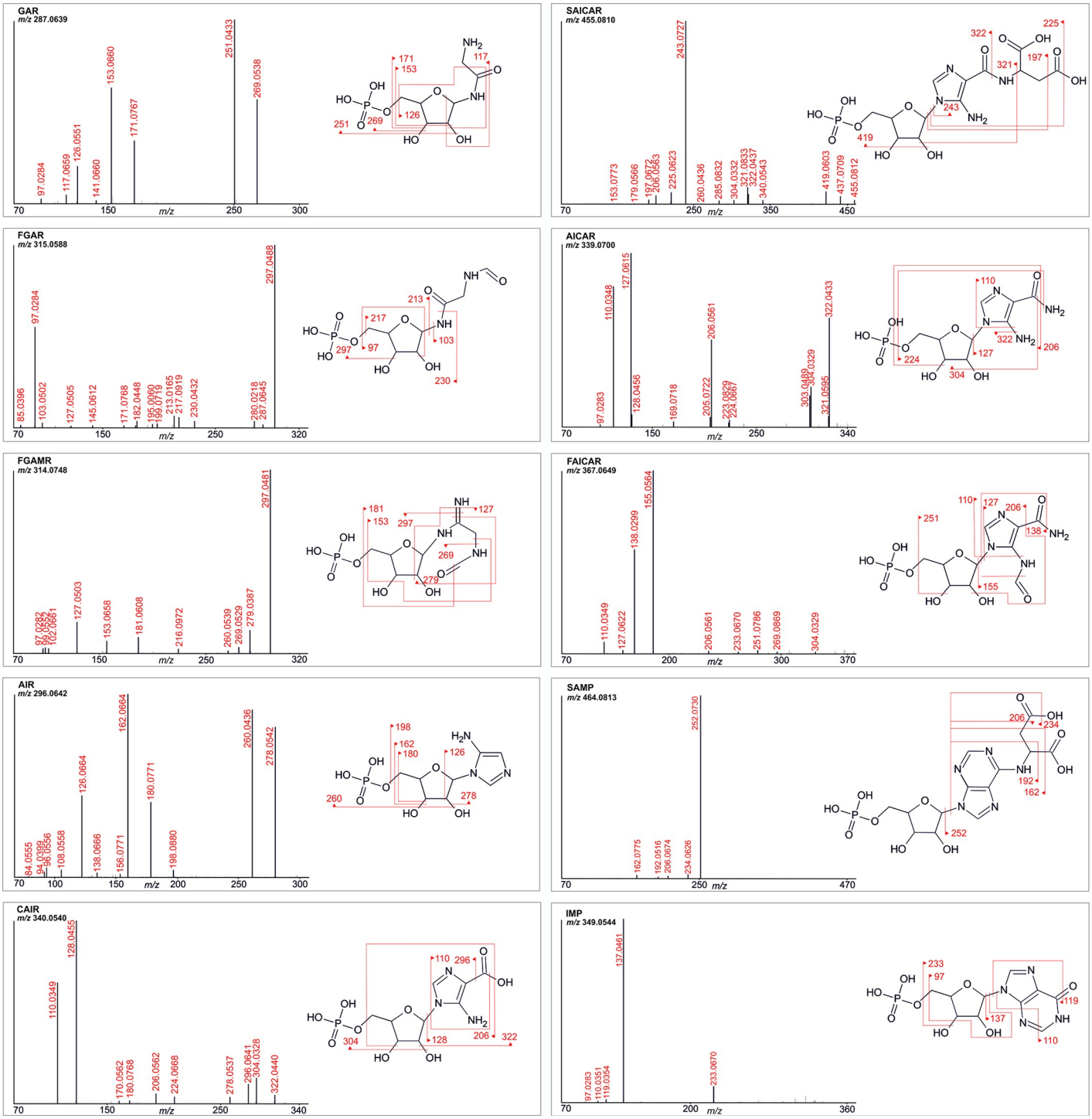

Fig 3. MS^2 fragmentation spectra of PDNS ribotides. The structure of the fragmented compound is shown next to every spectrum, and up to six of the most intense fragments are depicted in the structure.

https://doi.org/10.1371/journal.pone.0208947.g003

most-intense fragment ions were represented by a basic part that had lost either the amino or a hydroxyl group. The loss of one or more molecules of water from the ribosidic part of nucleosides was characteristic of the subsequent fragments.

To identify unknown structures, free online databases of fragmentation spectra can be used in advance. In the case of PDNS metabolites, databases (Metlin, HMDB, mzCloud) [24] do not contain experimental fragmentation spectra, just *in silico* predictions. Moreover, *in silico* fragmentation spectra are available for PDNS ribotides but not for ribosides. The MS^2 spectra of the PDNS ribotides acquired in our study were compared with *in silico* spectra provided by the Metlin database (Fig 4), except for AICAR and IMP, which both have only experimental spectra in the database.

Generally, the experimental spectra match the *in silico* predictions by roughly one-third. Metlin *in silico* spectra generated by a machine learning approach are characterized by prioritizing low-molecular-weight ions (less than *m/z* 100) under all three different fragmentation sets of conditions tested in positive mode (10, 20, and 40 eV). In contrast, our experimental spectra offered many ions higher than *m/z* 100; the low-molecular-weight ions were suppressed because of the mechanism of CID fragmentation. The diversity of the ions in the experimental spectra can be attributed to combined sites of fragmentation leading to a particular ion. For example, in the MS^2 experimental spectrum of GAR (Fig 4), the most significant fragments originate from the loss of one or two molecules of water from ribose (*m/z* 251 and 269) or the loss of one or two molecules of water from ribose in combination with the loss of the phosphate group (*m/z* 153 and 171). Of these four most significant ions, the *in silico* MS^2 spectrum of GAR (MID 3411) offers just the ion of *m/z* 269, suggesting that only one fragmentation site is preferred for *in silico* fragment prediction. This assumption could explain the difference observed between the *in silico* and experimental spectra of the PDNS metabolites. Another reason for the spectral disagreement could arise from the existence of predicted ions that would probably not be generated in a given ionization mode (in our case, positive). An example is the ion of *m/z* 98.9842, annotated as a positively charged phosphate group (using MassFrontier for annotation). This ion appears in all the *in silico* spectra of PDNS ribotides but is unlikely to arise in positive ESI mode. *In silico* fragmentation approaches often use experimental spectra of commercially available compounds in the prediction process of commercially unavailable compounds (e.g., PDNS metabolites). AICAR is an example of a commercially available PDNS metabolite whose experimental spectra are present in the Metlin database. Generally, a greater number of equivalent fragment ions were found when comparing the experimental and predicted spectra of metabolites that structurally resemble the AICAR metabolite from the second part of PDNS. In contrast, the fragmentation spectra of metabolites from the first part of PDNS (GAR, FGAR) differ significantly from the *in silico* predictions. Despite the known limitations, *in silico* spectra can be helpful in the process of the identification of unknown structures or confirmation of supposed structures.

The analysis of the HeLa cells enzymatically deficient in the individual steps of PDNS provided data for confirmation of the structures of the synthesized PDNS intermediates. The fragmentation patterns of the PDNS intermediates produced by cells were compared with those obtained by fragmentation analysis of the synthesized compounds. The HeLa cell lines (deficient and control) were cultivated in a glycine-free medium with the addition of isotopically labeled glycine. Glycine enters PDNS in the second enzymatic reaction catalyzed by a trifunctional GART enzyme, incorporating a glycine backbone into the forming purine structure. The PDNS pathway was stimulated by cultivating cells in purine-depleted media 24 hours before stable isotope labeling. Applying this procedure, we obtained naturally labeled PDNS intermediates serving as another means of confirmation of identity. Identity was confirmed by comparing the MS^2 spectra of synthesized compounds to the MS^2 spectra of these isotopically labeled metabolites on the basis of mass shift and considering the position of glycine incorporation and fragmentation. An example of the results of the mass shift experiment is shown in Fig 5. The majority of the PDNS metabolites detected in both cell lysates and growth media

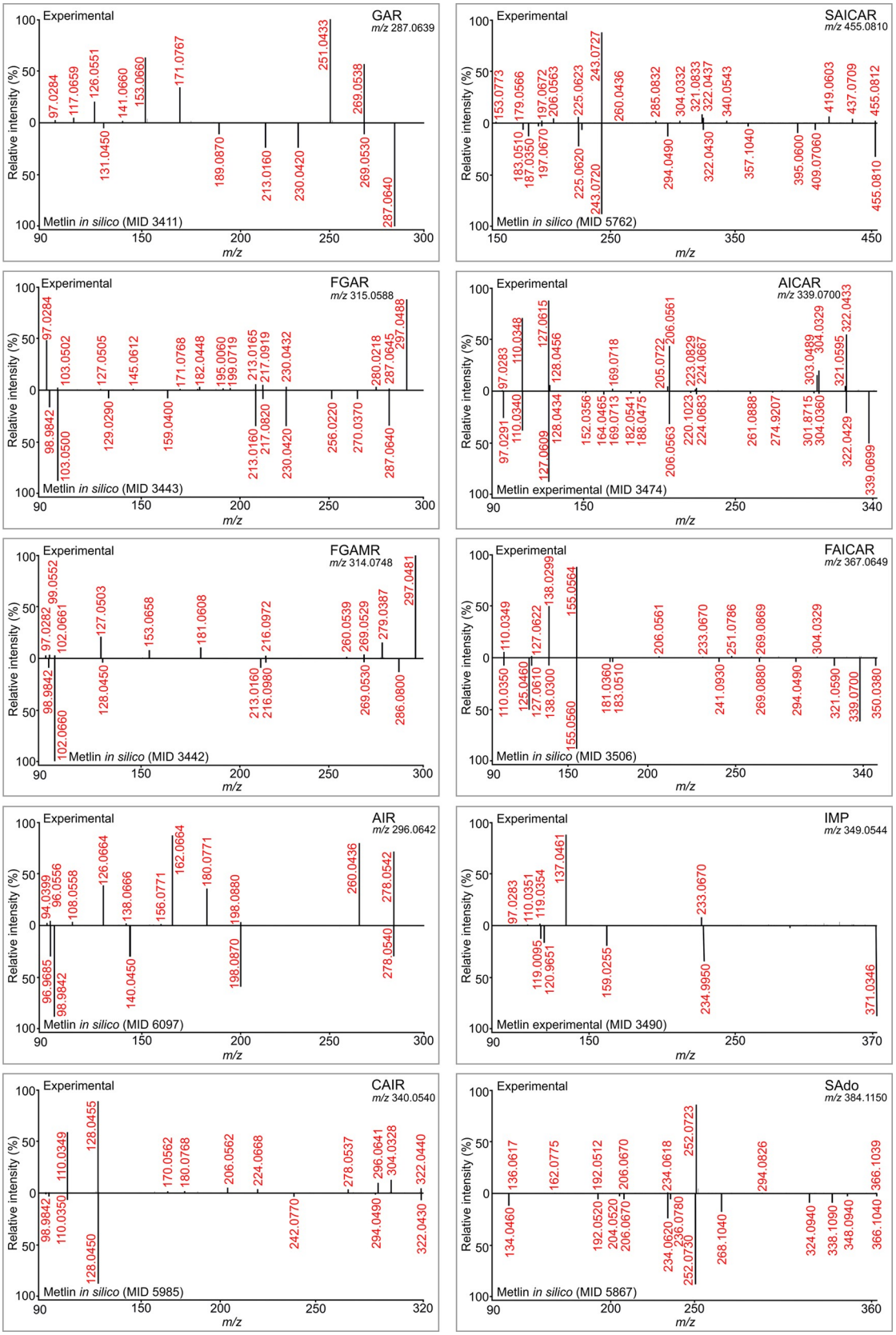
GAR
m/z 287.0639
Experimental
Metlin *in silico* (MID 3411)
SAICAR
m/z 455.0810
Experimental
Metlin *in silico* (MID 5762)
FGAR
m/z 315.0588
Experimental
Metlin *in silico* (MID 3443)
AICAR
m/z 339.0700
Experimental
Metlin experimental (MID 3474)
FGAMR
m/z 314.0748
Experimental
Metlin *in silico* (MID 3442)
FAICAR
m/z 367.0649
Experimental
Metlin *in silico* (MID 3506)
AIR
m/z 296.0642
Experimental
Metlin *in silico* (MID 6097)
IMP
m/z 349.0544
Experimental
Metlin experimental (MID 3490)
CAIR
m/z 340.0540
Experimental
Metlin *in silico* (MID 5985)
SAdo
m/z 384.1150
Experimental
Metlin *in silico* (MID 5867)
Relative intensity (%)
m/z

Fig 4. MS^2 spectral comparison. PDNS metabolites present in the Metlin database (either as *in silico* or experimental fragmentation spectra) were compared with experimental spectra acquired in our study. The mass range of fragmentation spectra from the database was adjusted to the mass range of the spectra from our study.

https://doi.org/10.1371/journal.pone.0208947.g004

were found in the labeled forms. PRA was not detected as a result of its known chemical instability [16]. We were not able to detect FAICAR, probably because of the specific kinetic properties of ATIC [25]. ATIC is a bifunctional enzyme catalyzing the final transformylation of AICAR and cyclization of FAICAR to IMP. The spatial proximity of the two active sites, in which the formylation reaction favors a backward direction while the terminal cyclohydrolase is essentially unidirectional, makes FAICAR difficult to diffuse.

Metabolic changes in edited HeLa cell line cultures

The regulation of PDNS has been studied since the 1950s. Enzyme kinetics experiments, as well as theoretical calculations, have proposed that only the first step of PDNS is limiting for the pathway and that no change in other steps has an impact on the overall flux [26–28]. AICAr and SAICAr are the only PDNS intermediates detectable in the bodily fluids of healthy humans by current analytical technologies [10, 17, 29, 30]. These observations imply that other regulatory places might exist within the PDNS pathway.

The first knockout human cellular models of both known and potentially novel genetically determined defects of PDNS, published in 2016 by Baresova et al. [11], were used in the study. The aim was to model the situation in the bodily fluids of patients. All cells were transferred into purine-depleted medium for 24 hours prior to the experiment to stimulate PDNS. The HPLC-HRMS method was applied to analyze the accumulated PDNS metabolites in the cell lysates and growth media. Overall, six CRISPR-Cas9 genome-edited defective HeLa cell lines (CR-GART, CR-PFAS, CR-PAICS, CR-ADSL, CR-ATIC, and CR-HGPRT) and control HeLa cells were analyzed. All the ribotides and ribosides detected in control and ADSL-defective HeLa cells are listed in Fig 6 (see other defective cell lines in S6 Fig). The majority of the PDNS metabolites detected in both cell lysates were found in the labeled forms. In all the deficient cell lines, we were able to detect both intracellular and extracellular metabolites, except GART-deficient cells, because of the instability of the theoretically expected accumulating PRA, which has a half-life of 5 s under physiological conditions [15, 16]. The accumulation of intermediate ribotides of a particular defective enzyme causes a shift in the equilibria of upstream enzymatic reactions. Because of this effect, we also observed an accumulation of intermediates of PDNS enzymes up to five steps prior to the defective step. In these cases, we usually did not observe an accumulation of metabolites one by one in the opposite direction preceding the main enzyme block. Not all such intermediates were detected because of the chemical instability of the metabolite, differing enzyme kinetics across PDNS, and different ionization efficiencies of PDNS intermediates. The fragmentation method used generally favors ribosides over the more negatively charged ribotides. This might be the reason why ribotides are not detected in cells in some cases but the dephosphorylated analogues of the ribotides are present. Some of the dephosphorylated forms of PDNS intermediates were detected in both cell lysates and media. This is a usual route for defective cells in both the *de novo* and salvage purine pathways to eliminate toxic accumulated intermediates via equilibrative nucleoside transporters. These suggested mechanisms hold for purine salvage pathway defects [31] and are also supported by biochemical observations in patients deficient in ADSL and ATIC, where only ribosidic forms of substrates are detected in the body fluids of the patients [7, 32]. These mechanisms are of the utmost clinical importance because extracellular nucleosides are used as diagnostic biomarkers of these diseases [31]. Human equilibrative transporters possess highly different

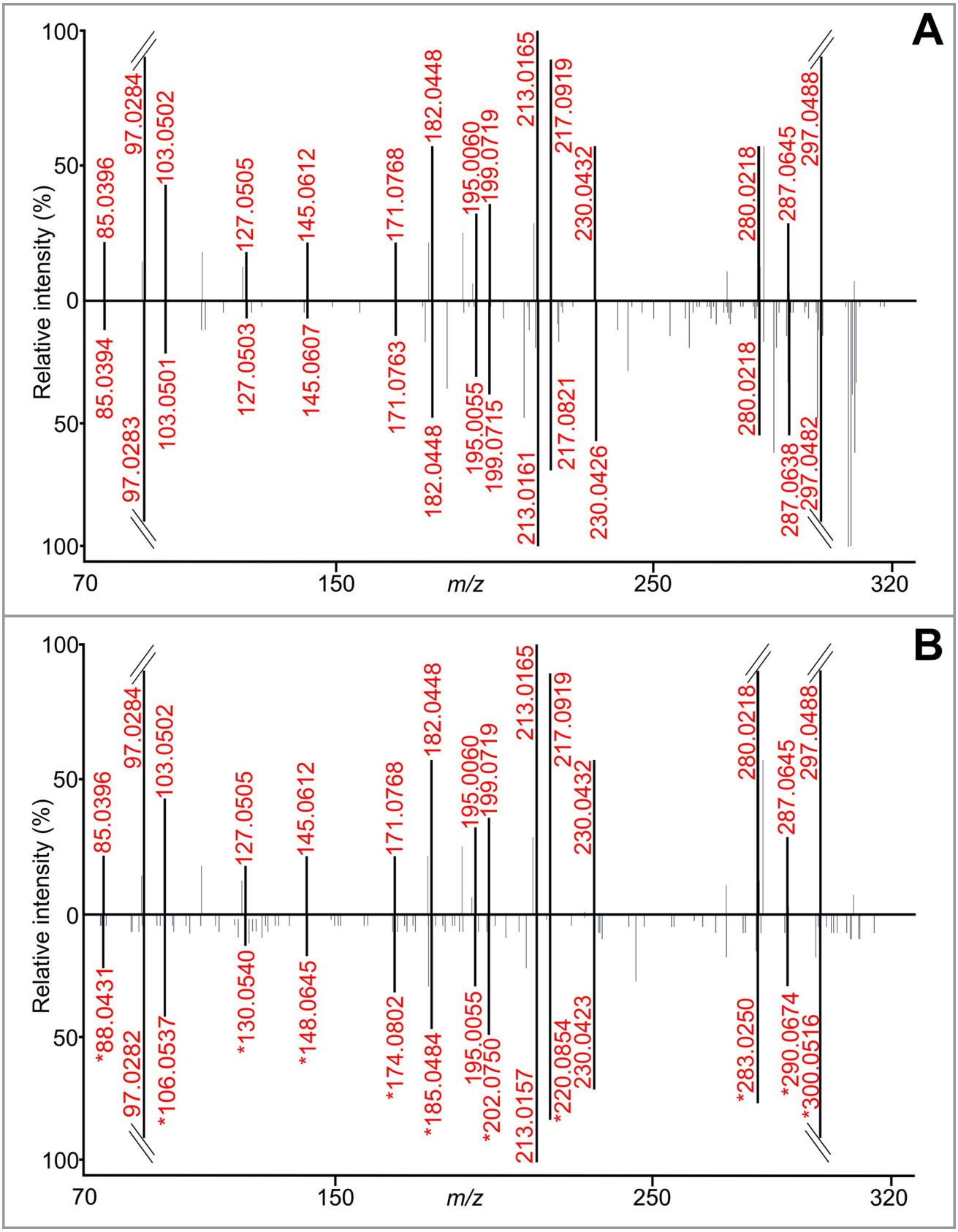
A
Relative intensity (%)
100
50
0
50
100
85.0396
97.0284
103.0502
127.0505
145.0612
171.0768
182.0448
195.0060
199.0719
213.0165
217.0919
230.0432
280.0218
287.0645
297.0488
85.0394
97.0283
103.0501
127.0503
145.0607
171.0763
182.0448
195.0055
199.0715
213.0161
217.0821
230.0426
280.0218
287.0638
297.0482
70
150
m/z
250
320
B
Relative intensity (%)
100
50
0
50
100
85.0396
97.0284
103.0502
127.0505
145.0612
171.0768
182.0448
195.0060
199.0719
213.0165
217.0919
230.0432
280.0218
287.0645
297.0488
*88.0431
97.0282
*106.0537
*130.0540
*148.0645
*174.0802
*185.0484
195.0055
*202.0750
213.0157
*220.0854
230.0423
*283.0250
*290.0674
*300.0516
70
150
m/z
250
320

Fig 5. Confirmation of the identity of FGAR. The MS^2 spectrum of synthesized FGAR was compared to the MS^2 spectra of FGAR (A) and isotopically labeled FGAR-L (B), both of which were accumulated in CR-PFAS HeLa cells. In B, fragments with a mass shift of 3.0038 Da (because of the U-$^{13}C_2$, ^{15}N labeling) are marked with an asterisk. The retention time of all compounds was 8.98 min.

https://doi.org/10.1371/journal.pone.0208947.g005

catalytic activities towards their substrates, and these substrates compete for the active site [33]. Additionally, there is an unknown specificity of purine nucleoside phosphorylase towards our metabolites. These facts make the interpretation of the levels of both natural and labeled PDNS metabolites difficult, and Fig 6 represents just an illustrative view.

In the cytoplasm of control HeLa cells cultured in purine-free medium (Fig 6), AICAR and SAICAR were detected, as were their dephosphorylated forms, which is in agreement with previous reports [29, 30]. Moreover, we were able to detect natural GAR/r and AIr in control cell

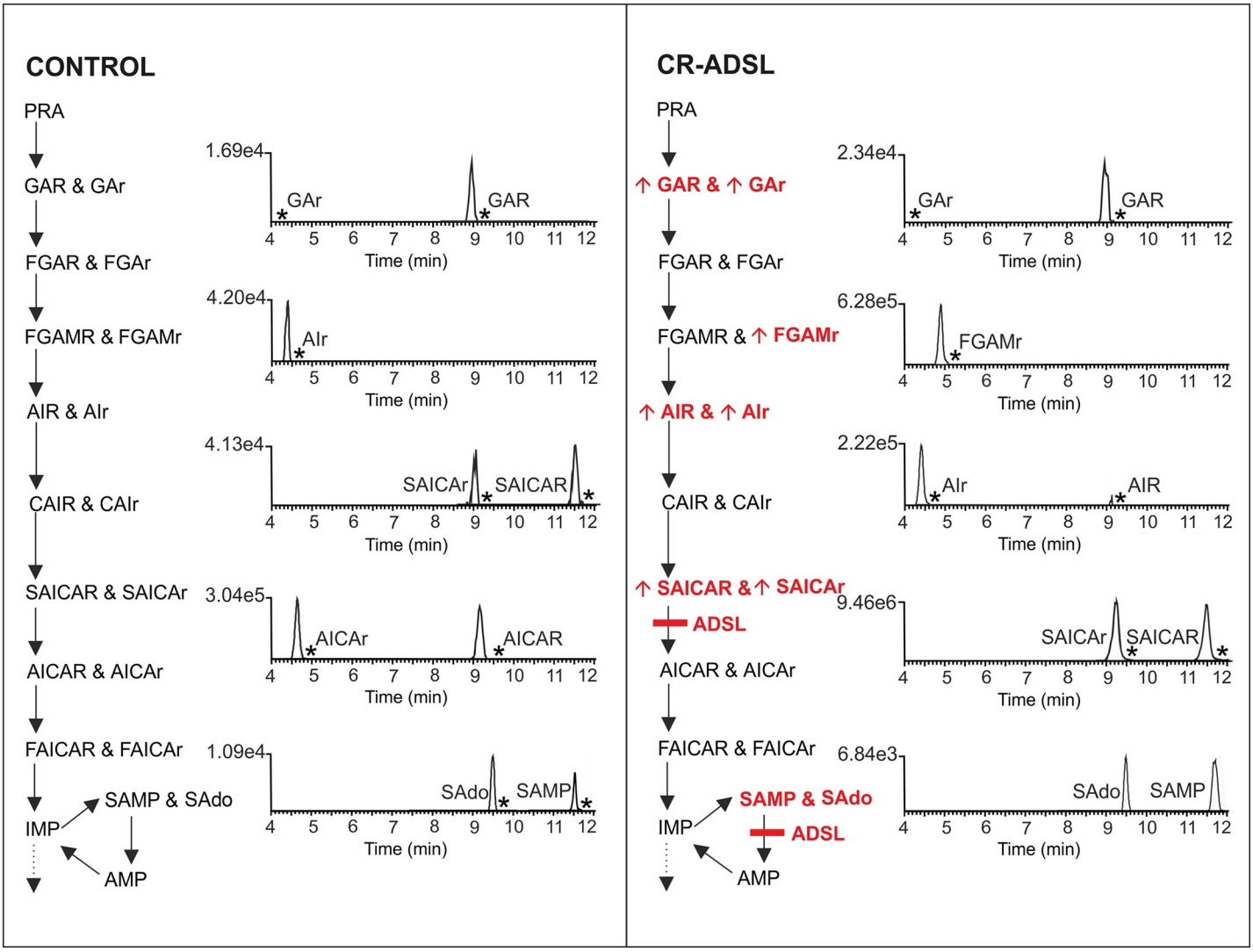

Fig 6. Ribotides and ribosides detected in cell lysates of ADSL-deficient and control HeLa cells. The deficient cell line is graphically represented by a PDNS pathway with an enzyme block marked by a red rectangle. Accumulating metabolites are marked with red bold letters with an arrow. Cell lines were measured in hexaplicate, and the value of the unlabeled peak intensity given above the baseline represents the average of a particular metabolite. Chromatographic peaks of metabolites that were detected also in labeled form are shown as an asterisk. Note: The ionization efficiency of ribotides and ribosides is substantially different, so the responses of these compounds are not directly comparable.

https://doi.org/10.1371/journal.pone.0208947.g006

lysates for the first time, suggesting higher sensitivity of the method. PDNS is considered to be a pathway with an initial rate-limiting step regulating the overall flux, leading to an assumption that its substrates are at low and mutually related concentrations. Thus, their detection probably depends on the ionization efficiency of the individual PDNS intermediates. The experiments could be influenced by the differing viability of the individual defective cell lines used, providing highly variable numbers of cells in each cultivation flask. There is a single study reporting the partial detection of intermediates at trace levels by radiolabeling with autoradiography [5]. The purine salvage metabolites SAMP and SAdo were also detected. Two ribosides (AICAr and AIr) were excreted into the growth media of the control cells.

PFAS-deficient cells (CR-PFAS cells) accumulated FGAR and its riboside, which was also detected in growth media. Most likely, accumulating FGAR causes a shift in equilibrium for trifunctional GART, resulting in a detectable amount of GAR. FGAR and GAR were also detected as isotopically labeled analogues.

The accumulation of AIR in CR-PAICS cells was previously described in Chinese hamster ovary cells. These cells deficient in PAICS activity also accumulated a second compound that the authors were not able to identify [8]. In our experiment, we detected three other ribotides preceding the enzymatic block in addition to the expected accumulation of AIR. The abundant ribotides were excreted into growth media in dephosphorylated forms. This observation suggests a shift in the equilibria of enzymatic reactions up to the PFAS enzyme, as FGAR and FGAr were the last detectable metabolites.

The deficiency of the bifunctional enzyme ADSL is characterized by the presence of the succinylpurines SAICAr and SAdo in bodily fluids [34]. In our experiment, CR-ADSL cells accumulated SAICAR and SAICAr; however, SAMP and SAdo were detected but not accumulated compared to the controls. This behavior could be explained by the experimental set-up, where the purine-free medium forces cells to use PDNS extensively. The purine nucleotide cycle, however, might not be used because of the low energy demands of the cultured cells, which do not possess high proliferation. Two other PDNS intermediates were detected in the cell lysates—AIR and GAR. These metabolites probably originate from the shifted equilibria of enzymes preceding the ADSL blockage. AIr, FGAMr, and GAr were other ribosides detected in cells. SAICAr, AIr, and FGAMr were found in growth media. The accumulation of AIR/AIr in cells and growth media is in accordance with the findings from ADSL-deficient Chinese hamster ovary cells (AdeI), where the authors detected the accumulation of AIR [8].

In the one patient suffering from ATIC deficiency reported so far, a massive accumulation of AICAr, SAICAr, and SAdo in bodily fluids was detected [7]. CR-ATIC cells accumulated AICAR and SAICAR. Corresponding ribosides were also found in growth media. SAMP and its riboside SAdo were not detected.

Patients with partial or complete HGPRT deficiency (Kelley-Seegmiller syndrome and Lesch-Nyhan syndrome, respectively) are known to have increased levels of AICAR in their erythrocytes [35] and AICAr in their urine [36]. As mentioned previously, erythrocytes lack an intact PDNS pathway but are capable of metabolizing exogenous ribosides to their corresponding mono-, di-, and triphosphates and accumulating the metabolites [35]. Several studies reported increased AICAR contents in the brains of HGPRT-deficient mice [37, 38]. We detected AICAR in cell lysates and AICAr in both the cell lysates and media of CR-HGPRT cells. The bifunctional enzyme ATIC, responsible for the last two steps of the pathway, is strongly inhibited by xanthosine-5'-monophosphate, which is accumulated in patients with Lesch-Nyhan syndrome because of the massive flux to uric acid production [39]. Another possible hypothesis for the accumulation of AICAR is enhanced histidine biosynthesis in HGPRT patients; however, there are no experimental data to support this hypothesis [38, 40]. As a result of shifted enzyme equilibria, labeled SAICAR was also detected.

Conclusion

In this study, we provide the first report of a comprehensive mass spectrometric fragmentation analysis of synthesized PDNS intermediates and their dephosphorylated analogues. HRMS fragmentation was possible in the third to sixth stages, and the spectra were compared with *in silico* spectra present in free online databases. The data acquired allowed the development of the method for the detection of these compounds in HeLa cells deficient in the individual steps of PDNS. Our method is applicable in various areas of PDNS research, such as studying cell cycle/purinosome formation. The detection of PDNS intermediates (ribotides) can be valuable in enzyme kinetics studies since numerous compounds are claimed to be inhibitors of this metabolic pathway. Medical applications include the development of diagnostic methods for known/putative inherited metabolic disorders of PDNS and understanding their pathobiochemistry.

Supporting information

S1 Table. List of initial concentrations of PDNS metabolites that were subjected to $HRMS^n$ fragmentation analysis.
(TIF)

S1 Fig. Fragmentation spectral trees of GAR/r, FGAR/r, FGAMR/r, AIR/r, CAIR/r, SAICAR/r, AICAR/r, FAICAR/r, IMP, SAdo and SAMP. All ribotides are marked with a capital R in the name; ribosides are marked with a lowercase r. Every *m/z* assigned with accurate mass in the spectra (in red) belongs to the fragmented structure. The other *m/z* represent coeluting compounds or masses belonging to fragmented structures that could not be identified using the given procedure.
(PDF)

S2 Fig. An example of in-source fragmentation. MS^2 spectra of GAr measured using decreasing spray voltages: 3 kV (A), 2.5 kV (B), and 2 kV (C). Intensities of the depicted fragments do not significantly change with altered conditions.
(TIF)

S3 Fig. An example of in-source fragmentation. MS^2 spectra of GAr measured using increasing S-lens parameters: 10% (A), 20% (B), and 40% (C). Intensities of the depicted fragments do not significantly change with altered conditions.
(TIF)

S4 Fig. An example of in-source fragmentation. MS^2 spectra of GAr measured using different temperatures of the heater (H) and capillary (CA): H 300˚C, CA 350˚C (A); H 300˚C, CA 300˚C (B); and H 250˚C, CA 250˚C (C). Intensities of the depicted fragments do not significantly change with altered conditions.
(TIF)

S5 Fig. MS^2 fragmentation spectra of PDNS ribosides. The structure of the fragmented compound is shown next to every spectrum, and up to six of the most intense fragments are depicted in the structure.
(TIF)

S6 Fig. Ribotides and ribosides detected in cell lysates of PFAS-, PAICS-, ATIC- and HGPRT-deficient HeLa cells. Deficient cell lines are graphically represented by a PDNS pathway with an enzyme block marked by a red rectangle. Accumulating metabolites are marked with red bold letters with an arrow. Cell lines were measured in hexaplicate, and the value of

the unlabeled peak intensity given above the baseline represents the average of a particular metabolite. Chromatographic peaks of metabolites that were also detected in labeled form are shown with asterisks. Note: The ionization efficiency of ribotides and ribosides is substantially different, so the responses of these compounds are not directly comparable.
(TIF)

Acknowledgments

The authors acknowledge Vladimir Cermak for providing the p6H vector.

Author Contributions

Data curation: Lucie Mádrová, Matyáš Krijt, Veronika Barešová, Jan Václavík, Dana Dobešová, Olga Součková, Václava Škopová, Tomáš Adam, Marie Zikánová.

Formal analysis: David Friedecký, Tomáš Adam.

Investigation: Lucie Mádrová, Matyáš Krijt, Veronika Barešová, Jan Václavík, David Friedecký, Dana Dobešová, Olga Součková, Václava Škopová, Tomáš Adam, Marie Zikánová.

Methodology: Marie Zikánová.

Software: David Friedecký.

Supervision: Tomáš Adam, Marie Zikánová.

Writing – original draft: Lucie Mádrová, Tomáš Adam.

Writing – review & editing: Marie Zikánová.

References

1. An S, Kumar R, Sheets ED, Benkovic SJ. Reversible compartmentalization of de novo purine biosynthetic complexes in living cells. Science. 2008; 320(5872):103–6. https://doi.org/10.1126/science.1152241 PMID: 18388293
2. Stone TW, Simmonds HA. Purines: basic and clinical aspects. Dordrecht; London: Kluwer Academic Publishers; 1991.
3. Baresova V, Skopova V, Sikora J, Patterson D, Sovova J, Zikanova M, et al. Mutations of ATIC and ADSL affect purinosome assembly in cultured skin fibroblasts from patients with AICA-ribosiduria and ADSL deficiency. Hum Mol Genet. 2012; 21(7):1534–43. https://doi.org/10.1093/hmg/ddr591 PMID: 22180458
4. Zhao H, Chiaro CR, Zhang L, Smith PB, Chan CY, Pedley AM, et al. Quantitative analysis of purine nucleotides indicates that purinosomes increase de novo purine biosynthesis. J Biol Chem. 2015; 290(11):6705–13. https://doi.org/10.1074/jbc.M114.628701 PMID: 25605736
5. Sant ME, Poiner A, Harsanyi MC, Lyons SD, Christopherson RI. Chromatographic analysis of purine precursors in mouse L1210 leukemia. Anal Biochem. 1989; 182(1):121–8. PMID: 2604037
6. Jurecka A, Zikanova M, Kmoch S, Tylki-Szymanska A. Adenylosuccinate lyase deficiency. J Inherit Metab Dis. 2015; 38(2):231–42. https://doi.org/10.1007/s10545-014-9755-y PMID: 25112391
7. Marie S, Heron B, Bitoun P, Timmerman T, Van Den Berghe G, Vincent MF. AICA-ribosiduria: a novel, neurologically devastating inborn error of purine biosynthesis caused by mutation of ATIC. Am J Hum Genet. 2004; 74(6):1276–81. https://doi.org/10.1086/421475 PMID: 15114530
8. Duval N, Luhrs K, Wilkinson TG 2nd, Baresova V, Skopova V, Kmoch S, et al. Genetic and metabolomic analysis of AdeD and AdeI mutants of de novo purine biosynthesis: cellular models of de novo purine biosynthesis deficiency disorders. Mol Genet Metab. 2013; 108(3):178–89. https://doi.org/10.1016/j.ymgme.2013.01.002 PMID: 23394948
9. Hornik P, Vyskocilova P, Friedecky D, Adam T. Diagnosing AICA-ribosiduria by capillary electrophoresis. J Chromatogr B Analyt Technol Biomed Life Sci. 2006; 843(1):15–9. https://doi.org/10.1016/j.jchromb.2006.05.020 PMID: 16798121

10. Zidkova L, Krijt J, Sladkova J, Hlobilkova A, Magner M, Zikanova M, et al. Oligodendroglia from ADSL-deficient patient produce SAICAribotide and SAMP. Mol Genet Metab. 2010; 101(2–3):286–8. https://doi.org/10.1016/j.ymgme.2010.06.014 PMID: 20674424
11. Baresova V, Krijt M, Skopova V, Souckova O, Kmoch S, Zikanova M. CRISPR-Cas9 induced mutations along de novo purine synthesis in HeLa cells result in accumulation of individual enzyme substrates and affect purinosome formation. Mol Genet Metab. 2016; 119(3):270–7. https://doi.org/10.1016/j.ymgme.2016.08.004 PMID: 27590927
12. Chakravarthi BV, Goswami MT, Pathi SS, Dodson M, Chandrashekar DS, Agarwal S, et al. Expression and Role of PAICS, a De Novo Purine Biosynthetic Gene in Prostate Cancer. Prostate. 2017; 77 (1):10–21. https://doi.org/10.1002/pros.23243 PMID: 27550065
13. Goswami MT, Chen G, Chakravarthi BV, Pathi SS, Anand SK, Carskadon SL, et al. Role and regulation of coordinately expressed de novo purine biosynthetic enzymes PPAT and PAICS in lung cancer. Oncotarget. 2015; 6(27):23445–61. https://doi.org/10.18632/oncotarget.4352 PMID: 26140362
14. Zikanova M, Krijt J, Hartmannova H, Kmoch S. Preparation of 5-amino-4-imidazole-N-succinocarboxamide ribotide, 5-amino-4-imidazole-N-succinocarboxamide riboside and succinyladenosine, compounds usable in diagnosis and research of adenylosuccinate lyase deficiency. J Inherit Metab Dis. 2005; 28(4):493–9. https://doi.org/10.1007/s10545-005-0493-z PMID: 15902552
15. Rudolph J, Stubbe J. Investigation of the mechanism of phosphoribosylamine transfer from glutamine phosphoribosylpyrophosphate amidotransferase to glycinamide ribonucleotide synthetase. Biochemistry. 1995; 34(7):2241–50. PMID: 7532005
16. Schendel FJ, Cheng YS, Otvos JD, Wehrli S, Stubbe J. Characterization and chemical properties of phosphoribosylamine, an unstable intermediate in the de novo purine biosynthetic pathway. Biochemistry. 1988; 27(7):2614–23. PMID: 2454658
17. Kmoch S, Hartmannova H, Stiburkova B, Krijt J, Zikanova M, Sebesta I. Human adenylosuccinate lyase (ADSL), cloning and characterization of full-length cDNA and its isoform, gene structure and molecular basis for ADSL deficiency in six patients. Hum Mol Genet. 2000; 9(10):1501–13. PMID: 10888601
18. Lukens L, Flaks J. Intermediates in Purine Nucleotide Synthesis. Method Enzymol. 1963; 6:671–702.
19. Baresova V, Skopova V, Souckova O, Krijt M, Kmoch S, Zikanova M. Study of purinosome assembly in cell-based model systems with de novo purine synthesis and salvage pathway deficiencies. PLoS One. 2018; 13(7):e0201432. https://doi.org/10.1371/journal.pone.0201432 PMID: 30059557
20. Wojtowicz P, Zrostlíková J, Šťastná V, Dostálová E, Žídková L, Bruheim P, et al. Comprehensive Two-Dimensional Gas Chromatography Coupled to Time-of-Flight Mass Spectrometry in Human Metabolomics. Salih B, editor: InTech; 2012.
21. Kasper PT, Rojas-Cherto M, Mistrik R, Reijmers T, Hankemeier T, Vreeken RJ. Fragmentation trees for the structural characterisation of metabolites. Rapid Commun Mass Spectrom. 2012; 26(19):2275–86. https://doi.org/10.1002/rcm.6340 PMID: 22956319
22. Ridder L, van der Hooft JJ, Verhoeven S, de Vos RC, van Schaik R, Vervoort J. Substructure-based annotation of high-resolution multistage MS(n) spectral trees. Rapid Commun Mass Spectrom. 2012; 26(20):2461–71. https://doi.org/10.1002/rcm.6364 PMID: 22976213
23. Sheldon MT, Mistrik R, Croley TR. Determination of ion structures in structurally related compounds using precursor ion fingerprinting. J Am Soc Mass Spectrom. 2009; 20(3):370–6. https://doi.org/10.1016/j.jasms.2008.10.017 PMID: 19041260
24. METLIN database [database on the Internet] [cited 22 May 2018]. Available from: https://metlin.scripps.edu.
25. Bulock KG, Beardsley GP, Anderson KS. The kinetic mechanism of the human bifunctional enzyme ATIC (5-amino-4-imidazolecarboxamide ribonucleotide transformylase/inosine 5'-monophosphate cyclohydrolase). A surprising lack of substrate channeling. J Biol Chem. 2002; 277(25):22168–74. https://doi.org/10.1074/jbc.M111964200 PMID: 11948179
26. Becker MA, Kim M. Regulation of purine synthesis de novo in human fibroblasts by purine nucleotides and phosphoribosylpyrophosphate. J Biol Chem. 1987; 262(30):14531–7. PMID: 2444588
27. Curto R, Voit EO, Sorribas A, Cascante M. Mathematical models of purine metabolism in man. Math Biosci. 1998; 151(1):1–49. PMID: 9664759
28. Hartman SC, Buchanan JM. Biosynthesis of the purines. XXI. 5-Phosphoribosylpyrophosphate amidotransferase. J Biol Chem. 1958; 233(2):451–5. PMID: 13563519
29. Thomas A, Vogel M, Piper T, Krug O, Beuck S, Schanzer W, et al. Quantification of AICAR-ribotide concentrations in red blood cells by means of LC-MS/MS. Anal Bioanal Chem. 2013; 405(30):9703–9. https://doi.org/10.1007/s00216-013-7162-0 PMID: 23828211

30. Zikanova M, Krijt J, Skopova V, Krijt M, Baresova V, Kmoch S. Screening for adenylosuccinate lyase deficiency using tandem mass spectrometry analysis of succinylpurines in neonatal dried blood spots. Clin Biochem. 2015; 48(1–2):2–7. https://doi.org/10.1016/j.clinbiochem.2014.10.004 PMID: 25445730

31. Hommes FA. Techniques in diagnostic human biochemical genetics: a laboratory manual. New York, NY: Wiley-Liss; 1991.

32. Zikanova M, Skopova V, Hnizda A, Krijt J, Kmoch S. Biochemical and structural analysis of 14 mutant adsl enzyme complexes and correlation to phenotypic heterogeneity of adenylosuccinate lyase deficiency. Hum Mutat. 2010; 31(4):445–55. https://doi.org/10.1002/humu.21212 PMID: 20127976

33. Huang W, Zeng X, Shi Y, Liu M. Functional characterization of human equilibrative nucleoside transporter 1. Protein Cell. 2017; 8(4):284–95. https://doi.org/10.1007/s13238-016-0350-x PMID: 27995448

34. Jaeken J, Van den Berghe G. An infantile autistic syndrome characterised by the presence of succinylpurines in body fluids. Lancet. 1984; 2(8411):1058–61. PMID: 6150139

35. Sidi Y, Mitchell BS. Z-nucleotide accumulation in erythrocytes from Lesch-Nyhan patients. J Clin Invest. 1985; 76(6):2416–9. https://doi.org/10.1172/JCI112255 PMID: 4077987

36. Newcombe DS. The urinary excretion of aminoimidazolecarboxamide in the Lesch-Nyhan syndrome. Pediatrics. 1970; 46(4):508–12. PMID: 5503686

37. Jinnah HA, Page T, Friedmann T. Brain purines in a genetic mouse model of Lesch-Nyhan disease. J Neurochem. 1993; 60(6):2036–45. PMID: 8492116

38. Tschirner SK, Bahre H, Kaever A, Schneider EH, Seifert R, Kaever V. Non-targeted metabolomics by high resolution mass spectrometry in HPRT knockout mice. Life Sci. 2016; 156:68–73. https://doi.org/10.1016/j.lfs.2016.05.031 PMID: 27221022

39. Lopez JM. Is ZMP the toxic metabolite in Lesch-Nyhan disease? Med Hypotheses. 2008; 71(5):657–63. https://doi.org/10.1016/j.mehy.2008.06.033 PMID: 18710792

40. Neychev VK, Mitev VI. The biochemical basis of the neurobehavioral abnormalities in the Lesch-Nyhan syndrome: a hypothesis. Med Hypotheses. 2004; 63(1):131–4. https://doi.org/10.1016/j.mehy.2004.01.019 PMID: 15193365

PLOS ONE

RESEARCH ARTICLE

Study of purinosome assembly in cell-based model systems with *de novo* purine synthesis and salvage pathway deficiencies

Veronika Baresova, Vaclava Skopova, Olga Souckova, Matyas Krijt, Stanislav Kmoch, Marie Zikanova*

Research Unit for Rare Diseases, Department of Paediatrics and Adolescent Medicine, First Faculty of Medicine, Charles University and General University Hospital, Prague, Czech Republic

* marie.zikanova@lf1.cuni.cz

OPEN ACCESS

Citation: Baresova V, Skopova V, Souckova O, Krijt M, Kmoch S, Zikanova M (2018) Study of purinosome assembly in cell-based model systems with *de novo* purine synthesis and salvage pathway deficiencies. PLoS ONE 13(7): e0201432. https://doi.org/10.1371/journal.pone.0201432

Editor: Pankaj K. Singh, University of Nebraska Medical Center, UNITED STATES

Received: February 28, 2018

Accepted: July 16, 2018

Published: July 30, 2018

Data Availability Statement: All relevant data are within the paper.

Funding: This work was supported by the Ministry of Health of the Czech Republic [grant AZV 15-28979A, http://www.azvcr.cz, recipient MZ] and by The Charles University Grant Agency [grant GAUK 818416, recipient MK and GAUK 1102217, recipient OS, https://www.cuni.cz/UK-33.html]. Institutional support was provided by Charles University [programmes PRIMUS/17/MED/6 - recipient MZ, PROGRES Q26/LF1, UNCE 204064 -

Abstract

Background

The enzymes involved in *de novo* purine synthesis (DNPS), one of the basic processes in eukaryotic cells, transiently and reversibly form a dynamic multienzyme complex called the purinosome in the cytoplasm. The purinosome has been observed in a broad spectrum of cells, but some studies claim that it is an artefact of the constructs used for visualization or stress granules resulting from the exposure of cells to nutrient-reduced growth media. Both may be true depending on the method of observation. To clarify this point, we combined two previously used methods, transfection and immunofluorescence, to detect purinosomes in purinosome-free cells deficient in particular DNPS steps (CR-DNPS cells) and in cells deficient in the salvage pathway, which resulted in construction of the purinosome regardless of purine level (CR-HGPRT cells).

Methods and findings

To restore or disrupt purinosome formation, we transiently transfected CR-DNPS and CR-HGPRT cells with vectors encoding BFP-labelled wild-type (wt) proteins and observed the normalization of purinosome formation. The cells also ceased to accumulate the substrate (s) of the defective enzyme. The CR-DNPS cell line transfected with a DNA plasmid encoding an enzyme with zero activity served as a negative control for purinosome formation. No purinosome formation was observed in these cells regardless of the purine level in the growth medium.

Conclusion

In conclusion, both methods are useful for the detection of purinosomes in HeLa cells. Moreover, the cell-based models prepared represent a unique system for the study of purinosome assembly with deficiencies in DNPS or in the salvage pathway as well as for the study of purinosome formation under the action of DNPS inhibitors. This approach is a promising

recipient VB and SVV 260367/2017 - recipients OS and MK, http://www.cuni.cz] and by the Ministry of Education, Youth and Sports of CR [LQ1604 National Sustainability Programme II, http://www.msmt.cz/].

Competing interests: The authors have declared that no competing interests exist.

step toward the treatment of purine disorders and can also provide targets for anticancer therapy.

Introduction

Purines, essential molecules for the synthesis of nucleic acids, universal carriers of chemical energy and components of signalling molecules in all living organisms, are synthesized in higher eukaryotes via 10 reaction steps catalysed by six enzymes, four of which are multifunctional. Once synthesized, they are efficiently recycled by the enzymes of the salvage pathway and eventually removed from cells in the form of uric acid or allantoin (Fig 1).

An important conceptual question is whether the purine-synthesizing enzymes are organized and interact directly within the cell. Because *de novo* purine synthesis (DNPS) produces unstable and/or toxic intermediates [1], the enzymes would need proximity to ensure this vital metabolic function. Knowledge of the composition and regulation of this multienzyme structure, the purinosome, would have important implications regarding human diseases and the treatment of cancer, inflammation and infections. The existence of purinosome has been therefore addressed by various biochemical, molecular and structural approaches [2].

The first direct evidence of purinosome formation was the detection of the spatial signal overlap of transiently expressed fluorescently labelled DNPS proteins in HeLa cells grown in purine-depleted media [3]. This model and its eventual utility for further research on purinosome structure and regulation has however been challenged. The formation of the purinosome bodies has been attributed to the aggregation of overexpressed proteins and to stress granules resulting from the exposure of cells to dialyzed and therefore nutrient-depleted growth media [4].

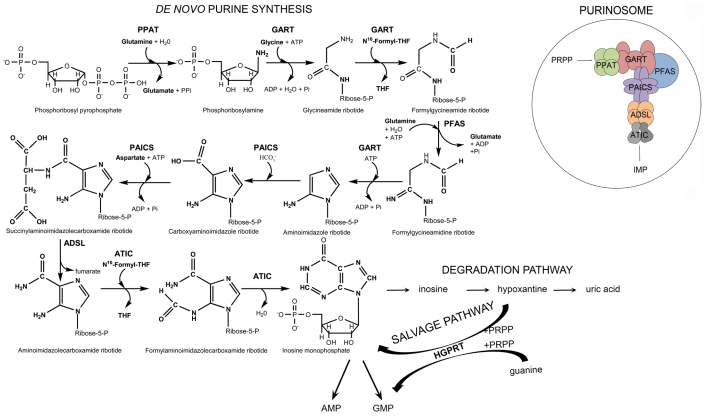

Fig 1. Scheme of *de novo* purine synthesis (DNPS), the salvage pathway, the degradation pathway and the purinosome. The initial substrate in DNPS is phosphoribosyl pyrophosphate (PRPP). Six enzymes are involved in DNPS and the purinosome multienzyme complex: phosphoribosyl pyrophosphate amidotransferase (PPAT), the trifunctional enzyme GART (glycinamide ribonucleotide synthetase/glycinamide ribonucleotide transformylase/aminoimidazole ribonucleotide synthetase), phosphoribosylformylglycinamidine synthetase (PFAS), the bifunctional enzyme PAICS (phosphoribosylaminoimidazole carboxylase/phosphoribosylaminoimidazolesuccinocarboxamide synthetase), adenylosuccinate lyase (ADSL), and the bifunctional enzyme ATIC (5-aminoimidazole-4-carboxamide ribonucleotide transformylase/inosine monophosphate cyclohydrolase). The final product is inosine monophosphate (IMP). IMP is converted into adenosine monophosphate (AMP) and guanosine monophosphate (GMP) and is also degraded to uric acid via the degradation pathway. The hypoxanthine intermediate can be recycled by the enzyme hypoxanthine-guanine phosphoribosyltransferase (HGPRT) into IMP or GMP.

https://doi.org/10.1371/journal.pone.0201432.g001

Further studies with transiently expressed fluorescently labelled DNPS proteins showed that a microtubule network appears to physically control the spatial distribution of purinosomes in the cytoplasm [5], that purinosomes colocalize and can be isolated together with mitochondria [6] and that they differ in size and cell density from stress granules and aggresomes [7].

Another way to detect purinosome complexes is the immunofluorescent labelling of endogenous proteins involved in the DNPS pathway. By this method, purinosome formation was observed in several cell types, including both cancer cell lines and primary cells, grown in purine-depleted medium [8]. The detection of endogenous proteins avoided the need for artificial protein overexpression. The disadvantage of this method is the inability to study purinosome formation *in vivo*.

Recently, we have developed model HeLa cell lines with DNPS enzyme knockouts. These cells represent human purinosome-free model systems [9]. In this work, we prepared model HeLa cells deficient in hypoxanthine-guanine phosphoribosyltransferase (HGPRT, EC 2.4.2.8), one of the key enzymes in a purine salvage pathway, that form purinosomes regardless of the level of purines in the medium. We combined both methods previously used for purinosome study, transfection and immunofluorescence, to investigate the effect of transiently expressed, fluorescently labelled recombinant wild-type (wt) and mutant human DNPS proteins on the formation of purinosome bodies in cells that otherwise never or always formed purinosomes.

Materials and methods

dx.doi.org/10.17504/protocols.io.qxfdxjn

Chemicals

Dulbecco's minimum essential medium (DMEM), F12 nutrition mix and foetal bovine serum (FBS) were obtained from Thermo Fisher Scientific, MA, US. All other chemicals were purchased from Sigma-Aldrich, Czech Republic.

HeLa cell line

The General University Hospital in Prague and Charles University, First Faculty of Medicine has possessed the HeLa cell line for many years; the original cells were obtained from ATCC (American Type Culture Collection).

CR-HGPRT cell preparation

We used the GeneArt® CRISPR Nuclease Vector with an OFP Reporter Kit (Life Technologies) to knockout the *HPRT1* gene in HeLa cells as described previously [9]. The sgRNA target sequence was designed by the program http://crispr.mit.edu/. We tested the cells for the presence of mutations, HGPRT enzyme activity and thioguanine inhibition.

Mutation analysis

We isolated gDNA and total RNA from HeLa cells according to standard procedures and transcribed the mRNA into cDNA with the ProtoScript®II Reverse Transcriptase Kit (New England BioLabs, MA, United States). PCR analysis was performed in 25 μl reaction mixtures containing Red PCR Master Mix (Rovalab, Germany), 1.5 mM $MgCl_2$, 8% DMSO and 0.4 μM specific primers. We gel-purified the amplification products and sequenced the amplicons by the ABI BigDye method (Thermo Fisher Scientific).

HGPRT enzyme activity assay

The reaction was performed for 1 h at 37˚C in a 40 μl reaction mixture containing 50 mM Tris (pH 7.4), 10 mM $MgCl_2$, 1.5 mM phosphoribosyl pyrophosphate (PRPP), 1 mM hypoxanthine, 37.5 mM KH_2PO_4 and cell lysate (4 μg of the protein). We measured the concentration of inosine monophosphate (IMP) formed using the previously described HPLC-DAD method [10]. The retention time of IMP was 10.8 min.

Thioguanine inhibition method and growth curves

First, 5 x 10^4 normal HeLa or CR-HGPRT cells were seeded in 6-well plates containing normal growth medium or medium supplemented with 0.03 mM 6-thioguanine (TG). Every 24 h, the full amount of cells grown in one well was harvested into 1 ml of growth medium and counted with a LUNA™ Automated Cell Counter (Logos Biosystems, Korea). Growth curves were established from the number of cells in 1 ml.

Cell culture

CRISPR-edited HeLa cells deficient in the trifunctional enzyme GART (glycinamide ribonucleotide synthetase (EC 6.3.4.13)/glycinamide ribonucleotide transformylase (EC 2.1.2.2.)/aminoimidazole ribonucleotide synthetase (EC 6.3.3.1)), phosphoribosylformylglycinamidine synthetase (PFAS, EC 6.3.5.3), the bifunctional enzyme PAICS (phosphoribosylaminoimidazole carboxylase (EC 4.1.1.21)/phosphoribosylaminoimidazolesuccinocarboxamide synthetase (EC 6.3.2.6)), adenylosuccinate lyase (ADSL, EC 4.3.2.2), the bifunctional enzyme ATIC (5-aminoimidazole-4-carboxamide ribonucleotide transformylase (EC 2.1.2.3)/inosine monophosphate cyclohydrolase (EC 3.5.4.10)), or HGPRT were maintained in DMEM/F12 nutrient mixture supplemented with 10% foetal bovine serum (FBS), 1% penicillin/streptomycin and 0.03 mM adenine. DMEM supplemented with dialyzed 10% FBS and 1% penicillin/streptomycin served as the purine-depleted media. The FBS was dialyzed against 0.9% NaCl at 4˚C for 48 h with a 10 kDa MWCO dialysis membrane to remove purines.

Cloning of mammalian expression plasmids

Wild-type (wt) DNPS genes were amplified from previously prepared pMAL-c2wt vectors [9, 11] and inserted into the pTagBFP-C vector (Evrogen, Russia). The vector pTagBFP_Y114-H_ADSL was prepared by introducing the mutation *c340T>C* (p.Y114H) into the initial vector pTagBFP_ADSL by using the GeneArt Site-Directed Mutagenesis System (Thermo Fisher Scientific) according to standard procedures. All sequences were verified by DNA sequencing.

Transfection

For transfection, 1 x 10^5 CRISPR-edited HeLa cells were transiently transfected with 1.5 μg of constructs using the Neon® Transfection System (Thermo Fisher Scientific) with the following parameters: pulse voltage: 1400 V, pulse width: 20 ms, number of pulses: 2, tip type: 10 μl and seeded on 1.7 cm^2 glass chamber slides (Thermo Fisher Scientific). After 24 h, the cells were washed and subsequently incubated with purine-depleted or purine-rich medium. After another 24 h, immunofluorescence labelling was performed. PAICS-, PFAS-, ADSL- and ATIC- deficient cells transfected with wt proteins were grown on 6-well plates for 24 h in purine-depleted medium and then tested for DNPS substrate accumulation by LC-MS/MS as described previously [9]. The cells were not synchronized for the cell cycle.

Immunofluorescence

For immunofluorescence labelling, the cells were fixed with 4% paraformaldehyde in PBS, permeabilized in 0.1% TRITON, washed, blocked with 5% BSA in PBS and incubated in a humidified chamber for 1 h at 37˚C with the following primary antibodies: rabbit polyclonal IgG anti-PPAT (Sigma-Aldrich), mouse polyclonal IgG anti-GART (Abnova, Taiwan), and mouse monoclonal IgG2κ anti-PAICS (Sigma-Aldrich). For fluorescence detection, species-appropriate Alexa Fluor® 488 and 555 secondary antibodies (Thermo Fisher Scientific) were used. Slides were mounted with ProLong® Gold Antifade Mountant (Thermo Fisher Scientific) as the fluorescence mounting medium and analysed by confocal microscopy. All immunofluorescence experiments were repeated at least twice.

Image acquisition and analysis

The prepared slides were analysed by confocal microscopy. XYZ images were sampled according to the Nyquist criterion by using a LeicaSP8X laser scanning confocal microscope with an HC PL APO objective (63x, N.A. 1.40) and 405, 488 and 543 laser lines. The images were restored by a classic maximum likelihood restoration algorithm in Huygens Professional Software (SVI, Hilversum, The Netherlands) [12]. Colocalization maps with single-pixel overlap coefficient values ranging from 0–1 [13] were created in Huygens Professional Software. The resulting overlap coefficient values are presented in pseudocolour, and the scale is shown in the corresponding lookup tables (LUT). Image analysis was performed on at least ten cells from each cell type. The conditions for image acquisition were the same for all cells included in the experiment.

Results

Preparation of HeLa cells deficient in HGPRT (CR-HGPRT cells)

We knocked-out the *HPRT1* gene in HeLa cells using the CRISPR-Cas9 genome editing system. We detected positive clones via cDNA and gDNA sequencing, the thioguanine inhibition method and subsequent growth curves and activity assays (Fig 2). The homozygous mutation in the targeted gene *c. 373_378delTTAACT* (p. 125-126del) (Fig 2A) resulted in the expression of an HGPRT protein with undetectable enzyme activity (Fig 2B). The lack of HGPRT activity was also tested by establishing growth curves with and without the addition of 0.03 mM TG to the growth media. After the addition of TG, normal HeLa cells underwent cell death within 72 h (Fig 2C, dark blue), while CR-HGPRT cells survived for at least 6 days (Fig 2C, dark red). In normal medium, both cell types grew normally (Fig 2C, light red and blue).

Purinosome formation in CR-HGPRT cells

To determine whether mutations in the *HPRT1* gene affect the intracellular compartmentalization of DNPS proteins *in vivo*, we investigated purinosome formation in CR-HGPRT cells. We cultured HeLa cells for 24 h in purine-rich or purine-depleted media and immunolabelled the combination of the PPAT and GART enzymes. We observed purinosome formation independently of the amount of purines in the growth media (Fig 3A–3C and 3J–3L).

Transfection of knockout HeLa cells by constructs encoding wt proteins

We transiently transfected previously prepared HeLa cells with the knockout of individual DNPS genes (CR-DNPS cells) [9] and CR-HGPRT cells with vectors encoding pTagBFP-labelled wt proteins to restore or disrupt purinosome formation. We transfected HeLa cells deficient for GART (CR-GART) with the pTagBFP_wt GART vector (Fig 4), HeLa cells

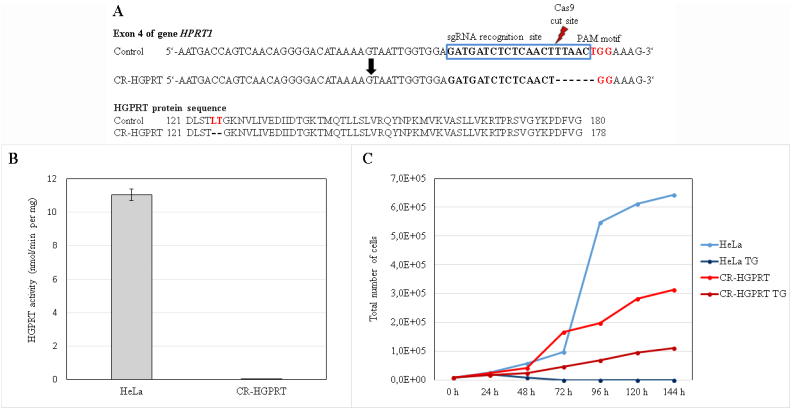

Fig 2. Characterization of the HGPRT knockout cells. (A): Illustration of the sgRNA targeting sequence in exon 4 of the *HPRT1* gene in control and CR-HGPRT cells and the protein sequences of wild-type and mutated HGPRT. The 20-bp target sgRNA sequence is indicated in the blue box, adjacent to the NGG (TGG) PAM motif sequence (red coloured). The probable Cas9 cut site is indicated by the red flash-shaped object. CR-HGPRT is shown with the appropriate c.373-378delTTAACT mutation. In the HGPRT protein sequence, the affected amino acids are coloured red; the CR-HGPRT protein shows a p. 125-126del deletion. (B): The activity of the HGPRT enzyme was determined in the control and CR-HGPRT cells. The activity of the enzyme in the CR-HGPRT cells was 0% of the activity in the control cells (n = 3). (C): Growth curves of CR-HGPRT cells and control HeLa cells. The cells were grown in normal growth medium and in growth medium containing 0.03 mM thioguanine (TG). The CR-HGPRT cells grew in the normal growth medium (light red line) and more slowly in the growth medium containing TG (dark red line). All the control cells in the medium containing TG died within 72 h (dark blue line), while the control cells in the normal medium showed ten times more growth at the same time point (light blue line).

https://doi.org/10.1371/journal.pone.0201432.g002

deficient for PFAS (CR-PFAS) with the pTagBFP_wt PFAS vector (Fig 5), HeLa cells deficient for PAICS (CR-PAICS) with the pTagBFP_wt PAICS vector (Fig 6), HeLa cells deficient for ADSL (CR-ADSL) with the pTagBFP_wt ADSL vector (Fig 7), HeLa cells deficient for ATIC (CR-ATIC) with the pTagBFP_wt ATIC vector (Fig 8), and CR-HGPRT cells with the pTagBFP_wt HGPRT vector (Fig 3).

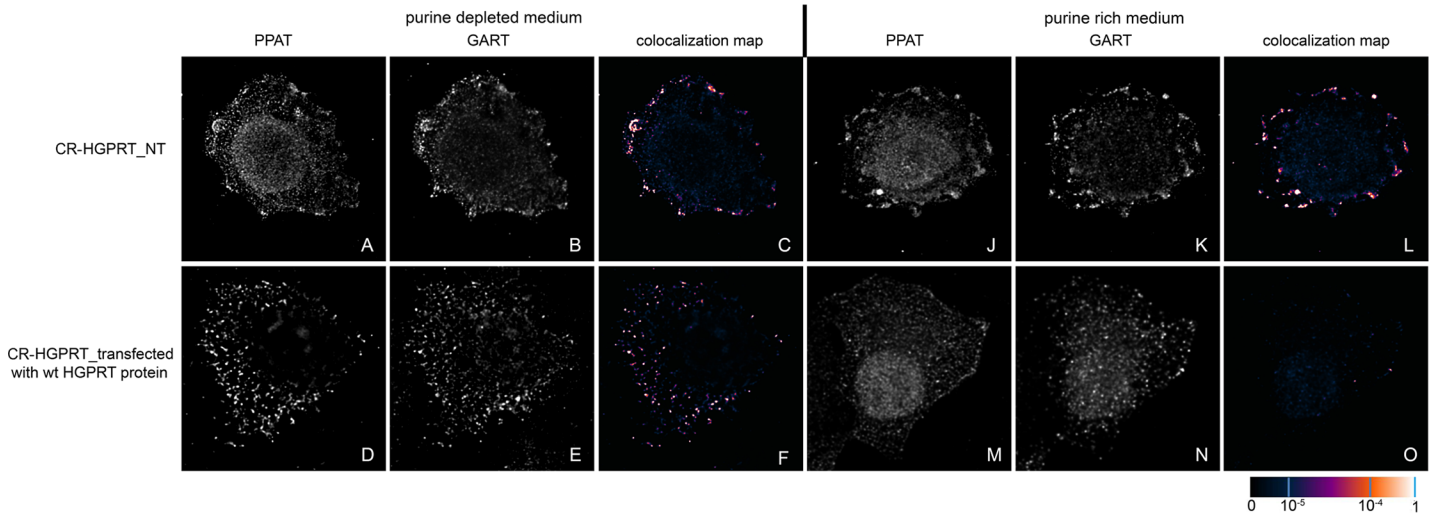

Fig 3. Immunodetection of GART and PPAT in CR-HGPRT cells. Non-transfected CR-HGPRT cells exhibited endogenous GART (B, K) and PPAT (A, J) proteins in the form of fine granules, and their fluorescent signals showed a high degree of overlap in both the purine-depleted medium (C) and the purine-rich medium (L). In cells transfected with a vector encoding the wt HGPRT protein, the endogenous proteins formed fine granules with high signal colocalization in the purine-depleted medium (D, F), whereas in the purine-rich medium, the proteins remained diffuse (M, N) with no colocalization (O). The values of the fluorescent signal overlaps are shown in pseudocolour, and the scale is shown at the lower right in the corresponding LUT.

https://doi.org/10.1371/journal.pone.0201432.g003

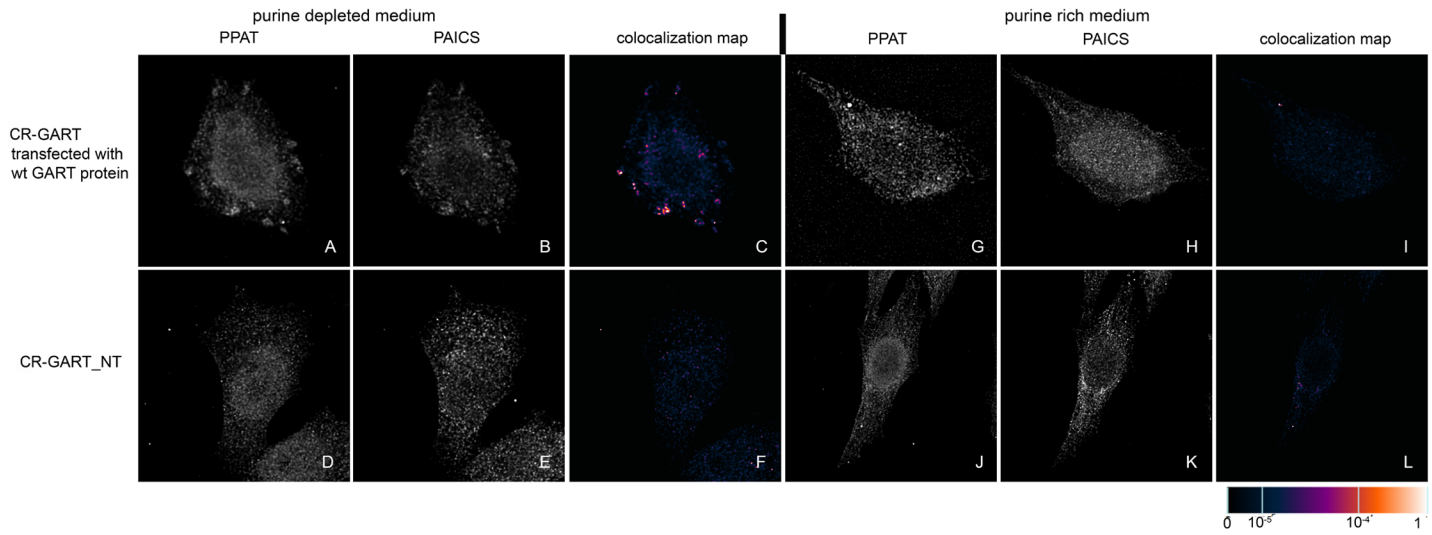

Fig 4. Immunochemical labelling of the endogenous proteins PPAT and PAICS in CR-GART cells transfected with constructs encoding wt-GART proteins. In cells transfected with constructs encoding the wt-GART protein, the endogenous proteins PPAT (A) and PAICS (B) were observed in the form of fine granules with their fluorescent signals showing a high degree of overlap in purine-depleted medium (C), whereas in purine-rich medium, the proteins PPAT (G) and PAICS (H) remained diffuse and did not colocalize (I). The same behaviour was observed in the control HeLa cells (Fig 9). Endogenous proteins in the non-transfected cells remained diffuse regardless of the level of purines in the media (D, E, J, K) and did not colocalize (F, L). The values of the fluorescent signal overlaps are shown in pseudocolour, and the scale is shown at the lower right in the corresponding LUT.

https://doi.org/10.1371/journal.pone.0201432.g004

All the transfected cells were grown in purine-rich and in purine-depleted medium. After 24 h, we immunofluorescently labelled and observed the colocalization of the DNPS protein phosphoribosyl pyrophosphate amidotransferase (PPAT) with GART (Figs 3 and 5–8) or with PAICS (CR-GART cell line, Fig 4). We observed the restoration of purinosome formation in CR-DNPS cells in the purine-depleted medium (Figs 4–8A–8C), whereas in the purine-rich

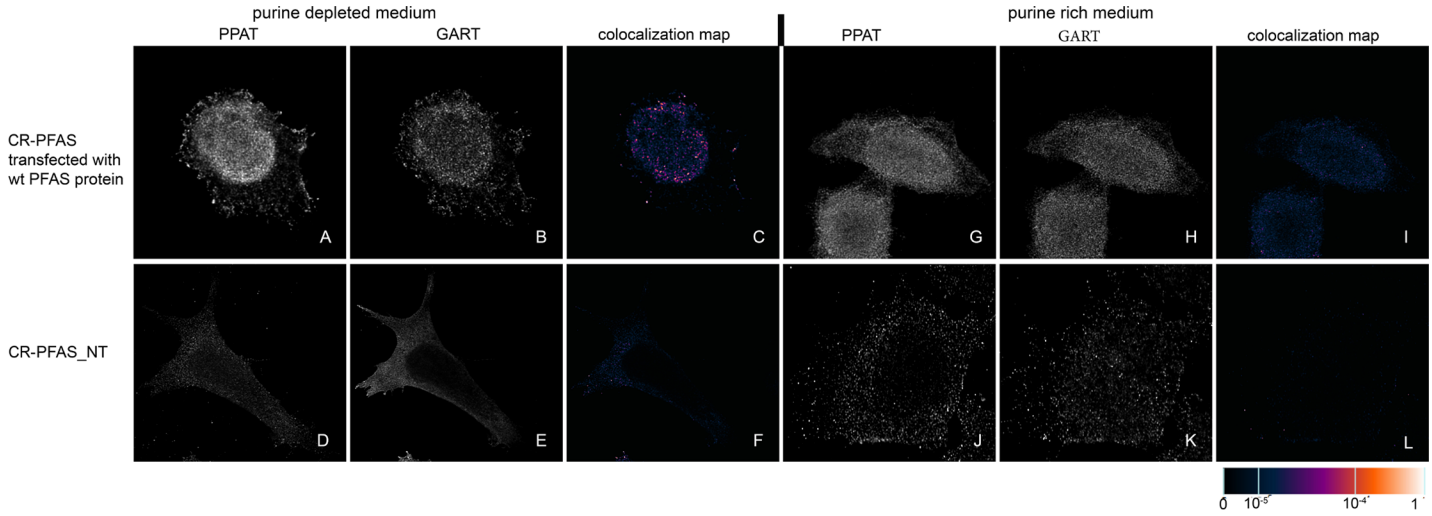

Fig 5. Immunodetection of PPAT and GART in CR-PFAS cells transfected with constructs encoding wt-PFAS proteins. In cells transfected with constructs encoding wt-PFAS protein, the endogenous proteins PPAT (A) and GART (B) were observed in the form of fine granules with their fluorescent signals showing a high degree of overlap in purine-depleted medium (C), whereas in purine-rich medium, the proteins PPAT (G) and GART (H) remained diffuse and did not colocalize (I). The same behaviour was observed in the control HeLa cells (Fig 9). When the cells were not transfected, the endogenous proteins remained diffuse regardless of the level of purines in the media (D, E, J, K) and did not colocalize (F, L). The values of the fluorescent signal overlaps are shown in pseudocolour, and the scale is shown at the lower right in the corresponding LUT.

https://doi.org/10.1371/journal.pone.0201432.g005

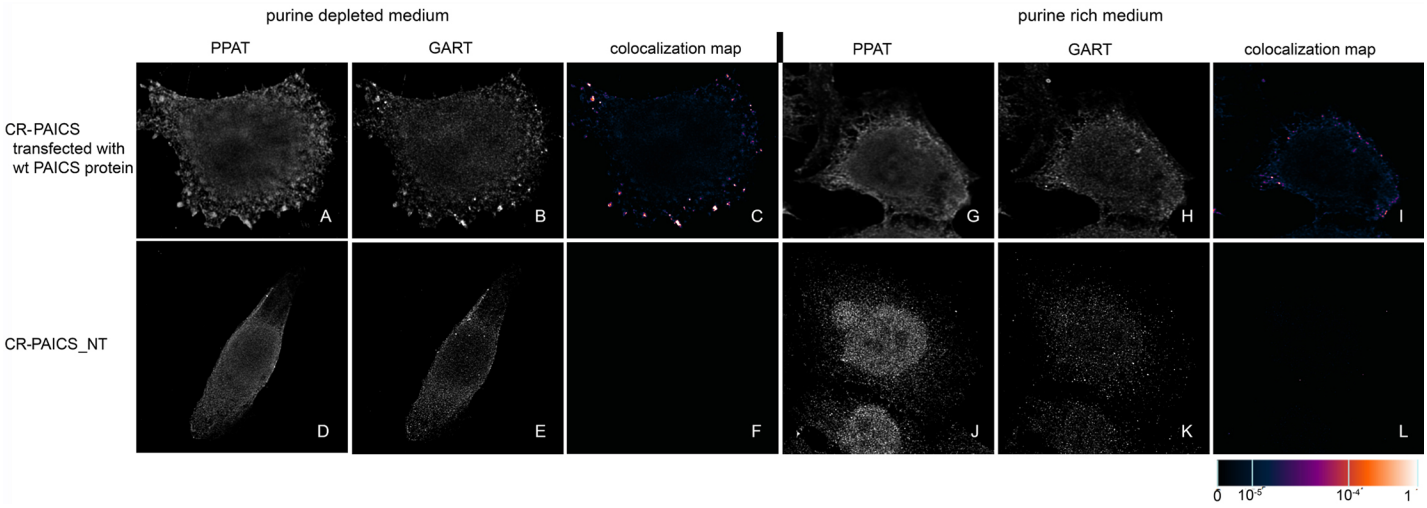

Fig 6. Immunodetection of PPAT and GART in CR-PAICS cells transfected with constructs encoding wt-PAICS proteins. In cells transfected with constructs encoding wt-PAICS protein, the endogenous proteins PPAT (A) and GART (B) were observed in the form of fine granules with their fluorescent signals showing a high degree of overlap in purine-depleted medium (C), whereas in purine-rich medium, the proteins PPAT (G) and GART (H) remained diffuse and did not colocalize (I). The same behaviour was observed in the control HeLa cells (Fig 9). Endogenous proteins in the non-transfected cells remained diffuse regardless of the level of purines in the media (D, E, J, K) and did not colocalize (F, L). The values of the fluorescent signal overlaps are shown in pseudocolour, and the scale is shown at the lower right in the corresponding LUT.

https://doi.org/10.1371/journal.pone.0201432.g006

medium, the proteins remained diffuse (Figs 4–8G–8I). In CR-HGPRT cells transfected with the pTagBFP_wt HGPRT vector, we observed the disruption of purinosome formation in the purine-rich medium (Fig 3M–3O), while purinosome formation remained unchanged in the purine-depleted medium (Fig 3D–3F). The control HeLa cells exhibited similar behaviour to the CR-DNPS and CR-HGPRT cells transfected with wt proteins (Fig 9). We also tested CR-PFAS, CR-PAICS, CR-ADSL and CR-ATIC cells grown in PD media and transfected with wt

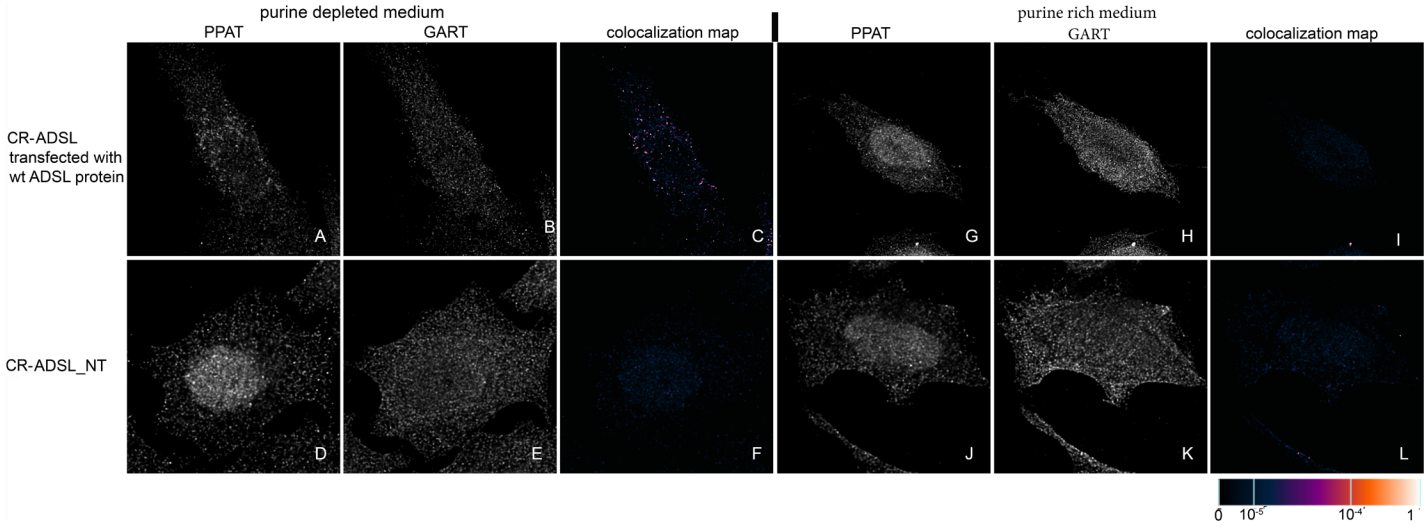

Fig 7. Immunodetection of PPAT and GART in CR-ADSL cells transfected with constructs encoding wt-ADSL proteins. In cells transfected with constructs encoding wt-ADSL protein, the endogenous proteins PPAT (A) and GART (B) were found in the form of fine granules with their fluorescent signals showing a high degree of overlap in purine-depleted medium (C), whereas in purine-rich medium, the proteins PPAT (G) and GART (H) remained diffuse and did not colocalize (I). The same behaviour was observed in the control HeLa cells (Fig 9). When the cells were not transfected, the endogenous proteins remained diffuse regardless of the level of purines in the media (D, E, J, K) and did not colocalize (F, L). The values of the fluorescent signal overlaps are shown in pseudocolour, and the scale is shown at the lower right in the corresponding LUT.

https://doi.org/10.1371/journal.pone.0201432.g007

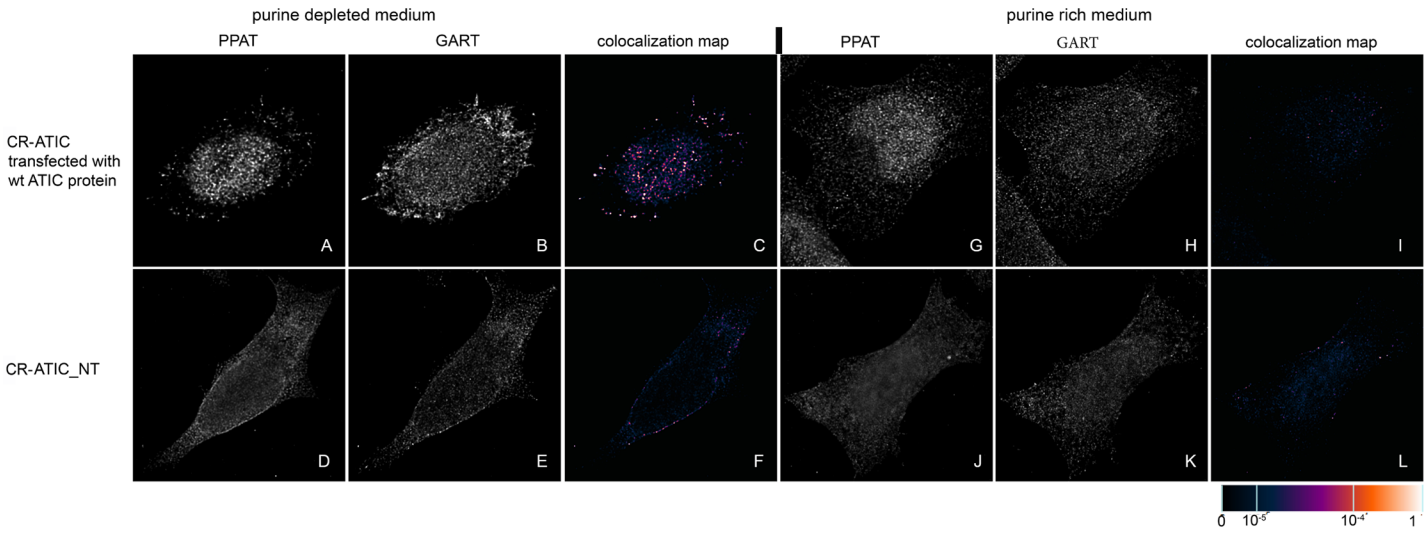

Fig 8. Immunodetection of PPAT and GART in CR-ATIC cells transfected with constructs encoding wt-ATIC proteins. In cells transfected with constructs encoding wt-ATIC protein, the endogenous proteins PPAT (A) and GART (B) were observed as fine granules with their fluorescent signals showing a high degree of overlap in purine-depleted medium (C), whereas in purine-rich medium, the proteins PPAT (G) and GART (H) remained diffuse and did not colocalize (I). The same behaviour was observed in the control HeLa cells (Fig 9). When the cells were not transfected, the endogenous proteins remained diffuse regardless of the level of purines in the media (D, E, J, K) and did not colocalize (F, L). The values of the fluorescent signal overlaps are shown in pseudocolour, and the scale is shown at the lower right in the corresponding LUT.

https://doi.org/10.1371/journal.pone.0201432.g008

proteins for DNPS substrate accumulation in the cell lysates. The levels of N-formylglycinamide ribotide/riboside (FGAR/r) decreased after pTagBFP_wt PFAS vector transfection in CR-PFAS. Decreases were also observed in aminoimidazole ribotide/riboside (AIR/r) after pTagBFP_wt PAICS vector transfection in the CR-PAICS cells, succinylaminoimidazolecarboxamide ribotide/riboside (SAICAR/r) and succinyladenosine monophosphate (SAMP)/succinyladenosine (S-Ado) after pTagBFP_wt ADSL vector transfection in CR-ADSL cells and aminoimidazolecarboxamideribotide/riboside (AICAR/r) after pTagBFP_wt ATIC vector transfection in CR-ATIC cells (Table 1, S1 Fig).

Transfection of ADSL-deficient HeLa cells by a mutant ADSL protein

As a control to examine whether cells undergoing transient transfection and nutrition starvation formed purinosomes or stress bodies, we transfected CR-ADSL cells with the

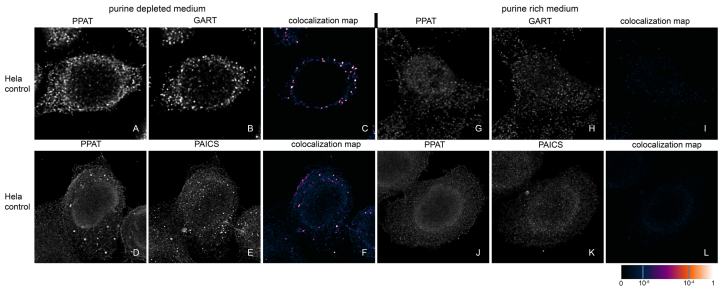

Fig 9. Immunodetection of PPAT, GART and PAICS in control HeLa cells. Control HeLa cells were immunolabelled with PPAT and GART (A, B, C, G, H, I) or with PPAT and PAICS (D, E, F, J, K, L). Both combinations of the endogenous proteins formed granules (A, B, D, E) with high signal colocalization in the purine-depleted medium (C, F), whereas in the purine-rich medium, the proteins remained diffuse (G, H, J, K) with no colocalization (I, L). The values of the fluorescent signal overlaps are shown in pseudocolour, and the scale is shown at the lower right in the corresponding LUT.

https://doi.org/10.1371/journal.pone.0201432.g009

Table 1. Purine metabolites in cell lysates of non-transfected (non TR) and wt transfected (TR) CR-cells (n = 3).

	HeLa	CR-PFAS		CR-PAICS		CR-ADSL		CR-ATIC	
metabolite	μmol/l	non TR μmol/l	TR μmol/l	non TR μmol/l	TR μmol/l	non TR μmol/l	TR μmol/l	non TR μmol/l	TR μmol/l
FGAr	nd	12.1±2.1	0.32±0.22	0.28±0.06	nd	nd	nd	nd	nd
FGAR	nd	2.1±0.9	0.07±0.06	0.13±0.04	nd	nd	nd	nd	nd
AIr	nd	nd	nd	1.0±0.1	0.004±0.001	nd	nd	nd	nd
AIR	nd	nd	nd	2.93±0.16	0.33±0.01	nd	nd	nd	nd
SAICAr	nd	nd	nd	nd	nd	0.40±0.04	0.072±0.002	0.05±0.01	≈ LOQ
SAICAR	nd	nd	nd	nd	nd	0.21±0.03	nd	nd	nd
S-Ado	≈ LOQ	≈ LOQ	≈ LOQ	≈ LOQ	≈ LOQ	10.5±1.1	1.9±0.2	≈ LOQ	≈ LOQ
SAMP	≈ LOQ	≈ LOQ	≈ LOQ	nd	nd	22.7±2.5	nd	nd	nd
AICAr	nd	nd	nd	nd	nd	nd	nd	0.09±0.03	nd
AICAR	nd	nd	nd	nd	nd	nd	nd	1.2±0.4	nd

nd–not detected

≈ LOQ—Values close to limit of quantification.

https://doi.org/10.1371/journal.pone.0201432.t001

pTagBFP_Y114H_ADSL vector encoding the ADSL enzyme with the mutation Y114H. This mutation is one of the most common mutations in patients suffering ADSL deficiency and results in zero enzyme activity [10]. We used the same conditions as for the transfection of the pTagBFP_wt ADSL vector into the CR-ADSL cells. We observed that the immunofluorescently labelled endogenous proteins remained diffuse regardless of the quantity of purines in the growth media (Fig 10).

Discussion and conclusions

Purinosomes have previously been detected in cells [3], but the argument was made that they may be artefacts of the constructs used for visualisation [4]. Both conclusions seemed possible depending on the cell state and the method of observation. The aim of this work was to detect purinosome formation by two previously described methods in non-purinosome-forming cells and in cells that form purinosomes regardless of purine levels. Furthermore, we aimed to determine the suitability of these systems for purinosome studies.

We built upon findings that purinosome formation is disrupted in fibroblasts deficient in ADSL and ATIC [8], which are affected by the flow of DNPS intermediates. By contrast, purinosome formation is increased in fibroblasts that are deficient in HGPRT, which results in a nonfunctional salvage pathway and therefore primarily depends on DNPS to generate purine nucleotides [14].

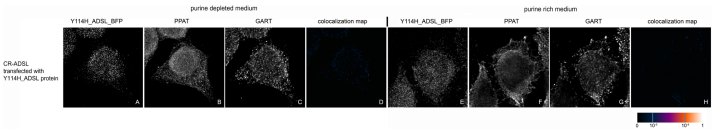

Fig 10. Immunochemical labelling of the endogenous proteins GART and PPAT in CR-ADSL cells transfected with a construct encoding a mutant inactive protein, p.Y114H ADSL. CR-ADSL cells were transfected with a vector encoding the BFP-labelled inactive protein p.Y114H ADSL (A, E) and seeded in purine-depleted medium (A, B, C, D) or purine-rich medium (E, F, G, H). The endogenous proteins PPAT (B, F) and GART (C, G) remained diffuse, and the signals did not colocalize, regardless of the amount of purines in the growth media (D, H). The values of the fluorescent signal overlaps are shown in pseudocolour, and the scale is shown at the lower right in the corresponding LUT.

https://doi.org/10.1371/journal.pone.0201432.g010

In our previous study, we introduced knockouts of individual DNPS genes into HeLa cells, in which we observed disrupted or greatly reduced purinosome formation (CR-DNPS cells) [9]. In this work, we prepared a CRISPR-Cas9-edited model HeLa cell system in which the purinosome forms independently of the purine level in the growth medium (CR-HGPRT cells).

Using the existing purinosomes-free systems, we checked whether purinosome assembly was restored in CR-DNPS cells grown in purine-depleted medium after transfection with vectors encoding BFP-labelled wt GART, PFAS, PAICS, ADSL or ATIC proteins. We also tested whether purinosome formation was affected in CR-HGPRT cells grown in purine-rich medium after transfection with a vector encoding BFP-labelled wt HGPRT protein.

To demonstrate purinosome formation, we used confocal microscopy and applied an established method of signal colocalization analysis based on single-pixel overlap coefficient values [13]. As the causal genetic defects often affect the amount of the corresponding mutant protein *in vivo*, we studied the intracellular localization of selected combinations of endogenous DNPS enzymes. Using this approach, we detected shared compartmentalization and spatial overlaps that suggested purinosome formation.

Purinosome formation in CR-DNPS cells transfected with constructs encoding wt DNPS proteins was restored to the level in the control HeLa cells in purine-depleted medium, whereas in purine-rich medium, the proteins remained diffuse. To prove that the structural bodies observed were real purinosomes, we transfected ADSL-deficient cells with a vector encoding a mutated ADSL protein (p.Y114H) with low enzyme activity [10]. We did not observe any purinosome assembly, and the proteins remained diffuse. This result is consistent with our knowledge that the fibroblasts of patients with the ADSL mutation Y114H likewise do not form purinosomes [8]. Based on these data, we conclude that purinosome formation by endogenous proteins can be restored by transiently introduced constructs encoding wt proteins. Furthermore, the restoration of purinosome function was verified in CR-DNPS cell lines transfected with wt proteins by measuring the level of substrates normally accumulated by deficient cells [9]. After transfection, substrate accumulation was significantly reduced or not detected.

HGPRT-deficient model cells transfected with a construct encoding the wt HGPRT protein ceased to form purinosomes in a purine-rich medium, which corresponds to the behaviour of healthy HeLa cells. This result supports the theory that the bodies observed are putative purinosomes.

We conclude that both methods, transient transfection and immunofluorescence, are useful for the detection of purinosome formation in HeLa cells. Moreover, the HGPRT knockout model of HeLa cells provides the ability to study purinosome formation in purine-rich medium without the need to expose the cells to stress conditions involving dialyzed and therefore nutrient-depleted growth media.

Cell-based models with specific deficiencies in the DNPS or salvage pathway provide a unique system for evaluating the efficacy and selectivity of DNPS inhibitors and activators at the biochemical level and the purinosome assembly level. The purinosome is a higher level of organization and regulation of metabolic enzymes in purine biosynthesis, and selective DNPS modulators can be used to better understand the role of its formation in both normal and disease states. This approach is a promising step toward the treatment of DNPS disorders and could provide a target for the treatment of cancer in which purine synthesis plays an essential role [15].

Supporting information

S1 Fig. LC-MS/MS chromatograms of purine metabolites in non-transfected and wt transfected CR-cell lines. Metabolites in non-transfected cells are labelled with a dashed line and in

transfected cells with a full line. The decrease in FGAR/r levels after pTagBFP_wt PFAS vector transfection in CR-PFAS cell lysate is shown in (A). The decrease in AIR/r levels after pTagBFP_wt PAICS vector transfection in CR-PAICS cell lysate is shown in (B). The decrease in SAICAR/r and SAMP/SAdo levels after pTagBFP_wt ADSL vector transfection in CR-ADSL cell lysate is shown in (C). The decrease in AICAR/r levels after pTagBFP_wt ATIC vector transfection in CR-ATIC cell lysate is demonstrated in (D).
(TIF)

Acknowledgments

The authors acknowledge Jana Sovova for the immunochemical staining of the cells.

We are grateful for access to computing and storage facilities owned by parties and projects contributing to the National Grid Infrastructure MetaCentrum provided under the programme "Projects of Large Research, Development, and Innovations Infrastructures" (CESNET LM2015042).

Author Contributions

Data curation: Stanislav Kmoch.

Formal analysis: Vaclava Skopova, Olga Souckova, Matyas Krijt.

Investigation: Veronika Baresova, Vaclava Skopova, Olga Souckova, Matyas Krijt, Stanislav Kmoch, Marie Zikanova.

Methodology: Veronika Baresova, Vaclava Skopova, Olga Souckova, Matyas Krijt.

Project administration: Marie Zikanova.

Software: Veronika Baresova.

Supervision: Marie Zikanova.

Validation: Veronika Baresova.

Visualization: Veronika Baresova.

Writing – original draft: Veronika Baresova.

Writing – review & editing: Marie Zikanova.

References

1. Jurecka A, Zikanova M, Kmoch S, Tylki-Szymanska A. Adenylosuccinate lyase deficiency. J Inherit Metab Dis. 2015; 38(2):231–42. https://doi.org/10.1007/s10545-014-9755-y PMID: 25112391
2. Pedley AM, Benkovic SJ. A New View into the Regulation of Purine Metabolism: The Purinosome. Trends Biochem Sci. 2017; 42(2):141–54. https://doi.org/10.1016/j.tibs.2016.09.009 PMID: 28029518
3. An S, Kumar R, Sheets ED, Benkovic SJ. Reversible compartmentalization of de novo purine biosynthetic complexes in living cells. Science. 2008; 320(5872):103–6. https://doi.org/10.1126/science.1152241 PMID: 18388293
4. Zhao A, Tsechansky M, Ellington AD, Marcotte EM. Revisiting and revising the purinosome. Mol Biosyst. 2014; 10(3):369–74.
5. An S, Deng Y, Tomsho JW, Kyoung M, Benkovic SJ. Microtubule-assisted mechanism for functional metabolic macromolecular complex formation. Proc Natl Acad Sci U S A. 2010; 107(29):12872–6. https://doi.org/10.1073/pnas.1008451107 PMID: 20615962
6. French JB, Jones SA, Deng H, Pedley AM, Kim D, Chan CY, et al. Spatial colocalization and functional link of purinosomes with mitochondria. Science. 2016; 351(6274):733–7. https://doi.org/10.1126/science.aac6054 PMID: 26912862

7. Chan CY, Zhao H, Pugh RJ, Pedley AM, French J, Jones SA, et al. Purinosome formation as a function of the cell cycle. Proc Natl Acad Sci U S A. 2015; 112(5):1368–73. https://doi.org/10.1073/pnas.1423009112 PMID: 25605889
8. Baresova V, Skopova V, Sikora J, Patterson D, Sovova J, Zikanova M, et al. Mutations of ATIC and ADSL affect purinosome assembly in cultured skin fibroblasts from patients with AICA-ribosiduria and ADSL deficiency. Hum Mol Genet. 2012; 21(7):1534–43. https://doi.org/10.1093/hmg/ddr591 PMID: 22180458
9. Baresova V, Krijt M, Skopova V, Souckova O, Kmoch S, Zikanova M. CRISPR-Cas9 induced mutations along de novo purine synthesis in HeLa cells result in accumulation of individual enzyme substrates and affect purinosome formation. Mol Genet Metab. 2016; 119(3):270–7. https://doi.org/10.1016/j.ymgme.2016.08.004 PMID: 27590927
10. Zikanova M, Skopova V, Hnizda A, Krijt J, Kmoch S. Biochemical and structural analysis of 14 mutant adsl enzyme complexes and correlation to phenotypic heterogeneity of adenylosuccinate lyase deficiency. Hum Mutat. 2010; 31(4):445–55. https://doi.org/10.1002/humu.21212 PMID: 20127976
11. Kmoch S, Hartmannova H, Stiburkova B, Krijt J, Zikanova M, Sebesta I. Human adenylosuccinate lyase (ADSL), cloning and characterization of full-length cDNA and its isoform, gene structure and molecular basis for ADSL deficiency in six patients. Hum Mol Genet. 2000; 9(10):1501–13. PMID: 10888601
12. Landmann L. Deconvolution improves colocalization analysis of multiple fluorochromes in 3D confocal data sets more than filtering techniques. J Microsc. 2002; 208(Pt 2):134–47. PMID: 12423263
13. Manders EMM, Verbeek FJ, Aten JA. Measurement of colocalization of objects in dual-color confocal images. J Microsc-Oxford. [Article]. 1993; 169:375–82.
14. Fu R, Sutcliffe D, Zhao H, Huang X, Schretlen DJ, Benkovic S, et al. Clinical severity in Lesch-Nyhan disease: the role of residual enzyme and compensatory pathways. Mol Genet Metab. 2015; 114(1):55–61. https://doi.org/10.1016/j.ymgme.2014.11.001 PMID: 25481104
15. Parker WB. Enzymology of purine and pyrimidine antimetabolites used in the treatment of cancer. Chem Rev. 2009; 109(7):2880–93. https://doi.org/10.1021/cr900028p PMID: 19476376

Příloha č. 5

Original Article

Metabolic Tools for Identification of New Mutations of Enzymes Engaged in Purine Synthesis Leading to Neurological Impairment

(de novo purine synthesis / aminoimidazole ribotide / 5-formamidoimidazole-4-carboxamide ribotide / PAICS / PFAS)

M. KRIJT, O. SOUCKOVA, V. BARESOVA, V. SKOPOVA, M. ZIKANOVA

Research Unit for Rare Diseases, Department of Paediatrics and Adolescent Medicine, First Faculty of Medicine, Charles University and General University Hospital, Prague, Czech Republic

Abstract. The cellular pool of purines is maintained by *de novo* purine synthesis (DNPS), recycling and degradation. Mutations in genes encoding DNPS enzymes cause their substrates to accumulate, which has detrimental effects on cellular division and organism development, potentially leading to neurological impairments. Unspecified neurological symptoms observed in many patients could not be elucidated even by modern techniques. It is presumable that some of these problems are induced by dysfunctions in DNPS enzymes. Therefore, we determined the concentrations of dephosphorylated DNPS intermediates by LC-MS/MS as markers of yet unpublished mutations in *PFAS* and *PAICS* genes connected with dysfunctions of carboxylase/phosphoribosylaminoimidazolesuccinocarboxamide synthase (PAICS) or phosphoribosylformylglycinamidine synthase (PFAS). We determined the criteria for normal values of metabolites and investigated 1,447 samples of urine and 365 dried blood spots of patients suffering from various forms of neurological impairment. We detected slightly elevated aminoimidazole riboside (AIr) concentrations in three urine samples and a highly elevated 5-formamidoimidazole-4-carboxamide riboside (FGAr) concentration in one urine sample. The accumulation of AIr or FGAr in body fluids can indicate PAICS or PFAS deficiency, respectively, which would be new disorders of DNPS caused by mutations in the appropriate genes. Measurement of DNPS intermediates in patients with neurological symptoms can uncover the cause of serious cellular and functional impairments that are otherwise inaccessible to detection. Further genetic and molecular analysis of these patients should establish the causal mutations for prenatal diagnosis, genetic consultation, and reinforce the DNPS pathway as a therapeutic target.

Received May 30, 2019. Accepted June 104, 2019.

This work was supported by grant AZV 15-28979A from the Ministry of Health, Czech Republic.

Corresponding author: Marie Zikanova, Department of Paediatrics and Adolescent Medicine, First Faculty of Medicine, Charles University and General University Hospital, Prague, Czech Republic, Ke Karlovu 2, 121 08 Prague 2, Czech Republic, E-mail: marie.zikanova@lf1.cuni.cz

Abbreviations: ADSL – adenylosuccinate lyase, AICAR/r – aminoimidazole carboxyamide ribotide/riboside, AIR/r – aminoimidazole ribotide/riboside, ATIC – 5-aminoimidazole-4-carboxamide ribonucleotide transformylase/inosine monophosphate cyclohydrolase, CAIR/r – carboxyaminoimidazole ribotide/riboside, CSF – cerebrospinal fluid, DBS – dry blood spot, DNPS – *de novo* purine synthesis, FAICAR/r – 5-formamidoimidazole-4-carboxamide ribotide/riboside, FGAM – formylglycineamidine ribotide, FGAR/r – formylglycineamide ribotide/riboside, GAR/r – glycineamide ribotide/riboside, GART – glycinamide ribonucleotide synthetase/aminoimidazole ribonucleotide synthetase/glycinamide ribonucleotide transformylase, HPLC – high-performance liquid chromatography, IMP – inosine monophosphate, LC-MS/MS – liquid chromatography tandem mass spectrometry, PAICS – phosphoribosylaminoimidazole carboxylase/ phosphoribosylaminoimidazolesuccinocarboxamide synthase, PFAS – phosphoribosylformylglycinamidine synthase, PPAT – amidophosphoribosyltransferase, SAdo – succinyladenosine, SAICAR/r – succinylaminoimidazolecarboxamide ribotide/riboside

Introduction

Purines are essential molecules for nucleic acid synthesis and universal carriers of chemical energy in all dividing cells (Yin et al., 2018). The cellular metabolism of purines is managed by *de novo* purine synthesis (DNPS), salvage pathways and purine degradation. DNPS is one of the metabolic pathways crucial to cell division and to neural development. Mutations in genes encoding DNPS enzymes may lead to congenital neurological disorders. DNPS includes 10 reactions, in which six enzymes are involved, with three of them being multifunctional (Fig. 1). DNPS enzymes are organized into

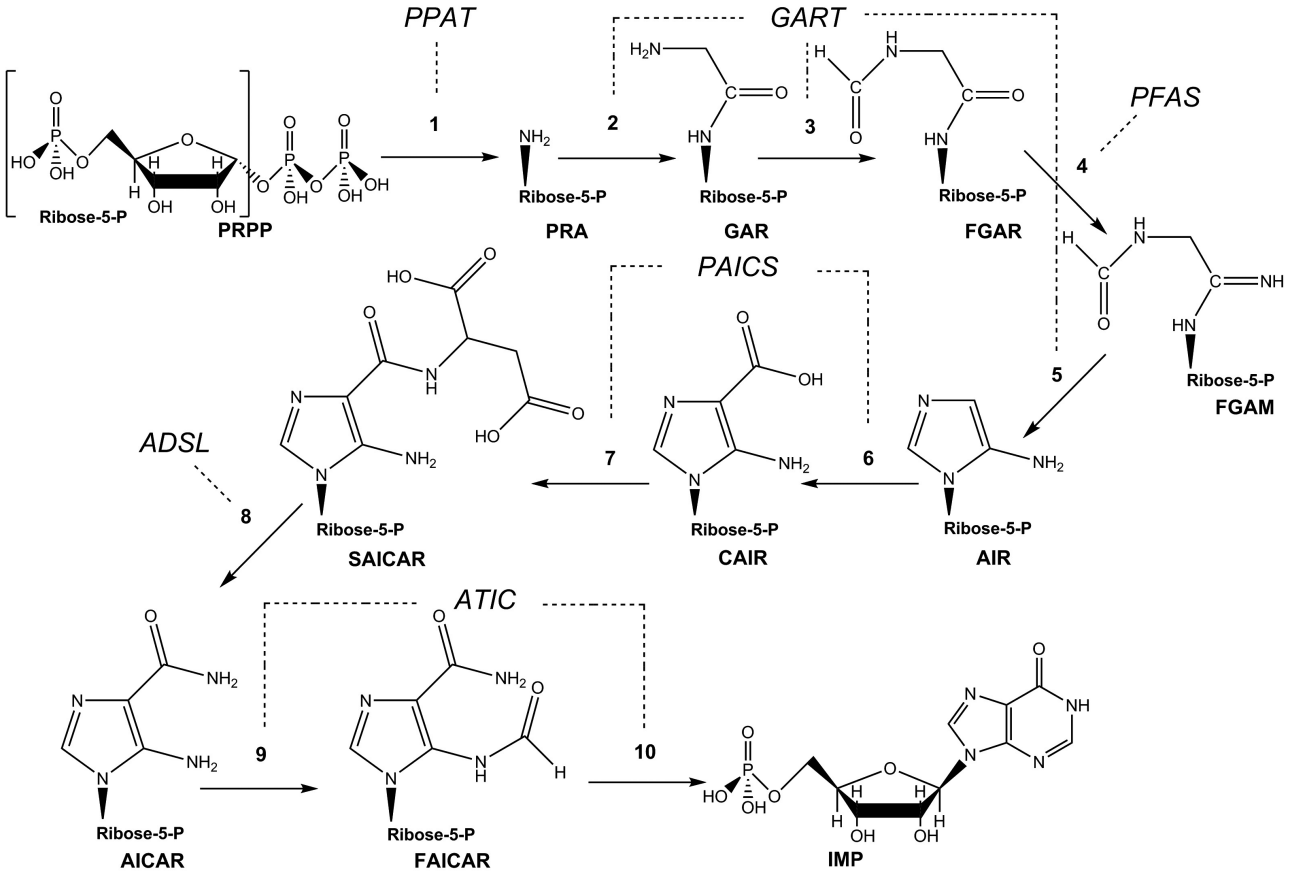

Fig. 1. Scheme of *de novo* purine synthesis (DNPS)
Phosphoribosylpyrophosphate (PRPP) substrate is metabolized by enzyme amidophosphoribosyl transferase (PPAT) to phosphoribosylamine (PRA) in the step 1. Steps 2, 3 and 5 are catalysed by trifunctional enzyme glycinamide ribonucleotide synthetase/aminoimidazole ribonucleotide synthetase/glycinamide ribonucleotide transformylase (GART). In step **2**, the whole molecule of glycine is connected to the amine group of PRA, resulting into glycineamide ribotide (GAR). The N^{10}-formyl tetrahydrofolate provides the formyl group to produce formylglycineamide ribotide (FGAR) during step **3**. In step **4**, the enzyme phosphoribosylformylglycinamidine synthase (PFAS) exchanges the oxo group of FGAR for the imino group provided by glutamine in order to create formylglycineamidine ribotide (FGAM). Step **5** leads to cyclization of FGAM into aminoimidazole ribotide (AIR). Steps **6** and **7** are catalysed by bifunctional enzyme phosphoribosylaminoimidazole carboxylase/ phosphoribosylaminoimidazolesuccinocarboxamide synthase (PAICS), which produces carboxyaminoimidazole ribotide (CAIR) and succinylaminoimidazolecarboxyamide ribotide (SAICAR), respectively. The bifunctional enzyme adenylosuccinate lyase (ADSL) catalysis occurs in step **8**, when the cleavage of fumarate from SAICAR occurs and forms aminoimidazolecarboxamide ribotide (AICAR). Steps **9** and **10** are catalysed by bifunctional enzyme 5-aminoimidazole-4-carboxamide ribonucleotide transformylase/inosine monophosphate cyclohydrolase (ATIC), which forms 5-formamidoimidazole-4-carboxamide ribotide (FAICAR) and inosine monophosphate (IMP), respectively.

a multienzyme complex called purinosome (An et al., 2008; Baresova et al., 2012). To date, two genetic defects in DNPS have been described: adenylosuccinate lyase (ADSL) deficiency (OMIM 103050) (Van den Berghe and Jaeken, 1986) and AICA-ribosiduria (OMIM 608688) (Marie et al., 2004). Both of these deficiencies result in serious damage of cellular homeostasis and functions manifested as neurological symptoms present at birth, causing accumulation of substrate(s) for the defected enzyme in cellular models or body fluids such as urine, plasma and/or cerebrospinal fluid (CSF) (Van den Bergh et al., 1991; Baresova et al., 2016).

The ADSL enzyme (ADSL, EC 4.3.2.2) catalyses the eighth reaction of DNPS (Fig. 1) and the second reaction of the purine nucleotide cycle. Mutations in this enzyme lead to ADSL deficiency (Kmoch et al., 2000). The cellular impairment clinically manifests in various disabilities classified as three basic types: (1) a neonatal form consisting of prenatal hyperkinesia, pulmonary hypoplasia and prenatal abortion of growth, followed by fatal neonatal encephalopathy and early death (Mouchegh et al., 2007); (2) a severe infantile form associated with severe psychomotor retardation and frequently with early death (Jaeken et al., 1988); (3) a mild/moderate form associated with less severe psychomotor retardation, hypotony and autism (Jaeken et al., 1988). The biochemical diagnostics of this condition is based on the detection of two dephosphorylated substrates of ADSL

– succinyladenosine (SAdo) and succinylaminoimidazolecarboxamide riboside (SAICAr). These substrates can be measured in the urine, plasma and/or CSF (Van den Bergh et al., 1991; Krijt et al., 2013). The genetic diagnosis of this condition is made through the detection of mutations in the *ADSL* gene (Jurecka et al., 2015).

AICA-ribosiduria is a recently identified autosomal recessive inherited disorder of DNPS (Marie et al., 2004). The cause of this condition is deficiency of bifunctional enzyme ATIC-5-aminoimidazole-4-carboxamide ribonucleotide transformylase (EC 2.1.2.3)/inosine monophosphate cyclohydrolase (EC 3.5.4.10), which catalyses the last two reactions of DNPS (Fig. 1). Similarly to patients with ADSL deficiency, the dephosphorylated substrate of the defective ATIC enzyme, aminoimidazolecarboxamide riboside (AICAr), accumulates in body fluids. SAICAr and SAdo accumulate as well, but at a lower level than in ADSL deficiency. The main pathogenic mechanism of ADSL and ATIC deficiencies has been attributed to the cytotoxicity of the accumulated dephosphorylated substrates (Stone et al., 1998; Marie et al., 2004; Jurecka et al., 2015).

To date, no other genetically determined defects of the DNPS pathway have been identified. However, the existence of such defects is highly probable. It is hypothesized that these defects will similarly manifest as nonspecific neurological symptoms accompanied by accumulation of DNPS intermediates in body fluids. Based on this hypothesis, we previously prepared and characterized DNPS deficiencies in a HeLa cell model system (Baresova et al., 2016; Madrova et al., 2018). Accumulation of dephosphorylated substrate(s) of the defective enzyme occurred in four DNPS knock-out cell lines, with the exception of cells deficient in trifunctional enzyme GART – glycinamide ribonucleotide synthetase (EC 6.3.4.13)/aminoimidazole ribonucleotide synthetase (EC 6.3.3.1)/glycinamide ribonucleotide transformylase (EC 2.1.2.2).

The main problem in developing analytical methods for detection of DNPS defects is the lack of commercial availability of DNPS intermediates. In our previous work, we developed procedures for preparation of phosphorylated and dephosphorylated DNPS substrates, which we characterized and detected by LC-MS/MS (Madrova et al., 2018).

In the presented work, we established physiological levels of DNPS metabolites 5-formamidoimidazole-4-carboxamide riboside (FGAr), aminoimidazole riboside (AIr) and carboxyaminoimidazole riboside (CAIr) in 40 control urine samples and in 50 control dried blood spots (DBS), and detected these metabolites in 1,447 urine samples and in 365 DBS of patients with various undiagnosed neurological defects. FGAr can serve as a marker for mutations in *PFAS*, which encodes phosphoribosylformylglycinamidine synthase (PFAS, EC 6.3.5.3) – for the fourth reaction of DNPS (Fig. 1). AIr and CAIr are markers for mutations of *PAICS*, which encodes the phosphoribosylaminoimidazole carboxylase (EC 4.1.1.21)/phosphoribosylaminoimidazolesuccinocarboxamide synthase (EC 6.3.2.6) (PAICS) bifunctional enzyme – for the sixth and seventh reactions of DNPS (Fig. 1). We hypothesized that the cytotoxicity of these markers would lead to neurological impairment similar to ADSL and AICA-ribosiduria deficiencies. Recently, a study of PFAS and PAICS expression in the rat brain and hippocampal neurons suggests the possibility of direct influence on neuronal functions caused by the cytotoxicity of accumulated substrates due to DNPS enzymatic deficiencies (Williamson et al., 2017).

Material and Methods

Chemicals

All chemicals were purchased from Sigma-Aldrich (St. Louis, MO) unless otherwise stated in the text.

Preparation of DNPS intermediates

DNPS substrates FGAr, AIr, CAIr and SAdo-$^{13}C_4$ were synthesized utilizing human and bacterial recombinant enzymes as described previously (Zikanova et al., 2005; Baresova et al., 2016; Madrova et al., 2018).

Briefly, enzymes catalysing each individual step of DNPS were prepared and used for synthesis of DNPS intermediates. Ribotidic forms of DNPS substrates obtained in enzymatic reactions were dephosphorylated in potassium phosphate buffer, pH 8.0 with calf intestine phosphatase (CIP) (New England Biolabs, Ipswich, MA) to ribosidic forms.

Preparation of samples

Control and neurologically impaired samples were anonymized prior to analysis.

Urine samples

Urine creatinine measurements were performed in a standard manner. All samples were adjusted to a creatinine concentration of 1 mmol/l and frozen. Prior to the analysis, the defrosted samples were spun down for 60 s in a mini centrifuge in order to remove any residual proteins. The supernatant, with a volume of minimum 30 µl to maximum 200 µl, was then pipetted into the insert and embedded into an HPLC vial for the purpose of LC-MS/MS analyses.

Dried blood spots

From each DBS sample, three 3-mm diameter disks were punched from a Guthrie card and placed in 100 µl of extraction buffer containing acetonitrile : methanol : water (1 : 1 : 1 ratio) with 100 nmol/l SAdo-$^{13}C_4$ internal standard. Samples were incubated for 15 min in an ultrasonic bath. An 80 µl aliquot of the extract was transferred to a clean tube and centrifuged for 5 min at 8,000 *g*. The supernatant was evaporated to dryness under a stream of nitrogen, dissolved in 30 µl of LC-MS water and embedded into an HPLC vial for the purpose of LC-MS/MS analyses.

HPLC-MS/MS analysis

The Agilent 1290 Infinity LC System (Agilent Technologies, Palo Alto, CA) coupled with an API 4000 triple quadrupole mass spectrometer operated with Analyst software version 1.4 (Applied Biosystems, Foster City, CA) was applied for identification and quantification of all DNPS substrates. The separation was performed with Prontosil 120 – 3 C18 – AQ column (200*4 mm, 3 μm) (Bischoff Chromatography, Leonberg, Germany) at 30 °C. The gradient elution consisted of 0.1% formic acid solution in water (mobile phase A) and 0.1% formic acid solution in acetonitrile (mobile phase B). The flow rate of 400 μl/min was performed by changing % B as follows: 0.0–12.0 min: 0 % to 20 %, 12.0–13.0 min: 20 % to 60 %, 13.0–15.5 min: 60 %, 15.5–16.0 min: 60 to 0 %. The column was then regenerated with 100 % A for 9 min, with an increased flow rate 700 μl/min between 16.2 and 24.2 min. The injection sample volume was 5 μl. The parameters of MS detection were set as previously (Baresova et al., 2016).

Results

The aim of our work was to study the flux of DNPS intermediates under physiological conditions and its alteration under pathological conditions designated by neurological symptoms. The levels of DNPS intermediates FGAr, AIr and CAIr were determined by LC-MS/MS in the urine and DBS in patients with undiagnosed neurological impairment.

Linearity and limits of detection (LOD) and quantification (LOQ) were defined using signal-to-noise ratios of 3 : 1 and 10 : 1, respectively. We confirmed the linearity of the method by generating linear calibration curves with high correlation coefficients ($r^2 > 0.9911$) in the indicated concentration range (Table 1).

Reference values of metabolites in the urine and DBS were determined by analysis of 40 control urine samples and 50 control DBS samples. The physiological values of FGAr, AIr and CAIr detected in urine samples vary from tens to hundreds of nmol/l concentrations (Table 2). In DBS samples, only FGAr was detected; AIr and CAIr were below LOD.

Screening of DNPS metabolites was performed in 1,447 anonymized samples of urine and 365 samples of DBS of patients suffering from neurological disability (Fig. 2). We detected an elevated FGAr level (386 times vs controls) in one patient (Fig. 2A); the elevated FGAr levels may be a marker of defective PFAS enzyme. In three urine samples, we detected slightly elevated AIr levels, a marker for defective PAICS enzyme (Fig. 2C). In DBS samples, we did not detect any markedly elevated values of the analysed DNPS metabolites.

Discussion

Purines play irreplaceable roles in all living organisms, utilized as universal energy source and storage, coenzymes, neurotransmitters, basic building blocks of nucleic acids, as well as for signal transduction and enzyme activity alterations. DNPS supplies the organism with newly synthesized molecules of purines during times of higher purine consumption, such as cell division and development. This pathway consists of 10 reactions driven by six enzymes. Mutations in genes encoding enzymes of DNPS lead to genetically determined disorders with a primary effect on neurological functions and physiological growth. Detection and investigation of DNPS disorders is difficult due to the nonspecific nature of the neurological findings caused by cytotoxic accumulation of substrate(s) of deficient enzymes and by the absence of commercially available DNPS substrates for development of analytical methods. In the

Table 1. Limits of detection (LOD) and quantification (LOQ) of DNPS metabolites in the urine and DBS

	URINE		DBS	
	LOD [μmol/l]	**LOQ [μmol/l]**	**LOD [μmol/l]**	**LOQ [μmol/l]**
FGAr	0.001	0.004	0.05	0.16
AIr	0.023	0.076	0.03	0.11
CAIr	0.003	0.009	0.03	0.09

Table 2. Physiological ranges of DNPS intermediate concentration detected in the urine and DBS

	URINE [μmol/mmol creat.]			DBS [μmol/l]		
	min	**max**	**median**	**min**	**max**	**median**
FGAr	0.00	0.32	0.098	0.24	0.55	0.35
AIr	0.00	0.43	0.068	n.d.	n.d.	n.d.
CAIr	0.00	0.17	0.052	n.d.	n.d.	n.d.

n.d. – not detected

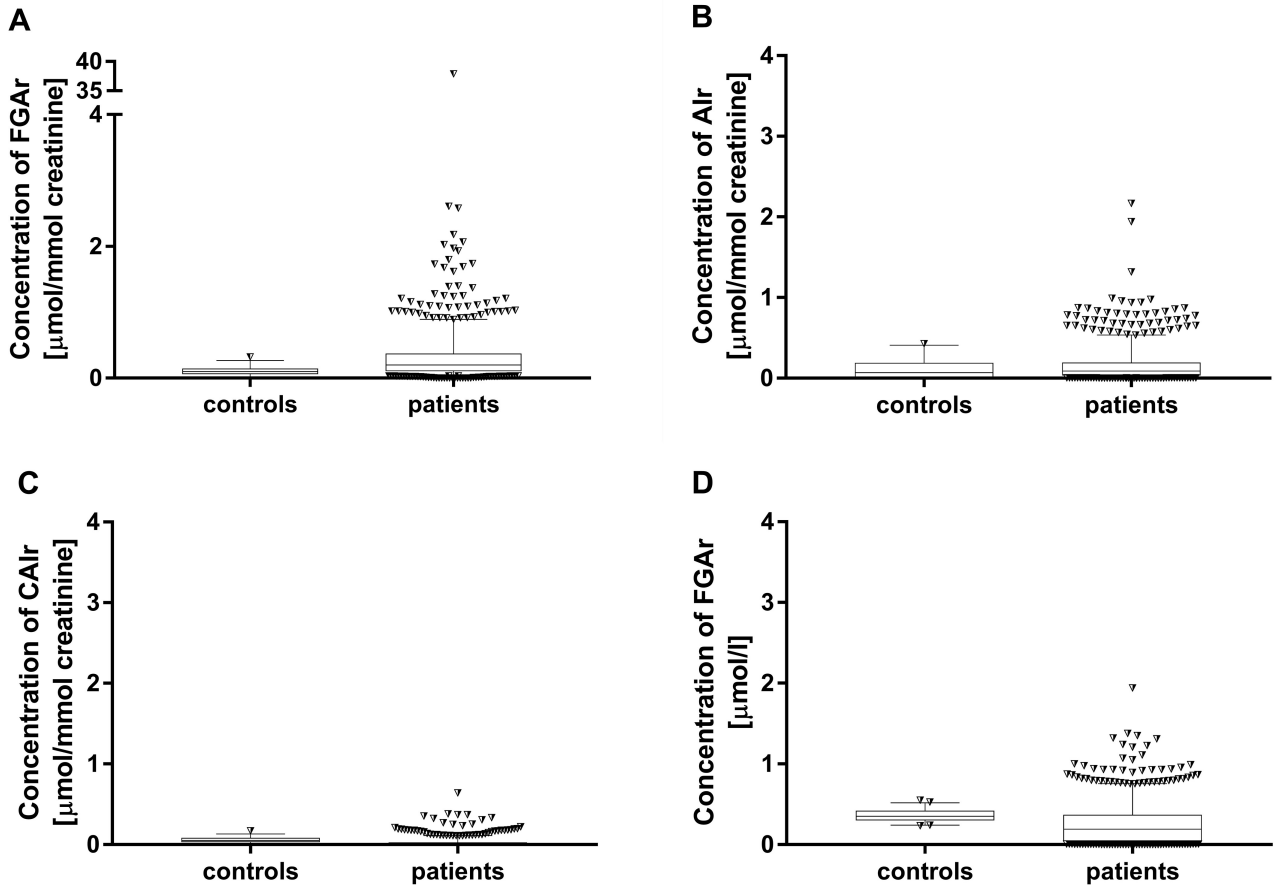

Fig. 2. *De novo* purine synthesis (DNPS) metabolites determined in urine samples and dried blood spots (DBS) Randomized urine samples of 40 controls and 1,447 patients with neurological impairment were screened for the presence of A/ formylglycineamide riboside (FGAr), B/ aminoimidazole riboside (AIr) and C/ carboxyaminoimidazole riboside (CAIr) metabolites by the HPLC-MS/MS method. With the same approach we also screened DBS samples of 50 controls and 365 patient samples; however, only D/ formylglycineamide riboside (FGAr) was detected. The box extends from the 25th to 75th percentiles with plotted median by the horizontal line, and whiskers mark the 5th and 95th percentiles.

case of severe phenotypes, mostly resulting in early death, the disease often remains undiagnosed (Mouchegh et al., 2007). This lack of diagnosis results in inadequate genetic counselling and inability to predict the outcomes of future pregnancies.

Furthermore, specialized laboratory investigation for metabolic disorders may not show satisfactory results due to the limited number of diagnostic methods that can detect DNPS disorders (Hartmann et al., 2006; Chrastina et al., 2007). Most of the specialized metabolic laboratories test only for ADSL deficiency, and rarely also AICA-ribosiduria. To date, no other genetically determined defects of DNPS enzymes have been identified. However, the range of the genetic variation provided in the gnomAD database indicates that, except for *PPAT,* there are no evolutionary constraints against loss of function or missense mutations in these genes in the population (Baresova et al., 2016). It can be anticipated that these mutations will be manifested by severe neurological impairment caused by the cytotoxicity of accumulated DNPS intermediates in body fluids, as shown in HeLa cell models (Baresova et al., 2016; Madrova et al., 2018).

In this work, we determined DNPS intermediates in the urine and DBS samples from patients with undiagnosed neurological impairment. We detected a higher urinary concentration of AIr in three samples and accumulation of FGAr in one sample. The accumulation of AIr or FGAr in body fluids can indicate mutations in the *PAICS* or *PFAS* gene and lead to the discovery of currently undiagnosed genetic disorders. Subsequently, AIr and FGAr nominate among applicable diagnostic markers.

Based on our results, we conclude that detection of DNPS intermediates, especially AIr and FGAr in patients with neurological symptoms, can show serious cellular and functional impairments resulting in novel metabolic defects of DNPS that have previously been inaccessible to detection. Genetic and molecular analysis of these patients should follow to establish the causal mutation(s) for future prenatal diagnosis and genetic consultation. Proving the existence of putative DNPS

disorders provides a new insight in the cellular metabolism. Broader cognitive knowledge brings possibilities to investigate the physiological and pathological conditions of the DNPS pathway and the effects on general and neurological development. Better understanding of the DNPS metabolism may also reveal the mechanisms of the pathway modulation, which could support not only the treatment of DNPS disorders, but also manage uncontrolled cell division (Chakravarthi et al., 2018; Meng et al., 2018), reinforcing DNPS as a potential therapeutic target.

References

An, S., Kumar, R., Sheets, E. D., Benkovic, S. J. (2008) Reversible compartmentalization of de novo purine biosynthetic complexes in living cells. *Science* **320**, 103-106.

Baresova, V., Skopova, V., Sikora, J., Patterson, D., Sovova, J., Zikanova, M. Kmoch, S. (2012) Mutations of ATIC and ADSL affect purinosome assembly in cultured skin fibroblasts from patients with AICA-ribosiduria and ADSL deficiency. *Hum. Mol. Genet.* **21**, 1534-1543.

Baresova, V., Krijt, M., Skopova, V., Souckova, O., Kmoch, S., Zikanova, M. (2016) CRISPR-Cas9 induced mutations along de novo purine synthesis in HeLa cells result in accumulation of individual enzyme substrates and affect purinosome formation. *Mol. Genet. Metab* **119**, 270-277.

Chakravarthi, B., Rodriguez Pena, M. D. C., Agarwal, S., Chandrashekar, D. S., Hodigere Balasubramanya, S. A., Jabboure, F. J., Matoso, A., Bivalacqua, T. J., Rezaei, K., Chaux, A., Grizzle, W. E., Sonpavde, G., Gordetsky, J., Netto, G. J., Varambally, S. (2018) A role for de novo purine metabolic enzyme PAICS in bladder cancer progression. *Neoplasia* **20**, 894-904.

Chrastina, P., Bartl, J., Stastna, S., Paulova, M., Koubikova, H., Elleder, M., Zeman, J. (2007) Screening of inherited metabolic disorders by tandem mass spectrometry. *J. Inherit. Metab. Dis.* **30 (Suppl. 1)**, 02-008P.

Hartmann, S., Okun, J. G., Schmidt, C., Langhans, C. D., Garbade, S. F., Burgard, P., Haas, D., Sass, J. O., Nyhan, W. L., Hoffmann, G. F. (2006) Comprehensive detection of disorders of purine and pyrimidine metabolism by HPLC with electrospray ionization tandem mass spectrometry. *Clin. Chem*. **52**, 1127-1137.

Jaeken, J., Wadman, S. K., Duran, M., van Sprang, F. J., Beemer, F. A., Holl, R. A., Theunissen, P. M., de Cock, P., van den Bergh, F., Vincent, M. F., van den Berghe, G. (1988) Adenylosuccinase deficiency: an inborn error of purine nucleotide synthesis. *Eur. J. Pediatr.* **148**, 126-131.

Jurecka, A., Zikanova, M., Kmoch, S., Tylki-Szymanska, A. (2015) Adenylosuccinate lyase deficiency. *J. Inherit. Metab. Dis*. **38**, 231-242.

Kmoch, S., Hartmannova, H., Stiburkova, B., Krijt, J., Zikanova, M., Sebesta, I. (2000) Human adenylosuccinate lyase (ADSL), cloning and characterization of full-length cDNA and its isoform, gene structure and molecular basis for ADSL deficiency in six patients. *Hum. Mol. Genet.* **9**, 1501-1513.

Krijt, J., Skopova, V., Adamkova, V., Cermakova, R., Jurecka, A., Kmoch, S., Zikanova, M. (2013) The need for vigilance: false-negative screening for adenylosuccinate lyase deficiency caused by deribosylation of urinary biomarkers. *Clin. Biochem.* 46, 1899-1901.

Madrova, L., Krijt, M., Baresova, V., Vaclavik, J., Friedecky, D., Dobesova, D., Souckova, O., Skopova, V., Adam, T., Zikanova, M. (2018) Mass spectrometric analysis of purine de novo biosynthesis intermediates. *PLoS One* **13**, e0208947.

Marie, S., Heron, B., Bitoun, P., Timmerman, T., Van Den Berghe, G., Vincent, M. F. (2004) AICA-ribosiduria: a novel, neurologically devastating inborn error of purine biosynthesis caused by mutation of ATIC. *Am. J. Hum. Genet.* **74**, 1276-1281.

Meng, M., Chen, Y., Jia, J., Li, L., Yang, S. (2018) Knockdown of PAICS inhibits malignant proliferation of human breast cancer cell lines. *Biol. Res.* **51**, 24.

Mouchegh, K., Zikanova, M., Hoffmann, G. F., Kretzschmar, B., Kuhn, T., Mildenberger, E., Stoltenburg-Didinger, G., Krijt, J., Dvorakova, L., Honzik, T., Zeman, J., Kmoch, S., Rossi, R. (2007) Lethal fetal and early neonatal presentation of adenylosuccinate lyase deficiency: observation of 6 patients in 4 families. *J. Pediatr.* **150**, 57-61.e2.

Stone, T. W., Roberts, L. A., Morris, B. J., Jones, P. A., Ogilvy, H. A., Behan, W. M., Duley, J. A., Simmonds, H. A., Vincent, M. F., van den Berghe, G. (1998) Succinylpurines induce neuronal damage in the rat brain. *Adv. Exp. Med. Biol.* **431**, 185-189.

Van den Bergh, F., Vincent, M. F., Jaeken, J., Van den Berghe, G. (1991) Radiochemical assay of adenylosuccinase: demonstration of parallel loss of activity toward both adenylosuccinate and succinylaminoimidazole carboxamide ribotide in liver of patients with the enzyme defect. *Anal. Biochem.* **193**, 287-291.

Van den Berghe, G., Jaeken, J. (1986) Adenylosuccinase deficiency. *Adv. Exp. Med. Biol.* **195**, 27-33.

Williamson, J., Petralia, R. S., Wang, Y. X., Mattson, M. P., Yao, P. J. (2017) Purine biosynthesis enzymes in hippocampal neurons. *Neuromolecular Med.* 19, 518-524.

Yin, J., Ren, W., Huang, X., Deng, J., Li, T., Yin, Y. (2018) Potential mechanisms connecting purine metabolism and cancer therapy. *Front. Immunol.* **9**, 1697.

Zikanova, M., Krijt, J., Hartmannova, H., Kmoch, S. (2005) Preparation of 5-amino-4-imidazole-N-succinocarboxamide ribotide, 5-amino-4-imidazole-N-succinocarboxamide riboside and succinyladenosine, compounds usable in diagnosis and research of adenylosuccinate lyase deficiency. *J. Inherit. Metab. Dis.* **2,** 493-499.

Příloha č. 6

Human Molecular Genetics, 2019, Vol. 28, No. 22 3805–3814

doi: 10.1093/hmg/ddz237
Advance Access Publication Date: 10 October 2019
General Article

GENERAL ARTICLE

PAICS deficiency, a new defect of *de novo* purine synthesis resulting in multiple congenital anomalies and fatal outcome

Anna Pelet[1,†], Vaclava Skopova[2,†], Ulrike Steuerwald[3], Veronika Baresova[2], Mohammed Zarhrate[1], Jean-Marc Plaza[1], Ales Hnizda[4], Matyas Krijt[2], Olga Souckova[2], Flemming Wibrand[5], Guðrið Andorsdóttir[6], Fróði Joensen[3], David Sedlak[7], Anthony J Bleyer[2,8], Stanislav Kmoch[2], Stanislas Lyonnet[1] and Marie Zikanova[2,*]

[1]Laboratory Embryology and Genetics of Congenital Malformation, INSERM UMR1163, Imagine Institute, Université de Paris, F-75015 Paris, France, [2]Research Unit for Rare Diseases, Department of Paediatrics and Adolescent Medicine, First Faculty of Medicine, Charles University and General University Hospital, 12808 Prague, Czech Republic, [3]Pediatric Unit, Medical Department, The Faroese Hospital System, FO 100 Tórshavn, Faroe Islands, [4]Department of Biochemistry, University of Cambridge, CB2 1TN Cambridge, UK, [5]Department of Clinical Genetics, Rigshospitalet, 2100 Copenhagen, Denmark, [6]FarGen, The Genetic Biobank of the Faroe Islands, FO 100 Tórshavn, Faroe Islands, [7]CZ-OPENSCREEN, Institute of Molecular Genetics, Czech Academy of Sciences, 140 00 Prague, Czech Republic. [8]Section on Nephrology, Wake Forest School of Medicine, 271 03 Winston-Salem, NC, USA

*To whom correspondence should be addressed at: Department of Pediatrics and Adolescent Medicine, Ke Karlovu 2, 12808 Prague 2, Czech Republic. Tel: +420224967208; Email: marie.zikanova@lf1.cuni.cz

Abstract

We report for the first time an autosomal recessive inborn error of *de novo* purine synthesis (DNPS)—PAICS deficiency. We investigated two siblings from the Faroe Islands born with multiple malformations resulting in early neonatal death. Genetic analysis of affected individuals revealed a homozygous missense mutation in *PAICS* (c.158A>G; p.Lys53Arg) that affects the structure of the catalytic site of the bifunctional enzyme phosphoribosylaminoimidazole carboxylase (AIRC, EC 4.1.1.21)/phosphoribosylaminoimidazole succinocarboxamide synthetase (SAICARS, EC 6.3.2.6) (PAICS). The mutation reduced the catalytic activity of PAICS in heterozygous carrier and patient skin fibroblasts to approximately 50 and 10% of control levels, respectively. The catalytic activity of the corresponding recombinant enzyme protein carrying the mutation p.Lys53Arg expressed and purified from *E. coli* was reduced to approximately 25% of the wild-type enzyme. Similar to other two known DNPS defects—adenylosuccinate lyase deficiency and AICA-ribosiduria—the *PAICS* mutation prevented purinosome formation in the patient's skin fibroblasts, and this phenotype was corrected by transfection with the wild-type

[†]These authors contributed equally.

Received: August 2, 2019. **Revised:** September 10, 2019. **Accepted:** September 12, 2019

but not the mutated PAICS. Although aminoimidazole ribotide (AIR) and aminoimidazole riboside (AIr), the enzyme substrates that are predicted to accumulate in PAICS deficiency, were not detected in patient's fibroblasts, the cytotoxic effect of AIr on various cell lines was demonstrated. PAICS deficiency is a newly described disease that enhances our understanding of the DNPS pathway and should be considered in the diagnosis of families with recurrent spontaneous abortion or early neonatal death.

Introduction

Purines are critical to energy production and are the fundamental units that transmit the genetic code. *De novo* purine synthesis (DNPS) includes a series of 10 enzymatic reactions that are critical to purine formation (Fig. 1). To date, two genetically determined defects of DNPS have been identified—adenylosuccinate lyase (ADSL) deficiency (ADLSD [OMIM 103050]) (1,2) and 5-aminoimidazole-4-carboxamide ribosiduria (AICA-ribosiduria) (OMIM 608688) (3), which are caused by mutations in *ADSL* or *ATIC* genes, respectively. Both disorders are characterized by neurological involvement of variable severity (4).

Inherited defects in the four other enzymes involved in the early steps of DNPS—phosphoribosyl pyrophosphate amidotransferase (PPAT, EC 2.4.2.14), trifunctional GART—glycinamide ribonucleotide synthetase (EC 6.3.4.13)/phosphoribosylglycinamide formyltransferase (EC 2.1.2.2)/phosphoribosylaminoimidazole synthetase (EC 6.3.3.1), phosphoribosylformylglycinamidine synthetase (PFAS, EC 6.3.5.3) and bifunctional enzyme phosphoribosylaminoimidazole carboxylase (AIRC, EC 4.1.1.21)/phosphoribosylaminoimidazole succinocarboxamide synthetase (SAICARS, EC 6.3.2.6) (PAICS)—have not yet been identified in humans and have been found to be lethal in respective knockout models in mouse (5), zebrafish (6) and *Drosophila melanogaster* (7). However, the range of genetic variation provided in the gnomAD database (https://gnomad.broadinstitute.org/) indicates that, except for *PPAT*, there are no evolutionary constraints against loss of function or missense mutations in these genes in the population (8).

In this investigation, we report for the first time an autosomal recessive condition resulting from mutations in *PAICS*. We demonstrate similar laboratory findings as in ADSL deficiency and AICA-ribosiduria and a similar but very severe neonatal phenotype with fatal outcome. PAICS deficiency is a newly described disease entity that increases our understanding of the DNPS pathway and the critical nature of the participating enzymes.

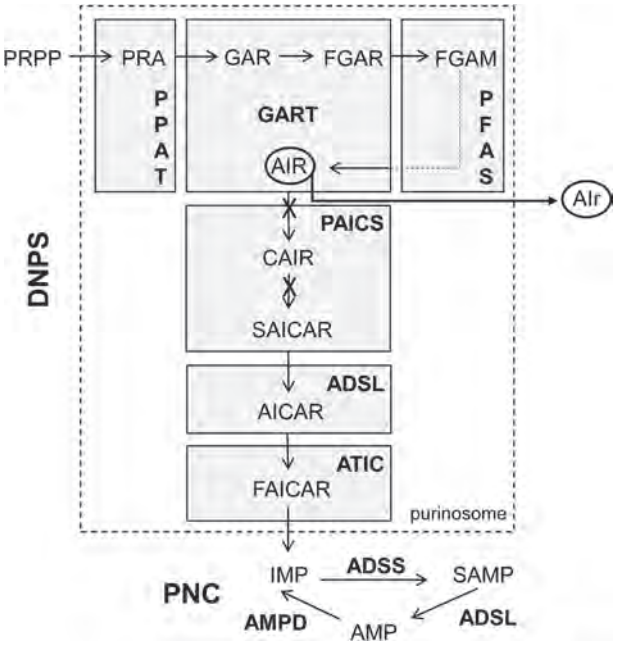

Figure 1. *De novo* purine synthesis (DNPS) and purine nucleotide cycle (PNC). The inosine monophosphate (IMP), the final product of DNPS, is generated from phosphoribosyl pyrophosphate (PRPP) in 10 enzymatic reactions catalyzed by six enzymes: phosphoribosyl pyrophosphate amidotransferase (PPAT), trifunctional GART glycinamide ribonucleotide synthetase/phosphoribosylglycinamide formyltransferase/phosphoribosylaminoimidazole synthetase, phosphoribosylformylglycinamidine synthetase (PFAS), bifunctional PAICS phosphoribosylaminoimidazole carboxylase/phosphoribosylaminoimidazole succinocarboxamide synthetase, adenylosuccinate lyase (ADSL) and bifunctional ATIC 5-aminoimidazole-4-carboxamide ribonucleotide transformylase/inosine monophosphate cyclohydrolase. In response to purine need, these enzymes transiently assemble into a multi-enzyme structure, the purinosome. The IMP is transformed in PNC to adenosine monophosphate (AMP) in reactions catalyzed by adenylosuccinate synthetase (ADSS) followed by ADSL. AMP could by converted back to IMP by adenosine monophosphate deaminase (AMPD). PAICS deficiency should lead to accumulation of aminoimidazole ribotide (AIR) and its dephosphorylated derivative aminoimidazole riboside (AIr).

Results

A family with recurrent polyhydramnios associated with fetal malformations and resulting in early neonatal death

Through an international collaboration and GeneMatcher (9), we investigated a family from the Faroe Islands that had total of seven pregnancies (Fig. 2A). Four pregnancies were uneventful and resulted in three healthy unaffected males and one healthy unaffected female. One pregnancy ended in a spontaneous abortion at 13 weeks of gestation based on polyhydramnios, and two pregnancies led to the live births of two children with multiple malformations who died on Days 2 and 3 based on progressive hypotension and hypoxia.

Case 1 (II.4). The index case was a male noted to have polyhydramnios during a routine ultrasound at 20 weeks of gestation. Ultrasound images also indicated an unspecified malformation of one leg. Spontaneous birth occurred at 36 weeks accompanied by discharge of 7 l of clear amniotic fluid. Moderate asphyxia was noted at birth, with APGAR scores of 3/1, 5/8 and 8/8. The birth weight was 1850 g (P3—200 g), length 41 cm (P3—2.5 cm) and head circumference 33.5 cm (P50). Multiple malformations were identified, including a small body, short neck, short stature, brachycephaly, craniofacial dysmorphism especially of midface with flat face, severe nasal hypoplasia, low nasal bridge, anteverted nostrils, bilateral choanal atresia, hypertelorism, low-set and poorly modulated ears, mild clinodactyly of the fifth fingers bilaterally, shortened distal part of the left leg with club foot, duplication of the left first toe, broadened first toe on right foot, small penis with subcoronal hypospadias, bilateral cryptorchidism, esophageal atresia without tracheoesophageal fistula, several costal and vertebral malformations and hypoplasia of left lung (Fig. 2B and C). Normal muscle tone and reflexes,

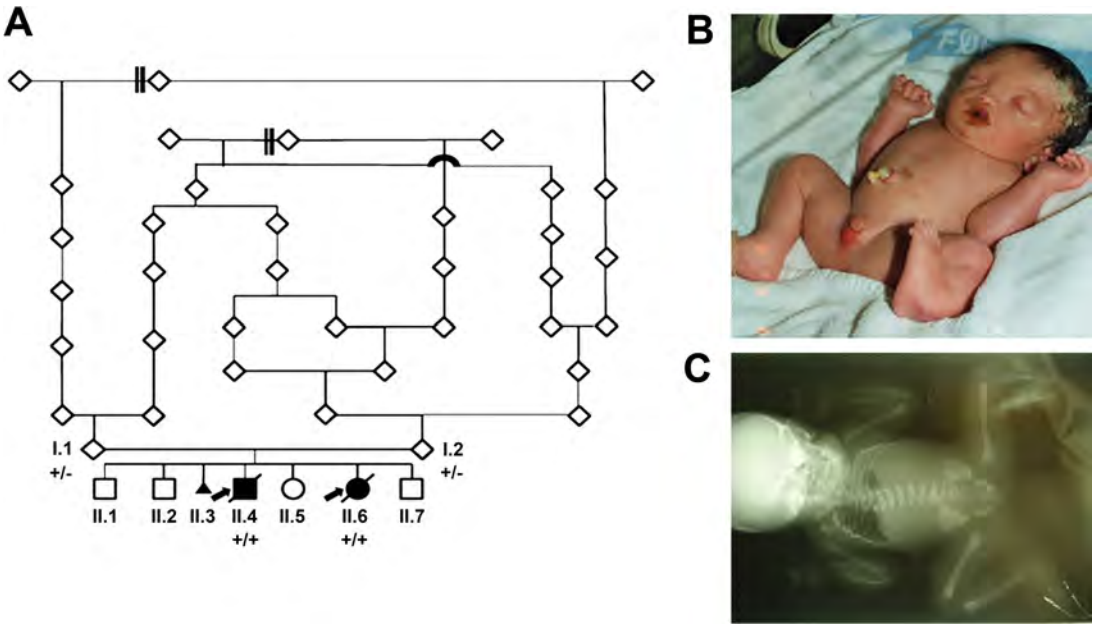

Figure 2. Pedigree and clinical picture of the proband II.4 with PAICS deficiency. (**A**) Pedigree of the family with several common ancestors. Black symbols denote affected individuals, open symbols denote unaffected parents and siblings. (+/−) denotes presence (+) or absence (−) of the chr4:57307970 A/G variant. (**B**) Multiple malformations including small body, short neck, flat face with hypertelorism, nasal hypoplasia, low nasal bridge, low set ears, small penis, clubfoot left in Proband 1 (patient is breathing through an oral Guedel tube for bilateral choanal atresia). (**C**) Whole body X-rays of proband showing multiple aplasias of costae (only eight rips present), hypoplasia of left thorax, multiple deformations of cervical and thoracic vertebrae (multiple butterfly and hemi-vertebrae) and hypoplasia of left tibia leading to clubfoot.

good spontaneous movements and reactions were noted. Ultrasound of the heart, kidneys and brain was without abnormalities. The patient was intubated 2.5 h after delivery based on respiratory failure. Progressive hypotension and hypoxia developed despite standard ventilation. The baby succumbed from cardiorespiratory failure on Day 3 before further diagnostics could be performed.

Case 2 (II.6). An affected sister of the index case was born spontaneously at 34 weeks of pregnancy. Polyhydramnios was observed. The APGAR scores were 7/1 and 8/5. The umbilical cord pH was 7.28. The weight was 2020 g (P10–P25). Short neck, brachycephaly, flat face, low-set ears and small nose with a low nasal bridge were noted. There was right choanal atresia and left choanal stenosis. No fluid was returned with nasogastric suction. An X-ray confirmed esophageal atresia with a tracheoesophageal fistula. Malformation of several ribs and lumbar hemivertebrae were observed. Cystic malformation of the left lung was suspected. The infant had a similar downhill course with progressive hypotension and hypoxia and died at 28 h of age.

Homozygosity mapping and exome sequencing identified a candidate homozygous missense variant in the *PAICS*

Genealogy and pedigree structure revealed that both parents have several common ancestors (Fig. 2A), and genomic analysis was pursued. We first genotyped genomic DNA using the Affymetrix 250K NspI SNP array. Using data derived from SNP probes, we did not identify any copy-number alterations that were compatible with an expected autosomal recessive inheritance model. In agreement with the expected founder effect, we identified three homozygous regions, on Chromosome 6 (chr6: 26393539–28 555 894), Chromosome 8 (chr8: 70174745–73 185 849) and Chromosome 4 (chr4: 54484130–62 069 735), which were shared by both probands (data not shown).

To identify potential disease-causing mutations, we sequenced and analyzed the exomes of the father, mother and two affected children. We searched for variants that had allele frequencies less than 0.1% in the gnomAD database (10) and whose genotypes were compatible with an expected autosomal recessive model of the disease. This analysis revealed in the homozygous region on Chromosome 4 a single homozygous missense variant (chr4: 57307970 A/G) in the *PAICS*. The identified variant, rs192831239, located in Exon 2 of *PAICS* (c.158A>G; NM_001079525.1), encodes the substitution of a lysine 53 to an arginine (p.Lys53Arg) of the PAICS (NP_001072993.1). Using Sanger sequencing, we confirmed homozygosity for the chr4: 57307970 A/G variant in both affected children and the heterozygous status of the healthy parents and siblings (Fig. 2A). The 'G' allele has been identified in a heterozygous state at a maximum frequency of 0.001 in non-Finnish Europeans. At lower frequencies, it has been identified in Finnish (0.0002), Africans (0.0002), and Latinos (0.0007) (https://gnomad.broadinstitute.org/gene/ENSG00000128050). All 143 Faroe individuals tested for this SNP showed the homozygous wild-type genotype A/A.

p.Lys53Arg mutation is predicted to affect the catalytic site of PAICS

The human PAICS assembles into octameric complexes that form well-defined tunnels connecting the AIRC and SAICARS catalytic sites (11). Using the available crystal structure of PAICS (PDB 4JA0, http://www.rcsb.org/pdb/home/home.do) and structural modeling, we found that the presence of the arginine residue at position 53 (R53) may lead to more favorable

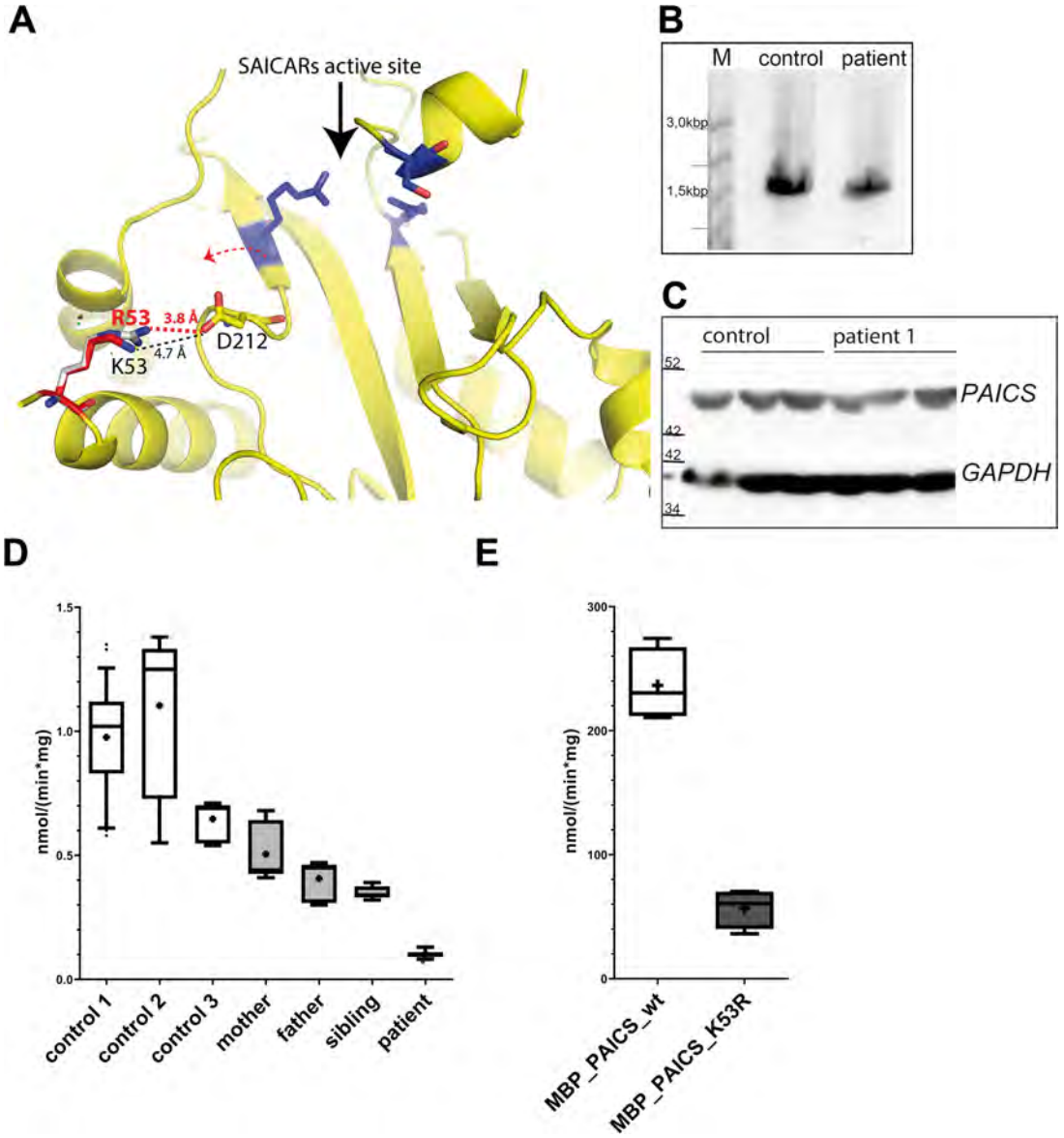

Figure 3. Structural effect of the p.Lys53Arg mutation and its impact on PAICS in cultured skin fibroblasts. (**A**) Analysis of PAICS structure (PDB 4JA0) suggesting that presence of the arginine residue at the position 53 (R53) may lead to a more favorable interaction of this residue with aspartic acid residue at the position 212 (D212). This may move the beta sheet 13, destabilize the catalytic pocket of the SAICARS and alter enzymatic activity of PAICS. (**B**) PAICS cDNA analysis; agarose gel electrophoresis profiles of RT-PCR products amplified from total RNA isolated from fibroblasts of control and proband. (**C**) Western blot analysis of PAICS in cell homogenates; detection with mouse monoclonal anti-PAICS antibody shows a specific immune-reactive protein of a molecular weight ~46 kDa corresponding to the predicted molecular weight of the processed PAICS. The amounts of PAICS were comparable in the proband and control when normalized to glyceraldehyde 3-phosphate dehydrogenase (GAPDH) detected with mouse monoclonal anti-GAPDH. (**D**) Enzyme activity of PAICS in lysates of fibroblasts was reduced to 10% in the proband and to 50% in heterozygous carriers in contrast to controls. Each data point represents the mean of three experiments. Whiskers represent 10 to 90 percentile values, and the mean is shown as plus and median as line ($n = 3$). (**E**) Enzyme activities of the recombinant maltose binding PAICS fusion proteins expressed in *E. coli* and purified on amylose resin. PAICS activity of mutated protein MBP-PAICS_K53R was reduced to 25% in contrast to the wild-type protein MBP-PAICS_wt. Each data point represents the mean of three expression experiments. Whiskers represent 10 to 90 percentile values, and the mean is shown as plus and median as line ($n = 3$).

interaction with the aspartic acid residue at Position 212 (D212), which would cause movement of beta sheet 13 and thus destabilize the catalytic pocket of the SAICARS. To further examine these structural effects, we performed bioinformatic analysis using mCSM software, which revealed significant destabilization of the mutant protein ($\Delta\Delta G = -0.165$ kcal/mol). These findings suggest that Lys53Arg mutation affects PAICS catalytic activity for succinyl aminoimidazole carboxamide ribotide (SAICAR) production based on impaired structural stability (Fig. 3A).

p.Lys53Arg mutation compromises PAICS activity in the patient's skin fibroblasts and of the corresponding purified recombinant protein

To characterize the molecular consequences of the identified mutation, we investigated cultured skin fibroblasts obtained from proband II.4 (Case 1), the heterozygous parents (I.1 and I.2), one heterozygous sibling and three healthy controls.

We isolated total RNA and performed reverse transcription polymerase chain reaction (RT-PCR) analysis and found a single PCR product of an expected size of 1509 bp in an amount that was

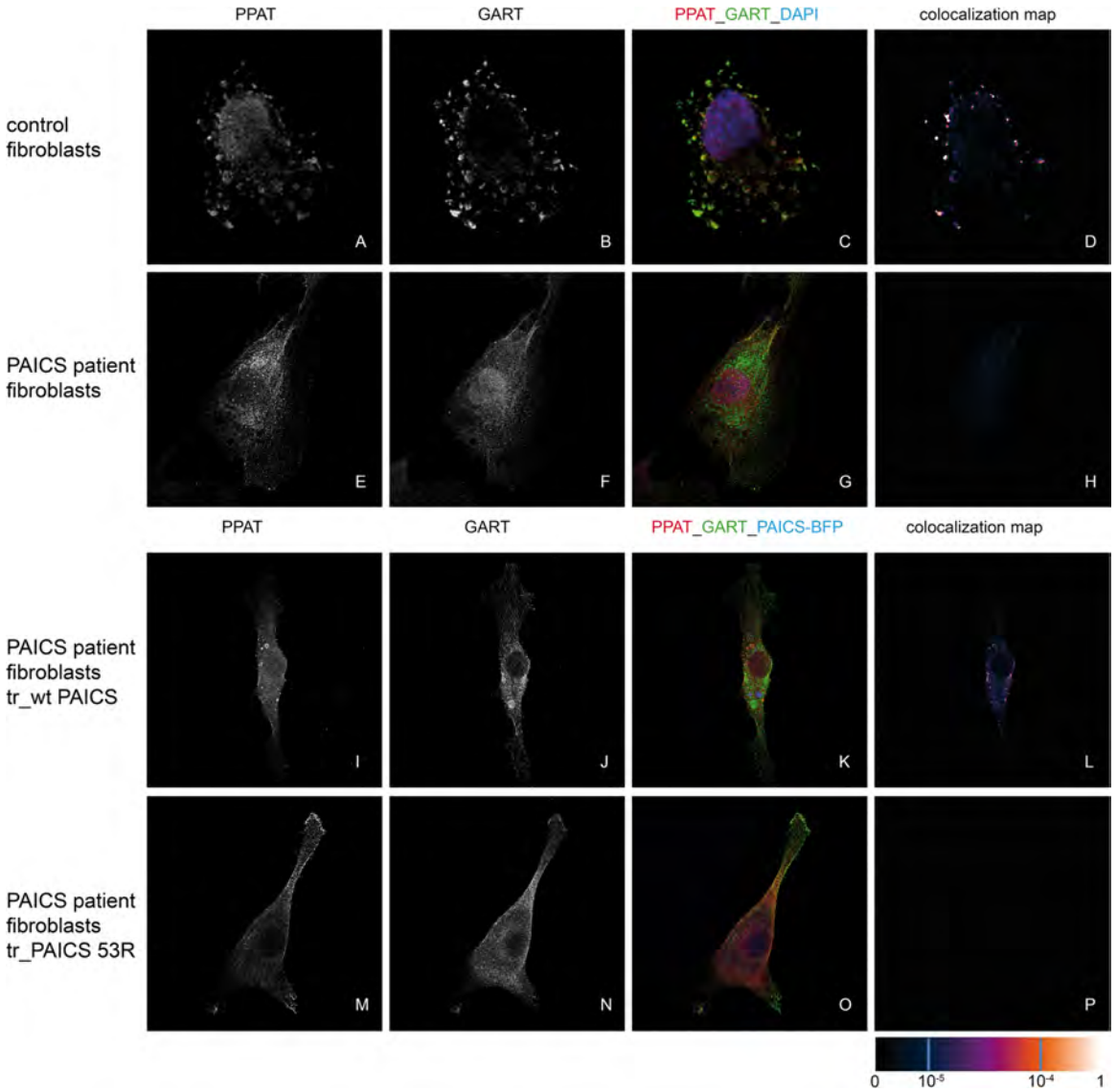

Figure 4. Purinosome formation in skin fibroblasts cultured in purine depleted media. (**A–D**) In control fibroblasts, (A) PPAT and (B) GART show coarsely granular staining and (C, D) significant colocalization in the cytoplasm that is characteristic for purinosome formation. (**E–H**) In affected fibroblasts, (E) PPAT and (F) GART show diffuse intracellular staining with (G, H) no significant signal overlap suggesting that the formation of purinosome is affected by the presence of structurally mutated PAICS. (**I–L**) Transfection of affected fibroblasts with wild-type PAICS restores purinosome formation as shown by granular staining of (I) PPAT and (J) GART and their (K, L) colocalization in the cytoplasm. (**M–P**) Transfection of affected fibroblasts with mutated PAICS does not restore purinosome formation. (D, H, L and P) The degree of PPAT and GART colocalization is demonstrated by the fluorescent signal overlap (Manders) coefficient values that range from 0 to 1. The resulting overlap coefficient values are presented as the pseudocolor whose scale is shown in the corresponding lookup table.

comparable to control specimens suggesting that the mutation has no negative effects on *PAICS* mRNA expression, splicing and stability (Fig. 3B).

Using western blot analysis, we found that the amounts of the PAICS enzyme were similar in the proband and controls (Fig. 3C). Using AIR as a substrate, we found in cell lysates, in contrast to controls, the enzyme activities of PAICS were reduced to approximately 10% in the proband and to 50% in heterozygous carriers (Fig. 3D).

Using established methods (12,13), we cloned the c.158A>G mutation into the pMAL-c2 vector and expressed and purified the wild type (MBP-PAICS_wt) and mutated MBP-PAICS_K53R proteins from *E. coli*. Using AIR as a substrate, we found that the mutant protein had reduced activity to 25% in contrast to the wild type (Fig. 3E).

Identified mutation prevents purinosome formation in the patient's skin fibroblasts, and this phenotype can be corrected by transfection with the wild-type but not the mutated *PAICS*

We showed earlier that mutations of DNPS enzymes affect purinosome assembly in fibroblasts from individuals with ADSL deficiency and AICA-ribosiduria (14) and in CRISPR-Cas9 genome-edited HeLa cells deficient for the individual steps of DNPS (12). To assess the effect of the K53R *PAICS* mutation on purinosome formation, we cultured skin fibroblasts of the proband in purine-depleted (PD) medium and immunodetected PPAT and GART using confocal fluorescent microscopy as previously described (14). When cultured in the PD medium, control fibroblasts demonstrated purinosome

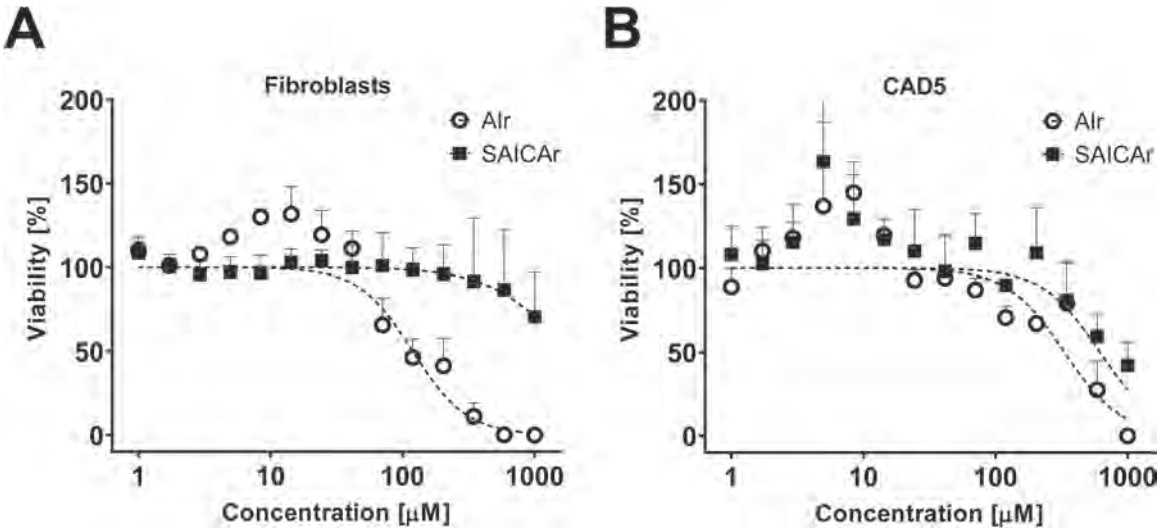

Figure 5. Cytotoxicity of AIr and SAICAr. Cells were cultured in a growth media containing either AIr (circles) or SAICAr (squares) at 14 concentrations ranging from 1.7 μmol/l to 1 mmol/l. Cell viability was assessed 72 h later with luminescent reagent ATPlite™ (PerkinElmer), which takes the level of intracellular ATP as a measure of cell viability. Data were normalized, and IC50 values were calculated using GraphPad Prism software. (**A**) AIr is cytotoxic to control fibroblasts with IC50 = 120 μmol/l in contrast to SAICAr which does not show any effect in the tested range of concentrations. (**B**) AIr and SAICAr are only mildly toxic to CAD5 cells with IC50 values 332 and 618 μmol/l, respectively. Each data point represents the mean of three experiments. Vertical bars represent S.D. ($n = 3$).

formation with characteristic granular staining and significant colocalization of PPAT and GART in the cytoplasm (Fig. 4A–D). In contrast, affected fibroblasts cultured under identical conditions showed diffuse intracellular staining of PPAT and GART with no significant signal overlap (Fig. 4E–H). Purinosome formation was restored in affected fibroblasts cultured in the PD medium after transient transfection with the eukaryotic expression vector encoding the wild-type PAICS (pTagBFP-PAICS_wt) (Fig. 4I–L). Transfection with the vector encoding mutant PAICS (pTagBFP-PAICS_K53R) did not restore purinosome formation (Fig. 4M–P).

AIR and AIr that accumulate in the cellular models of complete PAICS deficiency were not detected in the patient's skin fibroblasts

The other two known DNPS defects—ADSL deficiency and AICA-ribosiduria—are characterized by the accumulation of two dephosphorylated substrates of ADSL—succinyladenosine (SAdo) and succinylaminoimidazole carboxamide riboside (SAICAr). These substrates can be measured in the urine, plasma, cerebrospinal fluid (CSF) and dried blood spots of affected patients (15,16). Recently, we developed a quantitative liquid chromatography–tandem mass spectrometry (LC-MS/MS) method for detection of AIR and AIr, which are predicted to accumulate in the body fluids of patients with PAICS deficiency (17,18) similar to the accumulation of these metabolites in the growth media of Chinese hamster ovary (CHO) cells and HeLa cells that are completely deficient in PAICS (8,19). As there were no body fluids available from the affected individuals, we measured but could not detect AIR or AIr in the cell lysate and growth medium of the patient fibroblasts cultured in purine-depleted media and in purine-rich media. The limits of detection (LODs) and quantification (LOQs) of AIr (defined using signal-to-noise ratios of 3:1 and 10:1, respectively) were 12 and 62 nmol/l, respectively, in growth medium and 3.6 and 18.6 nmol/l, respectively, in water.

The metabolite AIr that is predicted to accumulate in the body fluids of patients with PAICS deficiency demonstrates higher cytotoxicity then SAICAr

The main pathogenic mechanism of ADSL and ATIC deficiencies has been attributed to the cytotoxicity of accumulated dephosphorylated succinylpurines, especially of SAICAr (20). To assess the cytotoxic and neurotoxic effects of AIr, which is expected to accumulate in PAICS deficiency, and compare it to SAICAr, which accumulates in ADSL deficiency, we cultured control fibroblasts and Cath a-differentiated catecholaminergic cells (CAD 5) (21) in a growth medium containing AIr or SAICAr in a concentration gradient from 1.7 μmol/l to 1 mmol/l.

Cell viability was assessed after 72 h of cultivation by determining the level of intracellular ATP with ATPlite™ (PerkinElmer) luminescence system. We observed cytotoxic activity of AIr on both fibroblasts and CAD 5 cells with an estimated half-maximal inhibitory concentration (IC50) of 120 and 332 μmol/l, respectively. In contrast to AIr, SAICAr demonstrated weaker cytotoxicity on both cell types. It was negligible on fibroblasts (IC50 > 1 mmol/l) and showed an IC50 of 618 μmol/l on CAD 5 cells (Fig. 5).

Stimulatory effects of AIr and SAICAr in concentrations <14.3 μM in CAD 5 cells and a stimulatory effect of AIr in concentrations <41.4 μM in fibroblasts were identified as well (Fig. 5).

Discussion

We describe two siblings from The Faroe Islands with multiple malformations and early neonatal death who were born to consanguineous parents. Both affected individuals were homozygous for a rare missense mutation in *PAICS* encoding PAICS, a bifunctional enzyme involved in DNPS. We demonstrate similar laboratory findings as in two known DNPS disorders, ADSL deficiency and AICA-ribosiduria, and a similar but very severe neonatal phenotype with fatal outcome (Table 1). The mutation affects the catalytic site of the enzyme and causes enzyme

Table 1. Comparison of malformations in three DNPS disorders processed by the OMIM database

	AICA-ribosiduria	ADSL deficiency	PAICS deficiency
Growth retardation		+	+ (Intrauterine)
Polyhydramnios			+
Brachycephaly	+	+	+
Microcephaly		(+)	
Short neck			+
Prominent forehead	+		
Prominent metopic suture		+	
Flat face			+
Hypertelorism			+/−
Low-set ears	+	+	+
Poorly modulated ears			+
Congenital blindness	+		n.a.
Optic atrophy	+		n.a.
Strabismus/nystagmus		+	
Small nose		+	+
High nasal bridge	+		
Low nasal bridge			+
Anteverted nostrils	+	+	+
Choanal atresia			+
Wide mouth	+	+	
Thin upper lip	+	+	
Long smooth philtrum		+	
Atrial septal defect	+		
Pulmonary hypoplasia/malformation			+
Esophagus atresia			+
Genitourinary abnormalities	Prominent clitoris, fused labia minora		Micropenis, subcoronal hypospadias
Multiple skeletal malformations			+++
Cognitive difficulties/encephalopathy	+	+	−

deficiency in affected skin fibroblasts and in corresponding recombinant mutant proteins. Moreover, it disturbs purinosome formation in the patient's skin fibroblasts, which can be corrected by transfection with the wild-type but not the mutated PAICS.

ADSL deficiency and AICA-ribosiduria lead to a diagnostic accumulation of the corresponding dephosphorylated enzyme substrates—SAICAr, SAdo and aminoimidazole carboxamide riboside (AICAr)—in the bodily fluids of patients (2,3). Similarly, PAICS deficiency should lead to intracellular accumulation of the enzyme substrate AIR and the presence of its dephosphorylated analog AIr in body fluids. Using liquid chromatography coupled either with electrochemical detection (LC-EMD) or with tandem mass spectrometry (LC-MS/MS), we also showed earlier that CHO cells and CRISPR-Cas9 genome-edited HeLa cells deficient in PAICS accumulate AIr in the growth medium (8,19). Based on the lack of body fluids from affected individuals, we measured but detected neither AIR nor AIr in patients' fibroblasts. This is similar to fibroblasts from individuals with ADSL deficiency, in which we did not detect SAICAr (data not shown). Our inability to detect AIr could be attributed to the approximatively 4-times higher LOD and LOQ of AIr in the growth medium in contrast to water.

The main pathogenic mechanism of ADSL deficiency has been attributed to the cytotoxicity of SAICAr (20), which has previously been reported to have levels of 0.12 mM in cerebrospinal fluid and 1.3 mM in the urine samples of affected individuals (22). Therefore, higher levels of AIr metabolite in bodily fluids may cause similar clinical impairment (Table 1). The neurotoxic and cytotoxic effects of presumably accumulating AIr were demonstrated on CAD5 and fibroblasts cells. Moreover, we found stimulatory effects of both AIr and SAICAr in these cells. The biphasic dose-response effect has been shown recently in a study of the anti-cancer effect of L-ascorbic acid in a colorectal cancer cell line (23,24). This phenomenon called also hormetic dose-response model is a biological feature commonly found in toxicological studies (25). The mechanism of stimulatory/inhibitory action can be explained by different affinity of molecule to particular receptor or part of the signaling pathway within the metabolism of the cell (26). This hypothesis considers further examination.

In conclusion, we have identified a new inherited metabolic disorder of *de novo* purine synthesis—PAICS deficiency. The previous lack of detection and rarity of this condition may be based on recurrent spontaneous abortion or early neonatal death. We are interested to study other similar cases and can provide the genetic testing and biochemical screening described here. Please contact marie.zikanova@lf1.cuni.cz.

Material and Methods

Study subjects and clinical examination

The study was approved by the appropriate institutional review boards and the investigations were performed according to the Declaration of Helsinki principles. Adults provided informed consent, and the siblings of the affected individuals provided assent with parental consent. Participants provided venous blood samples, and genomic DNA was isolated using standard technology. Punch skin biopsies were obtained under local anesthesia, and fibroblasts were cultured according to standard protocol.

Chemicals

DNPS intermediates—SAICAR, AIR and their dephosphorylated forms SAICAr and AIr—were synthesized as previously described (8,27). Dulbecco's minimum essential medium (DMEM), Opti-MEM/Reduced Serum Medium, F12 nutrition mix, Glutamax and fetal bovine serum (FBS) were obtained from Life Technologies. All other chemicals were purchased from Sigma-Aldrich unless otherwise stated in the text.

Homozygosity mapping and sequencing analysis

DNA was isolated by standard methods from venous blood and fibroblasts obtained after skin biopsies. Genotyping was performed on the Affymetrix 250K NspI array (262 000 SNPs) according to the manufacturer's instructions. SNP calling was calculated using the BRLMM algorithm in the Genotyping Console 3.0.2 software (Affymetrix). Homozygous regions were determined using the MERLIN algorithm. Whole exome sequencing (WES) was performed at the genomic platform of the Imagine Institute, Paris, France. Agilent SureSelect libraries were prepared using the exome capture kit 51 Mb SureSelect Human All Exon kit V5 (Agilent Technologies) from 3 µg of sheared genomic DNA with a Covaris S2 Ultrasonicator. NGS was carried out using HiSeq 2500 (Illumina) generating paired-end reads.

After demultiplexing, paired-end sequences were aligned to the reference human genome (NCBI build37/hg19 version) using the Burrows–Wheeler Aligner. Downstream processing was carried out with the Genome Analysis Toolkit (GATK), SAMtools and Picard (http://www.broadinstitute.org/gatk/guide/topic?name5best-practices). Variant calls were made with the GATK Unified Genotyper. For each sample, the mean depth of coverage obtained was 103 with at least 94% of the exome covered at least 30×. An in-house software (Poly-Web based on Ensembl release 71, http://www.ensembl.org/index.html) was used to annotate and filter variants according to a homozygous genetic model. We excluded variants from public data bases (dbSnp, 1000 genomes, Evs, Exac and gnomAD) with a frequency >1% as well as variants previously identified in 'in house exomes'.

In order to verify the familial segregation of the variant a bidirectional Sanger sequencing was performed using the ABI BigDye Terminator v.3.1 Cycle Sequencing Kit (Life Technologies).

RNA analysis and cDNA sequencing

Total RNA and cDNA were isolated from cultured skin fibroblasts of proband II.4 (Case 1) and the control by ProtoScript II First Strand cDNA Synthesis Kit (NEB). PCR analysis was performed according to standard procedures. The PCR was conducted in 25 µl reaction mixtures containing Red PCR Master Mix (Rovalab), 1.5 mM $MgCl_2$, 8% DMSO and 0.4 µM specific primers covering cDNA from start to stop codon. The amplicons were sequenced using the specific 813L primer by Sanger sequencing service (Eurofins Genomics).

Structural impact of the identified mutation

For structural mapping, available crystal structure of PAICS (PDB ID 2H31) (11) was analyzed. Structural models were visualized using the PyMOL Viewer (DeLano Scientific, Palo Alto, CA, USA). Protein stability of the mutant was further assessed using mCSM software (28).

Cell cultures

Primary skin fibroblasts were maintained in Dulbecco's minimum essential medium/F12 nutrient mixture (DMEM/F12, Gibco, Life Technologies) supplemented with 10% FBS (Gibco, Life Technologies), 1% penicillin/streptomycin (Sigma-Aldrich) and 0.03 mM adenine. The purine-depleted media was prepared from DMEM (Gibco, Life Technologies) supplemented with dialyzed 10% FBS and 1% penicillin/streptomycin. FBS was dialyzed against 0.9% NaCl at 4°C for 48 h using a 10 kDa MWCO dialysis membrane to remove purines.

CAD-2A2D5 (CAD5) cells derived from Catha-differentiated (CAD) cells were provided by Sukhvir Mahal, The Scripps Research Institute, FL, USA. CAD5 cells were maintained in modified Eagle's Minimum Essential Media (Opti-MEM/Reduced Serum Media, Gibco, Life Technologies) supplemented with 10% FBS, 2 mM Glutamax, 1 mM pyruvate, 1% penicillin/streptomycin without phenol red.

Preparation of fibroblasts' lysates

Cells (1.5×10^6) were washed with PBS and centrifuged at 400*g* for 5 min at 4°C. The pellet was suspended in 30 µl of lysis buffer containing 30 mM KH_2PO_4, pH 6.0, 0.5% polyethylene glycol ether W-1 (Sigma-Aldrich) and Protease Inhibitor Cocktail Tablets (Roche) and incubated on ice for 45 min. The solution was sonicated four times for 5 s and centrifuged at 17000*g* for 20 min at 4°C.

Catalytic activity of PAICS enzyme in patient's skin fibroblasts

Proband II.4 1.5×10^6 (Case 1), the heterozygous parents (I.1 and I.2), a heterozygous sibling and three control skin fibroblasts were lysed, and protein concentrations were determined by Bradford reagent (Sigma-Aldrich). PAICS activities were assayed at 37°C in 50 mM Tris, pH 7.4, 5 mM aspartate, 0.3 mM ATP, 180 mM $KHCO_3$, 24.5 mM $MgCl_2$, 350 mg/l SF lysate and 0.25 mM AIR for 2 h. The reaction product SAICAR was quantified by HPLC analysis as previously described (8,13). All experiments were repeated three times.

Western blot

The cell lysates were separated by 10% SDS-PAGE, and proteins were blotted onto a PVDF membrane. The membrane was blocked with 5% BSA in PBS-T (PBS with 0.05% Tween 20) and probed with primary antibodies: mouse monoclonal anti-PAICS (OriGene) and mouse monoclonal anti-GAPDH (Sigma-Aldrich) diluted in 5% BSA in PBS-T. The target proteins were detected using peroxidase conjugated secondary antibodies: goat anti-mouse IgG (Sigma-Aldrich) and goat anti-mouse IgM (Pierce).

Chemiluminescent detection was performed using the Clarity Western ECL Substrate (Bio-Rad) and visualized by x-ray imaging.

LC-MS/MS analysis

Before analysis, the cell media were concentrated from 1 mL to 60 µL under a nitrogen stream at 37°C. Five percent perchloric acid (16.6 µl) was added to 30 µl of concentrated medium or cell lysate, and samples were incubated 5 min at 4°C. After centrifugation, the supernatants were neutralized with 3.2 µl of 2.5 M $KHCO_3$, incubated 10 min at 4°C and centrifuged again.

Five microliters of the sample was injected into the LC-MS/MS system consisting of an Agilent 1290 Infinity LC System (Agilent Technologies) equipped with a ProntoSIL 120-3-C18 AQ column (200∗4 mm, 3 µm, Bischoff) coupled with an API 4000 triple quadrupole mass spectrometer with an electron spray ionization operated by Analyst software (Applied Biosystems), as previously described (8). The limits of detection and quantification were determined using signal-to-noise ratios of 3:1 and 10:1, resp. from 3 nM to 50 µM concentrations of AIr standard diluted in water or in the purine-depleted (PD) media. The AIr samples were treated in the same manner as the growth media of patient fibroblasts before LC-MS/MS analysis. A retention time of AIr in PD media was 5.2 min, in water 4.7 min.

Cloning of pMAL-PAICS_wt, pMAL-PAICS_K53R, pTagBFP-PAICS_wt and pTagBFP-PAICS_K53R

The cDNA coding for wild-type PAICS was cloned into the expression vectors pMAL-c2 (NEB) and pTagBFP-C (Evrogene) as previously described (8,12). The mutation K53R was cloned into both vectors by the GeneArt™ Site-Directed Mutagenesis System (Thermo Fisher Scientific) using standard procedures.

Catalytic activities of recombinant PAICS proteins

The proteins MBP-PAICS_wt and MBP-PAICS_K53R were expressed in *E. coli* and affinity purified as previously described (29). PAICS activities were assayed as described previously, using 25 mg/l of the purified fused protein.

Transfection and immunofluorescence

For transfection, 1×10^5 of patient or control skin fibroblasts were transiently transfected with 1.5 µg of pTagBFP-PAICS_wt or pTagBFP-PAICS_K53R. The transfection and immunofluorescence labeling was performed as previously described (12) with the following primary antibodies: rabbit polyclonal IgG anti-PPAT (Sigma-Aldrich) and mouse polyclonal IgG anti-GART (Abnova). For fluorescence detection, species appropriate Alexa Fluor® 488 and 555 secondary antibodies (Thermo Fisher Scientific) were used. All immunofluorescence experiments were repeated at least twice.

Image acquisition and analysis

Slides were mounted with ProLong® Gold Antifade Mountant (Thermo Fisher Scientific) as the fluorescence mounting medium and analyzed by confocal microscopy as previously described (12,14). The resulting overlap coefficient values are presented in pseudocolor, and the scale is shown in the corresponding lookup tables (LUT). Image analysis was performed on at least 10 cells from each cell type. The conditions for image acquisition were identical for all cells evaluated in the experiment.

Substrate toxicity testing

Cells (7×10^2) cells in 24 µl volume were seeded per well in a 384-well plate format. Cells were maintained in Dulbecco's minimum essential medium (DMEM) or a modified Eagle's Minimum Essential Media (Opti-MEM/Reduced Serum Media) supplemented with 10% FBS, 2 mM Glutamax, 1 mM pyruvate and 1% penicillin/streptomycin. For feeding experiments, cells were transferred to DMEM without phenol red supplementation as mentioned earlier or Opti-MEM for CAD5 cells, respectively. Cells were grown in 12 µl of media overnight at 37°C using a 5% CO_2 incubator. The following day, individual substrates, SAICAr and AIr, were prediluted in a media in a series of 14 concentrations between 1.7 µM and 1 mM. Twelve microliters of prediluted substrates was added to cells to achieve final concentration in a total volume of 24 µl per well.

The ATPlite™ luminescence assay system was purchased from Perkin Elmer. A luciferase-catalyzed reaction of ATP and luciferin results in production of light. The ATP concentration (representing cell viability) is proportional to emitted light. A total volume of 24 µl of media with cells was treated with 11 µl of ATPlite solution followed by 15 min incubation at room temperature and shaking on an orbital shaker. After the incubation step, luminescence was recorded on an EnVision plate reader (PerkinElmer) with proper optical aperture for a 384-well plate. Subsequent analysis was performed on standard software Microsoft Office Excel and GraphPad Prism software.

Funding

The part of work conducted at the First Faculty of Medicine was supported by Charles University [program numbers PRIMUS/17/MED/6, PROGRES Q26/LF1, UNCE/MED/007, SVV 260367/2017], by the Ministry of Health of Czech Republic [grant number NV19-07-00136] and by the Ministry of Education, Youth and Sports of CR: The National Center for Medical Genomics [grant number LM2015091], National Sustainability Programme II [grant number LQ1604] and National infrastructure for chemical biology [grant number LM2015063]. The part of work conducted at Imagine Institute was supported by State funding from the Agence Nationale de la Recherche, 'Investissements d'avenir' [program number ANR-10-IAHU-01].

Acknowledgements

We acknowledge the dedicated care of the index case by member of the Neonatal Intensive Care Unit at University Hospital, Copenhagen, and the pediatricians at the National Hospital of the Faroe Islands, Tórshavn, where both patients were treated; the Genetic Biobank of the Faroe Islands in Tórshavn for providing DNA of the patients' family and information used for creating the family pedigree; and Ernst Christensen and Marianne Schwartz at the Metabolic Laboratory as well as Susanne Kjærgaard at the Chromosome Laboratory at University Hospital, Copenhagen, for providing DNA of the deceased infants and fibroblasts of the patient 1.

Conflict of Interest statement. None declared.

References

1. Stone, R.L., Aimi, J., Barshop, B.A., Jaeken, J., Van den Berghe, G., Zalkin, H. and Dixon, J.E. (1992) A mutation in adenylosuccinate lyase associated with mental retardation and autistic features. *Nat. Genet.*, **1**, 59–63.
2. Van den Berghe, G. and Jaeken, J. (1986) Adenylosuccinase deficiency. *Adv. Exp. Med. Biol.*, **195**, 27–33.
3. Marie, S., Heron, B., Bitoun, P., Timmerman, T., Van Den Berghe, G. and Vincent, M.F. (2004) AICA-ribosiduria: a novel, neurologically devastating inborn error of purine biosynthesis caused by mutation of ATIC. *Am. J. Hum. Genet.*, **74**, 1276–1281.

4. Jurecka, A., Zikanova, M., Kmoch, S. and Tylki-Szymanska, A. (2015) Adenylosuccinate lyase deficiency. *J. Inherit. Metab. Dis.*, **38**, 231–242.
5. Dickinson, M.E., Flenniken, A.M., Ji, X., Teboul, L., Wong, M.D., White, J.K., Meehan, T.F., Weninger, W.J., Westerberg, H., Adissu, H. *et al.* (2016) High-throughput discovery of novel developmental phenotypes. *Nature*, **537**, 508–514.
6. Ng, A., Uribe, R.A., Yieh, L., Nuckels, R. and Gross, J.M. (2009) Zebrafish mutations in gart and paics identify crucial roles for de novo purine synthesis in vertebrate pigmentation and ocular development. *Development*, **136**, 2601–2611.
7. Thurmond, J., Goodman, J.L., Strelets, V.B., Attrill, H., Gramates, L.S., Marygold, S.J., Matthews, B.B., Millburn, G., Antonazzo, G., Trovisco, V. *et al.* (2019) FlyBase 2.0: the next generation. *Nucleic Acids Res.*, **47**, D759–D765.
8. Baresova, V., Krijt, M., Skopova, V., Souckova, O., Kmoch, S. and Zikanova, M. (2016) CRISPR-Cas9 induced mutations along de novo purine synthesis in HeLa cells result in accumulation of individual enzyme substrates and affect purinosome formation. *Mol. Genet. Metab.*, **119**, 270–277.
9. Sobreira, N., Schiettecatte, F., Valle, D. and Hamosh, A. (2015) GeneMatcher: a matching tool for connecting investigators with an interest in the same gene. *Hum. Mutat.*, **36**, 928–930.
10. Lek, M., Karczewski, K.J., Minikel, E.V., Samocha, K.E., Banks, E., Fennell, T., O'Donnell-Luria, A.H., Ware, J.S., Hill, A.J., Cummings, B.B. *et al.* (2016) Analysis of protein-coding genetic variation in 60,706 humans. *Nature*, **536**, 285–291.
11. Li, S.X., Tong, Y.P., Xie, X.C., Wang, Q.H., Zhou, H.N., Han, Y., Zhang, Z.Y., Gao, W., Li, S.G., Zhang, X.C. *et al.* (2007) Octameric structure of the human bifunctional enzyme PAICS in purine biosynthesis. *J. Mol. Biol.*, **366**, 1603–1614.
12. Baresova, V., Skopova, V., Souckova, O., Krijt, M., Kmoch, S. and Zikanova, M. (2018) Study of purinosome assembly in cell-based model systems with de novo purine synthesis and salvage pathway deficiencies. *PLoS One*, **13**, e0201432.
13. Kmoch, S., Hartmannova, H., Stiburkova, B., Krijt, J., Zikanova, M. and Sebesta, I. (2000) Human adenylosuccinate lyase (ADSL), cloning and characterization of full-length cDNA and its isoform, gene structure and molecular basis for ADSL deficiency in six patients. *Hum. Mol. Genet.*, **9**, 1501–1513.
14. Baresova, V., Skopova, V., Sikora, J., Patterson, D., Sovova, J., Zikanova, M. and Kmoch, S. (2012) Mutations of ATIC and ADSL affect purinosome assembly in cultured skin fibroblasts from patients with AICA-ribosiduria and ADSL deficiency. *Hum. Mol. Genet.*, **21**, 1534–1543.
15. Krijt, J., Skopova, V., Adamkova, V., Cermakova, R., Jurecka, A., Kmoch, S. and Zikanova, M. (2013) The need for vigilance: false-negative screening for adenylosuccinate lyase deficiency caused by deribosylation of urinary biomarkers. *Clin. Biochem.*, **46**, 1899–1901.
16. Van den Bergh, F., Vincent, M.F., Jaeken, J. and Van den Berghe, G. (1991) Radiochemical assay of adenylosuccinase: demonstration of parallel loss of activity toward both adenylosuccinate and succinylaminoimidazole carboxamide ribotide in liver of patients with the enzyme defect. *Anal. Biochem.*, **193**, 287–291.
17. Krijt, M., Souckova, O., Baresova, V., Skopova, V. and M., Z. (2019) Metabolic tools for identification of new mutations of enzymes engaged in purine synthesis leading to neurological impairment. *Folia Biol. (Praha)*, **65**, 152–157.
18. Madrova, L., Krijt, M., Baresova, V., Vaclavik, J., Friedecky, D., Dobesova, D., Souckova, O., Skopova, V., Adam, T. and Zikanova, M. (2018) Mass spectrometric analysis of purine de novo biosynthesis intermediates. *PLoS One*, **13**, e0208947.
19. Duval, N., Luhrs, K., Wilkinson, T.G., 2nd, Baresova, V., Skopova, V., Kmoch, S., Vacano, G.N., Zikanova, M. and Patterson, D. (2013) Genetic and metabolomic analysis of AdeD and AdeI mutants of de novo purine biosynthesis: cellular models of de novo purine biosynthesis deficiency disorders. *Mol. Genet. Metab.*, **108**, 178–189.
20. Stone, T.W., Roberts, L.A., Morris, B.J., Jones, P.A., Ogilvy, H.A., Behan, W.M., Duley, J.A., Simmonds, H.A., Vincent, M.F. and van den Berghe, G. (1998) Succinylpurines induce neuronal damage in the rat brain. *Adv. Exp. Med. Biol.*, **431**, 185–189.
21. Mahal, S.P., Baker, C.A., Demczyk, C.A., Smith, E.W., Julius, C. and Weissmann, C. (2007) Prion strain discrimination in cell culture: the cell panel assay. *Proc. Natl. Acad. Sci U S A*, **104**, 20908–20913.
22. Jaeken, J. and Van den Berghe, G. (1984) An infantile autistic syndrome characterised by the presence of succinylpurines in body fluids. *Lancet*, **2**, 1058–1061.
23. Kendig, E.L., Le, H.H. and Belcher, S.M. (2010) Defining hormesis: evaluation of a complex concentration response phenomenon. *Int. J. Toxicol.*, **29**, 235–246.
24. Cho, S., Chae, J.S., Shin, H., Shin, Y., Song, H., Kim, Y., Yoo, B.C., Roh, K., Kil, E.J., Byun, H.S. *et al.* (2018) Hormetic dose response to L-ascorbic acid as an anti-cancer drug in colorectal cancer cell lines according to SVCT-2 expression. *Sci. Rep.*, **8**, 11372.
25. Calabrese, E.J. and Baldwin, L.A. (2003) The hormetic dose-response model is more common than the threshold model in toxicology. *Toxicol. Sci.*, **71**, 246–250.
26. Calabrese, E.J. (2013) Hormetic mechanisms. *Crit. Rev. Toxicol.*, **43**, 580–606.
27. Zikanova, M., Krijt, J., Hartmannova, H. and Kmoch, S. (2005) Preparation of 5-amino-4-imidazole-N-succinocarboxamide ribotide, 5-amino-4-imidazole-N-succinocarboxamide riboside and succinyladenosine, compounds usable in diagnosis and research of adenylosuccinate lyase deficiency. *J. Inherit. Metab. Dis.*, **28**, 493–499.
28. Pires, D.E., Ascher, D.B. and Blundell, T.L. (2014) mCSM: predicting the effects of mutations in proteins using graph-based signatures. *Bioinformatics*, **30**, 335–342.
29. Zikanova, M., Wahezi, D., Hay, A., Stiburkova, B., Pitts, C., 3rd, Musalkova, D., Skopova, V., Baresova, V., Souckova, O., Hodanova, K. *et al.* (2018) Clinical manifestations and molecular aspects of phosphoribosylpyrophosphate synthetase superactivity in females. *Rheumatology (Oxford)*, **57**, 1180–1185.